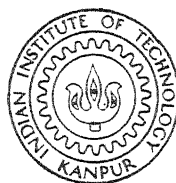


# SOME EXPERIMENTAL STRESS ANALYSIS TECHNIQUES FOR FIBROUS COMPOSITES

by

SHIVE KUMAR CHATURVEDI

ME <sup>TH</sup>  
1978 ME/1978/D  
DPhD < 3925  
CHA  
SOM



DEPARTMENT OF MECHANICAL ENGINEERING  
INDIAN INSTITUTE OF TECHNOLOGY KANPUR  
SEPTEMBER, 1978

सत यम् विष्णु सुन्दरम्

# **SOME EXPERIMENTAL STRESS ANALYSIS TECHNIQUES FOR FIBROUS COMPOSITES**

**A Thesis Submitted  
In Partial Fulfilment of the Requirements  
for the Degree of  
DOCTOR OF PHILOSOPHY**

**by  
SHIVE KUMAR CHATURVEDI**

**to the  
  
DEPARTMENT OF MECHANICAL ENGINEERING  
INDIAN INSTITUTE OF TECHNOLOGY KANPUR  
SEPTEMBER, 1978**

1.  
CENTRAL  
No. 58468


10 11 1979

ME-1578-D-CHA-SOM

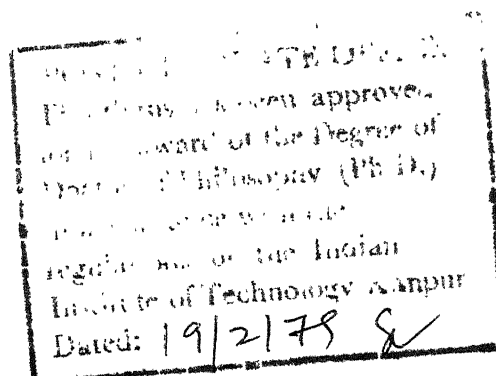


## CERTIFICATE

This is to certify that this thesis entitled, 'Some Experimental Stress Analysis Techniques for Fibrous Composites', by Mr. S.K. Chaturvedi is a record of work carried out under my supervision and has not been submitted elsewhere for a degree.

  
(B.D. Agarwal)  
Assistant Professor  
Department of Mechanical Engineering  
Indian Institute of Technology  
Kanpur

September 1978



## ACKNOWLEDGEMENTS

I wish to express my deep sense of gratitude to Prof. B.D. Agarwal for his valuable guidance and constructive criticism throughout the present investigations. His generous attitude has been a constant source of inspiration to me.

I am thankful to Professors V.K. Stokes, B.P. Singh and B.L. Dhoopar, successive coordinators of Experimental Stress Analysis Laboratories, for providing the facilities to carry out the experimental work. I wish to express my sincere thanks to Prof. P.N. Murthy for his useful discussions and encouragement during the work.

I deeply appreciate the thoughtprovoking discussions and helpful comments of my friends Messrs. K.N. Swamy Rao, S.K. Joneja and G. Kameshwar Rao during the course of this work. The indirect help extended by other friends is thankfully acknowledged.

I appreciate the cooperation and help of the technical staff of Mechanical Engineering Department, in particular of D.K. Sarkar, S.L. Srivastava, S.N. Yadav, B.L. Sharma, P.N. Mishra, B.P. Vishwakarma and M.M. Singh. I must also thank V.N. Pandey of Aeronautical Engineering Department for his help in developing the brittle coating.

I thank B.L. Arora for the illustrations in thesis and J.D. Varma for carefully typing the thesis.

Finally, I am indebted to my parents for their help and my wife Chandra Kanta for not only the help given by her in the laboratory work but keeping around me a peaceful and cheerful environment also. She has been a source of constant encouragement for devotion and hard work required for the completion of the present work.

S.K. Chaturvedi

## TABLE OF CONTENTS

	Page
LIST OF TABLES	viii
LIST OF FIGURES	ix
NOMENCLATURE	xii
SYNOPSIS	xv
CHAPTER	
1 INTRODUCTION	1
1.1 Introduction to Composite Materials	1
1.2 Literature Survey and Scope of Present Work	2
2. BRITTLE COATING STUDIES ON FIBROUS COMPOSITES	11
2.1 Introduction	11
2.2 Experimental Procedure	12
2.2.1 Coating Preparation	14
2.2.2 Specimen Material	15
2.2.3 Application of Coating to the Specimen	16
2.2.4 Calibration of Coating	18
2.3 Results and Discussion	19
2.3.1 Coating Behaviour under Uniaxial Stresses	19
2.3.2 Coating Behaviour under Biaxial Stresses	26
2.4 Analysis Technique	32

Chapter		Page
3	DEVELOPMENT AND CHARACTERISATION OF OPTICALLY SUPERIOR PHOTOELASTIC ORTHOTROPIC MODEL MATERIALS	39
3.1	Introduction	39
3.2	Optical Considerations for a Model Material	40
3.3	Fabrication of Material	48
3.4	Optical Suitability of Model Materials	52
3.4.1	Transparency	53
3.4.2	Resolution of Lines Through Model Materials	54
3.4.3	Image Forming Characteristics	57
3.4.4	Photoelastic Effects	62
3.5	Mechanical and Photoelastic Characteri- sation	64
4	EXACT THEORIES OF PHOTO-ORTHOTROPIC- ELASTICITY	69
4.1	Introduction	69
4.2	Assessment of Existing Theories of Photo- Orthotropic-Elasticity	70
4.3	Exact Strain-Optic Law	83
4.3.1	Experimental Determination of Principal Strain-Fringe Values	93
4.4	Some Important Observations	98
5	AN APPROXIMATE THEORY OF PHOTO- ORTHOTROPIC-ELASTICITY	103
5.1	Introduction	103
5.2	Approximate Strain-Optic Law	104

Chapter		Page
5.3	Assessment of Strain-Optic Laws	110
5.4	Error Estimation, Correction and Its Experimental Verification	114
5.5	Concluding Remarks	128
6	CONCLUSIONS	131
REFERENCES		134
APPENDIX		
A	TRANSFORMATION RELATIONS FOR STRESSES STRAINS AND MATERIAL PROPERTIES	139
B	FAILURE THEORY	142
C	EVALUATION OF STRAIN-OPTIC PROPERTY ( $P_{22} - P_{23}$ )	145

## LIST OF TABLES

Table		Page
2.1	Results for Coating Behaviour Under Uniaxial Stress	24
2.2	Results for Coating Behaviour Under Biaxial Stresses	31
3.1	Elastic Properties of Model Materials	68
3.2	Photoelastic Properties of Model Materials	68
4.1	Comparison of Photoelastic Properties and Anisotropic Ratios for Different Model Materials	99
5.1	Results of Photoelastic Analysis for a Uniaxial State of Stress	121
5.2	Results of Photoelastic Analysis for a Biaxial State of Stress	129
C.1	Properties of the Constituents of Unidirectional Model Material	148

## LIST OF FIGURES

Figure		Page
2.1	Test specimens (a) Cantilever beam for uniaxial stress (b) Circular disc under diametral compression for biaxial stresses.	17
2.2	Brittle coating crack patterns on the beam specimens under uniaxial state of stress. Left to right: Fibre orientations 5, 30, 45, 75 and 90 degree.	20
2.3	Schematic diagram showing directions of coating cracks, maximum principal stress and maximum principal strain on the beam specimen.	21
2.4	Brittle coating crack pattern on a partially reinforced beam specimen. Dotted line represents boundary of the reinforced region and the double arrow indicates fibre direction.	25
2.5	Brittle coating crack patterns on the circular disc specimens under diametral compression. Left to right: Fibre orientations 15, 45 and 60 degree.	27
2.6	Schematic diagram showing the positions of strain gauge rosettes mounted on the circular disc specimen.	29
3.1	Schematic representation of path of light through (a) Homogeneous solid (b) Two solid mediums with a straight interface and (c) Solid medium with another solid inclusion having a curved interface.	43
3.2	Arrangement of elements in optical bench.	45
3.3	Image of slit through a glass rods reinforced epoxy model. Angle of glass rods with the slit (a) $0^\circ$ , (b) $45^\circ$ and (c) $90^\circ$ , and (d) Image through unreinforced epoxy model.	46



Figure		Page
3.4	A mould in the vacuum chamber to remove- entrapped air.	51
3.5	View of parallel lines through (a) No model, (b) Unidirectional model material, (c) Bidirectional model material and (d) A material with small mismatch of refractive indices. Arrows indicate the direction of fibres.	56
3.6	Limit of resolution of lines for unidirec- tional materials.	58
3.7	Image of slit through unidirectional model material with fibres inclined at (a) $0^\circ$ , (b) $45^\circ$ and (c) $90^\circ$ , and (d) image through bidirectional model material.	60
3.8	Image of slit through inferior model mate- rials (a) Glass-polyester $0^\circ$ , (b) Glass- polyester $90^\circ$ (c) Glass-epoxy $0^\circ$ and (d) Glass-epoxy $90^\circ$ .	61
3.9	Isochromatic fringe patterns for (a) Uni- directional model (b) Bidirectional model (c) Glass-polyester model with small mis- match and (d) Glass-epoxy model with large mismatch of refractive indices.	63
4.1	Evaluation of off-axis stress-fringe value.	75
4.2	Stress fringe value as a function fibre orientation for uniaxial loading of tensile specimens.	77
4.3	Isoclinic angle as a function of the fibre orientation for uniaxial loading of tensile specimens. (Unidirectional material)	78
4.4	Isoclinic angle as a function of the fibre orientation for uniaxial loading of ten- sile specimens. (Bidirectional material)	79
4.5	Photoelastic characterisation-0-degree test.	95
4.6	Photoelastic characterisation-90-degree test.	96

Figure		Page
4.7	Variation of strain-fringe values with fibre orientation for unidirectional model material.	100
5.1	Predictions of isoclinic angle from exact and approximate theories.	111
5.2	Variations in directions of principal birefringence and stress as a function of fibre orientation for different biaxial states of strain.	113
5.3	Prediction of birefringence from exact and approximate theories for principal strain ratios of -0.25 and +0.25.	115
5.4	Prediction of birefringence from exact and approximate theories for principal strain ratios of -2.5 and -10.0.	116
5.5	Errors in corrected and uncorrected principal strain-difference.	123
5.6	Schematic diagram showing the locations of the three points considered for analysis.	124
5.7	Directions of major principal strain and birefringence at the three points for disc orientation of 0 - degree.	125
5.8	Directions of major principal strain and birefringence at the three points for disc orientation of 30 - degree.	126
5.9	Isochromatics for disc orientation of (a) 0° and (b) 30° and isoclinics for disc orientation of 30° with isoclinic parameter (c) 0° and (d) 15°.	127
A.1	An orthotropic plane lamina	139

## NOMENCLATURE

$A$	Variable defined in Eq. (2.8)
$a$	Strain-optic coefficient
$B$	Variable defined in Eq. (2.8)
$b_1, b_2, b_3$	Reciprocals of strain fringe values
$C$	Variable defined in Eq. (2.8)
$c$	Strain-optic coefficient
$E$	Modulus of elasticity
$f_e$	Strain-fringe value
$f_e'$	Strain-fringe value defined by Eq. (4.33)
$f_\sigma$	Stress-fringe value
$G$	Shear modulus
$K$	Brittle-coating strength ratio
$K_1, K_2$	Variables defined in Eq. (4.14)
$m$	Shear coupling coefficient
$N$	Isochromatic fringe order
$N_{ij}$	Birefringence tensor
$P_{qr}$	Strain-optic coefficients
$P_{ijkl}$	Anisotropic strain-optic property tensor
$P_{ijkl}^o$	Isotropic strain-optic property tensor
$R_1, R_2, R_3$	Variables defined in Eq. (C.4)
$r$	Variable defined in Eq. (2.12)
$S_1, S_2$	Slopes of straight lines defined by Eqs. (4.38) and (4.40)
$v$	Volume fraction

$X$	Ratio of principal stress difference
$x, y, z$	Orthogonal Cartesian coordinate axes

### Greek Symbols

$\alpha, \beta$	Angles defined in Figure 2.3
$\gamma$	Shear strain
$\delta_{ij}$	Kronecker delta
$\epsilon$	Strain
$\epsilon_{kl}$	Strain tensor
$\epsilon_t^r$	Threshold strain of coating
$\theta$	Fibre orientation
$\lambda$	Wavelength of light
$\nu$	Poisson's ratio
$\sigma$	Normal stress
$\tau$	Shear stress
$\phi$	Isoclinic angle

### Subscripts

ap	Approximate, principal strain-difference
c	Composite
cr	Corrected principal strain-difference
ex	Exact principal strain-difference
g	Glass fibres
L	Longitudinal axis of a composite lamina
LT	Properties referred to L-T coordinate axes
m	Matrix

$p$	Major principal strain-direction
$q$	Minor principal strain-direction
$pq$	Properties referred to $p - q$ coordinate axes
$T$	Transverse axis of a composite lamina
$u_c$	Compressive strength
$u_t$	Tensile strength
$x_c$	Average coordinate stress in composite
$x_g$	Average coordinate stress along $x -$ axis in glass
$x_m$	Average coordinate stress along $x -$ axis in matrix
$xy$	Properties referred to $x - y$ coordinate axes
$y_g$	Average coordinate stress along $y -$ axis in glass
$y_m$	Average coordinate stress along $y -$ axis in matrix
$\epsilon$	Principal strain direction
$\theta$	Variables referred to fibre orientation
$\sigma$	Principal stress direction

### Superscripts

$c$	Coating
$p$	Load fraction
$s$	Specimen

## SYNOPSIS

SOME EXPERIMENTAL STRESS ANALYSIS TECHNIQUES  
FOR FIBROUS COMPOSITES

A Thesis Submitted  
In Partial Fulfilment of the Requirements  
for the Degree of  
DOCTOR OF PHILOSOPHY

by

SHIVE KUMAR CHATURVEDI

to the

Department of Mechanical Engineering  
Indian Institute of Technology, Kanpur

September, 1978

Due to increasing importance of glass fibre reinforced plastics in various industries, it is necessary to develop accurate and efficient stress analysis techniques for them. With this in mind, the present investigations have been carried out to improve the brittle coating method and the technique of transmission photoelasticity to a state where they can be easily applied to the problems of stress analysis involving orthotropic materials.

The studies with brittle coating have been performed using an indigenous coating developed in the laboratory which permits an easy variation in the properties required for its application on the polymer matrix surfaces of composite materials. The coating behaviour has been studied on unidirectionally reinforced glass

fibre epoxy composite subjected to uniaxial and biaxial stress fields. It has been established that the cracks represent the directions of principal strains and not the directions of principal stresses and that the threshold strain for the coating remains unaffected by the orthotropy of the specimen material. Details of a data analysis procedure have been worked out so as to readily obtain specimen stresses from crack patterns.

Optically superior photoelastic orthotropic model materials have been developed with glass fibres and polyester resin. A systematic method of assessing the suitability of heterogeneous materials to photoelastic applications has been developed through considerations of laws of optics. The newly developed model materials exhibit better transparency, higher resolution of closely spaced lines, negligible distortion of a directed beam of light and sharper isochromatic fringes compared to the materials reported in the literature.

An assessment of existing theories of photo-orthotropic-elasticity shows that some of the theories are capable of predicting photoelastic response of orthotropic materials quite accurately. However, no theory permits evaluation of the individual strain or stress components or even the difference between their principal values from birefringence measured in a polariscope. The directions

of principal stresses or strains also can not be determined. An exact strain-optic law derived on the basis of theory of photoelasticity for anisotropic crystals also suffers from these limitations.

In order to overcome the above limitations in the application of photoelasticity to the stress analysis of fibrous composites, an approximate strain-optic law has been derived by minimising error between approximate and exact laws. A method has been developed to estimate the error introduced by the approximations. Thus, it has been possible to establish, with a reasonable degree of accuracy, the difference between principal strains at every point in a model. The theoretical predictions regarding the error estimation have been verified through experiments conducted on orthotropic circular disc under diametral compression and on rectangular specimens under uniaxial tension.

With the above developments, the technique of transmission photoelasticity can now be applied to solve problems of the stress analysis of orthotropic elasticity as easily as it is employed for isotropic materials.



## CHAPTER 1

### INTRODUCTION

#### 1.1 INTRODUCTION TO COMPOSITE MATERIALS

Demands of materials imposed by today's advanced technologies have become so diverse and severe that they often can not be met by single component materials acting alone. It is frequently necessary to combine two or more materials into a composite to which each constituent not only contributes its share, but whose combined action transcends the sum of the individual properties and provides new performance unattainable by the constituents acting alone. Many engineering applications impose requirements that are best met and in many instances met only by composite materials. Different types of composite materials are developed employing various techniques best suited for a particular application. The fibre reinforced materials are probably the most important class of composite materials. They are very widely used in structural applications particularly when the weight saving is a premium because they offer high strength to weight and modulus to weight ratios, excellent corrosion resistance, formability and mechanical properties which can be controlled to a significant degree. For an efficient utilisation of

these materials and their adoption to newer applications, it is necessary to develop accurate and efficient stress analysis techniques applicable to such materials.

## 1.2 LITERATURE SURVEY AND SCOPE OF PRESENT WORK

An important characteristic of the fibre reinforced materials is that they have high strength and modulus in the direction of fibres and the properties in other directions are different from those in the fiber direction that is; the properties change with the direction. Macroscopically fibrous composites can be idealised as orthotropic materials, a class of anisotropic materials having three mutually orthogonal axes of material symmetry. Analytical solutions to the stress analysis problems involving anisotropic materials are extremely difficult. The general approach to the theory of anisotropic elasticity has been discussed by Lekhniskii [1]. Analytical solutions to some simplified problems with thin infinite bodies have been obtained by Lekhniskii [1] Savin [2] and others [3, 4]. However, analytical solutions to more realistic problems are not available. An alternative approach to solve such problems appears to be numerical one. Out of the various numerical methods, finite element technique is considered generally a very useful and powerful tool in analysing structural components. Complex geometries and complicated

loadings can be handled with ease. Solutions to classical and special problems are being developed [5, 6] using this technique. However, a greater confidence into the numerical solutions can be placed only when they are well supported by experimental observations. In fact numerical methods and experimental techniques can be employed to supplement each other. They two together can provide more information about the problem being analysed than either method taken alone. An example of this has been provided by Sanford and Beaubien[ 7] who analysed a complex part made of single phase isotropic material.

There are a number of experimental methods available to solve the stress analysis problems involving isotropic materials. Some of the methods can be directly applied to anisotropic materials also whereas others require modifications. Electrical resistance strain gauges are widely used for measuring surface strains. They can be applied to isotropic or anisotropic materials with equal ease. They are efficient and accurate in measuring strains at a point. Recently the techniques in strain gauges have been further developed to measure internal strains. For example, the gauges can be embedded in the composite material to measure residual strains [8]. The strain gauges can be employed very efficiently to measure strains when the critical areas are known, however, their use becomes

very cumbersome and expensive if complete strain distributions over large areas are to be determined.

Moire technique is also based on the measurement of surface displacements and hence can be applied to anisotropic materials. This technique has been employed to obtain strain distributions around holes and other free edges in laminated composites [ 9 - 11 ]. However, this technique requires more sophisticated instrumentations which are not available in many laboratories. Holographic technique has also been extended for stress analysis of anisotropic materials [ 12 ]. But this technique requires even more complicated and expensive set-up so that it may not be adopted as a routine stress analysis method.

The present investigations have been carried out to develop techniques of brittle coating and transmission photoelasticity to a state where they can be easily applied to the problems of stress analysis involving orthotropic materials. Brittle coating technique is a very useful method for locating critical areas in structures and machine components through preliminary stress analysis. The critical areas can then be analysed using one of the more accurate stress analysis methods. The technique of brittle coating for isotropic materials is fairly well developed. Cunningham and Yavorsky [ 13 ] applied brittle coating to wood which is an orthotropic material. However, there are many problems associated with the

application of this technique to orthotropic materials and in the interpretation of experimental observations. Such problems have remained unexplored yet, probably because of the limited use of wood in engineering applications. Now with the development of fibrous composites, a fresh look at the brittle coating technique and associated problems is necessary. The present work gives a lead in this direction.

Photoelastic stress analyses of orthotropic materials are performed either by applying a birefringent coating on structures and machine components or by making models of transparent birefringent materials. Dally and Alfievich [14] applied an isotropic birefringent coating on glass fibre epoxy composite to obtain stress distributions around a hole. They encountered difficulties due to mismatch of Poisson's ratio between the specimen material and the birefringent coating. The situation is further complicated because the Poisson's ratio of the specimen material changes with direction. Pipes and Dalley[15] carried out a theoretical analysis which could be used in the interpretation of birefringent-coating-isochromatic data for laminated-composite-material applications. They, however, pointed out that the birefringent coating method is likely to produce greater inaccuracies near the free edges like holes, cutouts etc. and also in the areas of high strain-gradients.

In recent years several investigators have successfully initiated work on extending the technique of transmission photoelasticity to the stress analysis of fibre reinforced materials. There are two primary requirements for such applications; one, the composite model material should possess appropriate optical properties such as transparency and birefringence, and two, an appropriate theory to translate the photoelastic measurements into desired stresses and strains. It is interesting to note that although first attempt to develop transparent composites for photoelastic analysis seems to have been made by Horridge [16] in 1955, the real photoelastic investigations on fibrous composites started much later with the publication of results of Pih and Knight [17] in 1969. Since then many investigators developed composite model materials and used them in photoelastic investigations. However, no scientific approach was developed either to produce optically superior model materials or to assess their suitability to sophisticated applications. This has been done in the present investigations.

Several theories of photo-orthotropic-elasticity have been proposed in the literature. Some of them have been recently reviewed and assessed by Agarwal and Chaturvedi [18]. Pih and Knight [17] were probably the first to propose a stress-optic law for orthotropic

materials, however, their approach was unrealistic that they proposed a single photoelastic constant for orthotropic materials. It was not pursued any further by other investigators. Sampson [19] developed the concept of Mohr circle of birefringence by simple analogy and introduced the concept of three photo-elastic constants for orthotropic materials which are to be determined experimentally. Once the three constants are known for a material, the birefringent response of the material can be predicted through the stress-optic law formulated by Sampson. He supported his theory by limited experimental results.

Dally and Prabhakaran [20], like Sampson [19], assumed that the photoelastic response of orthotropic materials can be predicted through three independent photoelastic constants. Their experimental results for uniaxial state of stress agreed with their theory and with that of Sampson. Dally and Prabhakaran [20], using fundamental concepts of fibrous composite, developed a method of theoretically predicting the three photoelastic constants from the known photoelastic and elastic constants of the constituents and the volume content of glass fibres. Accuracy of such predictions is greatly influenced by the accuracy with which stresses in the constituents can be evaluated. This becomes a limitation of the approach particularly because it is very difficult to predict transverse stresses accurately. Another limitation of their work had been

that they did not discuss the isoclinics or their interpretation with regard to orthotropic materials. Prabhakaran [ 21] in a later paper did discuss the interpretation of isoclinics in photo-orthotropic-elasticity. His experimental results agreed well with Sampson's theoretical predictions for isoclinics.

Bert [ 22 ] modelled fibrous composites by an orthorhombic crystalline system and applied the theory of photoelasticity of crystals first proposed by Pockels [23] and later modified by Bhagavantam [24] . Bert showed that the concept of a Mohr circle of birefringence as intuitively proposed by Sampson is a direct result of tensorial nature of birefringence. More recently, Knight and Pih [ 25], again using Bhagavantam theory, derived general stress - optic law and then simplified it to a two dimensional case. Their formulation is general and accounts for initial birefringence also. However, their simplified equations are of the same form as those of Sampson and Bert.

Pipes and Rose [ 26 ] proposed the use of strain-optic law in place of stress-optic law. They assumed that the isotropic strain-optic law (with single strain-fringe value) is applicable for low fibre volume fraction birefringent composites. They experimentally verified this assumption for material with low degree of orthotropy. Prabhakaran [ 27] proposed a strain-optic law analogous to



stress-optic laws discussed in the preceding paragraphs. In the same paper, Prabhakaran has proposed a simplified strain-optic law with the single strain-fringe value which is taken as the arithmetic average of the three principal-fringe values. The approaches of Pipes and Rose and of Prabhakaran are really some kind of ad hoc approaches having no fundamental basis of material behaviour. Moreover, no added advantages have been gained by the use of strain-optic laws over the stress-optic laws.

Besides what has been discussed above, photoelastic investigations on composite materials have been carried out in other directions also. For example, the effects of residual birefringence [28 - 30] and the study of stress-waves propagation in fibrous composites [31, 32] have also been reported in the literature.

From the preceding discussion on the theories of photo-orthotropic-elasticity, it is quite clear that the photoelastic response of orthotropic composites can be accurately predicted through three independent photoelastic constants. It is, however, not clear if the existing stress-optic and strain-optic laws are adequate to interpret the photoelastic observations and translate them into the desired stresses or strains. Experiments were conducted on the superior unidirectional and bidirectional materials to assess the suitability of existing theories

of photo-orthotropic-elasticity. The results have been described in Chapter 4. Limitations of the existing stress-optic laws have been pointed out. An exact strain-optic law has been derived using well established theory of photoelasticity of anisotropic crystals. An approximate strain-optic law has been derived in Chapter 5 from the exact strain-optic law. The approximations have been made to ensure minimisation of the error. Finally a method has been developed to estimate the error with a reasonable degree of accuracy. Experiments have been performed to verify the hypothesis of error estimation.

## CHAPTER 2

### BRITTLE COATING STUDIES ON FIBROUS COMPOSITES

#### 2.1 INTRODUCTION

Brittle coating method is a very useful stress analysis technique which can be applied on actual structural components. This avoids the preparation of models and conversion of results from model to prototype. Brittle coatings are widely applied for locating critical areas in structures and machine components through preliminary stress analysis. Its technology and the method of interpretation of results are well understood for the case when it is applied on isotropic materials. However, not much work seems to have been done for its application on orthotropic materials which may present many more problems.

Cunningham and Yavorsky [13] applied the brittle lacquer on wood which is an anisotropic material. They performed tests under uniaxial state of stress and indicated that the coating cracks obtained on wood-specimens form trajectories of principal strains and not principal stresses. A transformation is needed to obtain the stress pattern in the specimen material. They had envisaged a future exploration of associated problems such as the relations between the law of failure of isotropic brittle coating and the strains and stresses in the anisotropic specimen. However,

such problems have remained unexplored yet probably because of the limited use of wood in engineering applications. Now with the development of fibrous composites, a fresh look at the brittle coating technique and associated problems is necessary.

The present investigations were aimed at studying the behaviour of brittle coating on orthotropic materials and also studying the technological and interpretational problems. The coating has been applied to the unidirectionally reinforced glass-fibre epoxy composite and its behaviour has been studied under uniaxial and biaxial stress fields. Differences arising due to the specimens being made of an orthotropic material rather than an isotropic material have been discussed. A data analysis procedure has been worked out so as to readily obtain specimen stresses from crack pattern.

## 2.2 EXPERIMENTAL PROCEDURE

Since commercial brittle coatings are not available in India, it was decided to develop a coating in the laboratory on the lines suggested by Ram Chand [33]. Moreover, the indigenously developed coating permits an easy variation in the properties which is very helpful, almost essential, when the coating has to be applied on different materials such as epoxy or

polyester matrices used in the composites. Following are the basic constituents of a brittle coating:

- (i) Base Material: It is the most important constituent of the coating and significantly affects its ultimate properties. Zinc resinate has been used as the base material. Naturally occurring rosin and zinc oxide have been used for its preparation. The rosin is crystalline and very brittle in nature. It has a specific gravity of about 1.1 and melting point  $84^{\circ}\text{C}$ . Its natural colour varies from pale to dark yellow, which, however, does not affect the colour of the resulting coating.
- (ii) Solvent and Thinner: For brittle coating applications, besides being a good solvent for the base material, the solvent should evaporate also reasonably fast when exposed to atmosphere. Carbon di-sulphide has been used as the solvent and thinner in the present coating. However, it must be mentioned here that carbon di-sulphide is an extremely hazardous solvent. It can easily ignite and its vapour, if inhaled, can cause health hazard. Therefore, extreme precautions should be taken in its use as described in reference [34].

(iii) Plasticiser: The plasticiser is added to control the strain-sensitivity and brittleness of the coating. Unplasticised coating may tend to "craze" (random cracks formed due to residual stresses) whereas, on the other hand, excessive plasticiser will reduce the brittleness so much that cracks once formed will close upon the release of the strain which caused the crack formation. In general, the plasticiser adversely affects adhesion characteristics of the coating. Dibutylphthalate is a common plasticiser. In the initial stages of the present coating development, it was used. However, it was affecting the adhesion characteristics too adversely and hence had to be dispensed with. The present unplasticised coating did not exhibit any tendency to craze.

#### 2.2.1 Coating Preparation

The coating is prepared by first cooking 100 gm rosin with 1.6 gm zinc oxide at a temperature of  $220 \pm 5^{\circ}\text{C}$  for about 30 minutes. Continuous stirring is necessary during cooking to achieve a thorough mixing of constituents. The resulting resinate, a dark brown semi-solid material, is allowed to cool down to room temperature and then dissolved in 100 cc. solvent, that is, carbon disulphide.

The solution is filtered to remove unreacted elements. Additional 100 cc of carbon di-sulphide is added to the filtrate. The resulting dark brown solution is the desired brittle coating ready to be sprayed on to the specimens. It may, however, be pointed out that before finally arriving at the above procedure, several other procedures were tried. Relative proportions of the ~~rosin~~ and zinc-oxide were changed as was curing time and temperature. A plasticiser was also used in the initial stages of development.

### 2.2.2 Specimen Material

Brittle coating studies were performed on commonly used fibrous composites. Unidirectionally reinforced glass-fibre epoxy composite was selected as the specimen material. The specimen material which was also fabricated in the laboratory exhibited the following average elastic properties in a tension test:

Longitudinal modulus,	$E_L$	$= 10005.5 \text{ MN/m}^2$
Transverse modulus	, $E_T$	$= 3835.5 \text{ MN/m}^2$
Shear modulus	, $G_{LT}$	$= 1481.0 \text{ MN/m}^2$
Major Poisson's ratio	, $\nu_{LT}$	$= 0.38$

For studying the behaviour of coating under uniaxial state of stress, rectangular cantilever beam specimens of size 125 x 20 x 3.5 mm shown in Figure 2.1a, were machined.

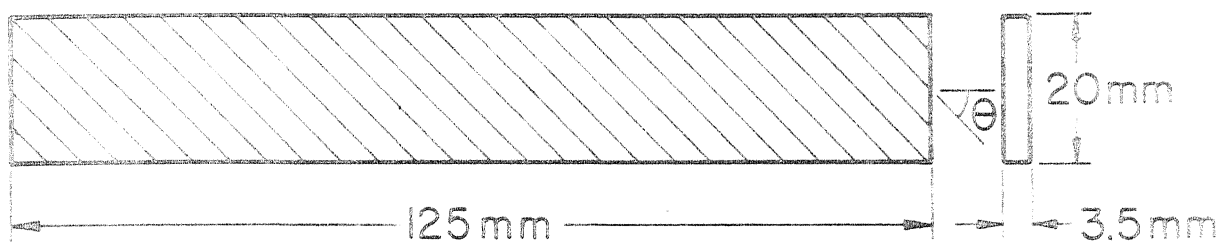
The fibre orientation,  $\theta$ , was kept at 0, 5, 30, 45, 75 and 90 degree in different specimens. The behaviour of coating under biaxial stress-field was studied through circular disc specimen of 100 mm diameter. The disc was loaded in diametral compression as shown in Figure 2.1b. Angle between the loading axis and the fibres was kept at 15, 45, and 60 degree in different tests.

### 2.2.3 Application of Coating to the Specimen

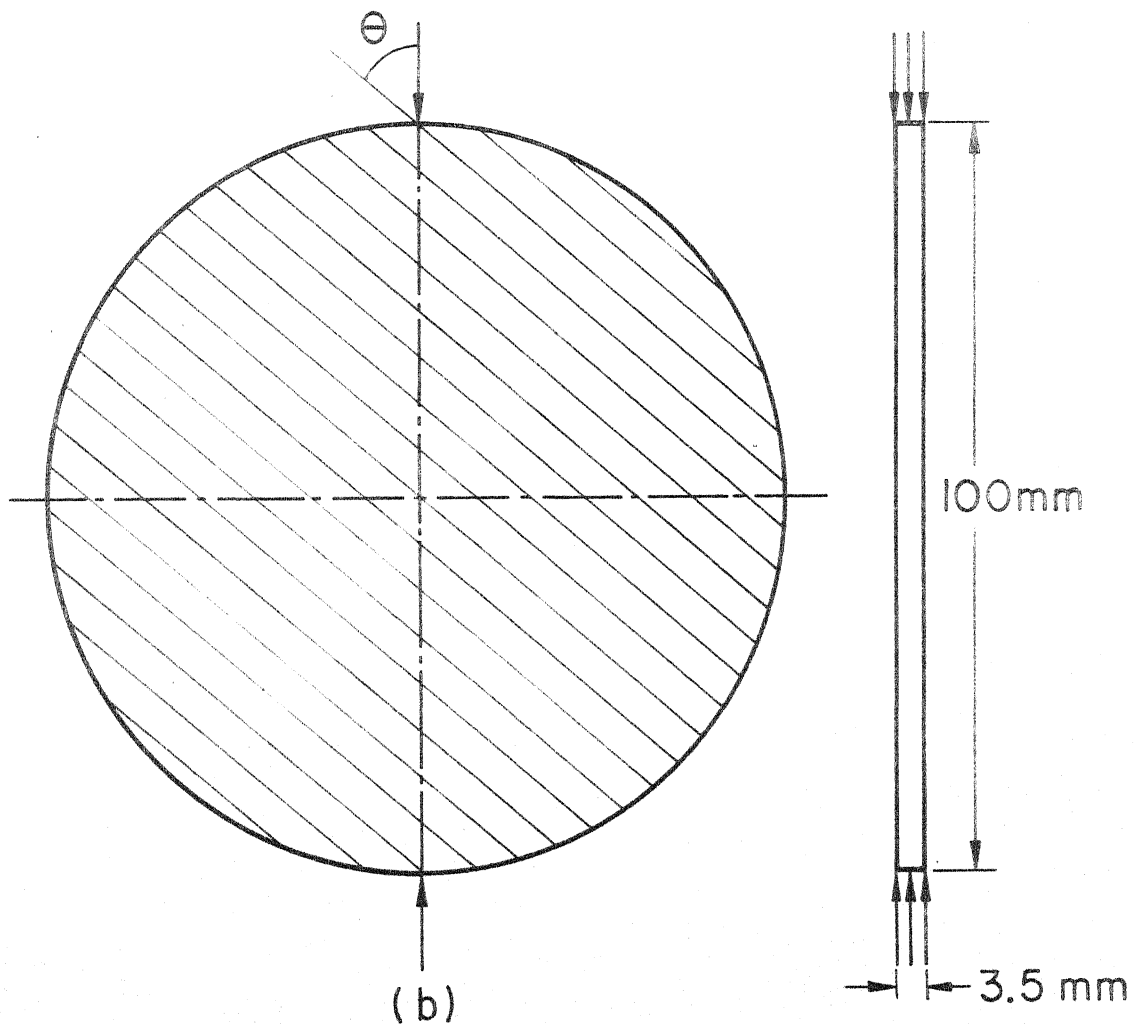
The coating was sprayed on the epoxy composite specimens degreased by acetone and further cleaned by carbon di-sulphide. An air compressor, which maintained a gauge pressure of  $0.14 \text{ MPa} \pm 10 \text{ percent}$ , was used for spraying. In order to obtain a uniform thickness of coating the spray gun was slowly moved along the length of the specimen and the gun was kept at a height of about 10 cm from the specimen surface. The number of passes of the spray were adjusted to obtain a coating thickness of about 0.4 mm.

The coating was cured in a temperature controlled oven at  $120^\circ\text{C}$  for 2 hours and then the coated specimens were allowed to cool in the oven itself so that a slow rate of cooling is maintained. Rapid cooling outside the oven may cause thermal crazing of the coating. The coating thus obtained exhibits satisfactory properties for





(a)



(b)

Figure 2.1 Test specimens (a) Cantilever beam for uniaxial stress (b) Circular disc under diametral compression for biaxial stresses.

carrying out brittle coating stress analysis. Properties in question include adequate sensitivity, good adhesion to the specimen surface and clearly visible cracks. The cracks produced during loading remain open after removing the load. However, if there is a significant rise in the room temperature, the cracks tend to close partially or completely. The tests were conducted under conditions of controlled temperature and humidity at 25 °C and 40 per-cent relative humidity.

#### 2.2.4 Calibration of Coating

Calibration of coating consists of finding out the threshold strain for the coating. The threshold strain is defined as the minimum strain which will produce cracks in the coating. It was obtained by applying the coating to a specimen with 0 - degree fibre orientation. The specimen was loaded as a cantilever beam and a known deflection (4 mm) was given to its free end. Position of the crack nearest to the free end was noted. The strain at this point gives the threshold strain for the coating. Magnitude of the strain was obtained experimentally by strain gauge measurements. The electrical resistance strain gauges were mounted at the desired position on the same specimen after removing the coating. The same known deflection was given to the free end and the strain was measured by a strain indicator. The magnitude of the

strain was also checked by theoretical calculations from the knowledge of the elastic constants and the position of the crack. The complete process was repeated five times with different specimens. An average value of threshold strain,  $\epsilon_t^*$ , was obtained to be  $675 \mu$  strain.

## 2.3 RESULTS AND DISCUSSION

### 2.3.1 Coating Behaviour Under Uniaxial Stress

The brittle coating was applied to the cantilever beam specimens with fibre orientations of 5, 30, 45, 75 and 90 degree. A uniaxial state of stress was produced in the specimens by giving a known deflection to the free ends. Photographs of the resulting fringe patterns have been shown in Figure 2.2. It may be noted that cracks are not perpendicular to the direction of maximum principal stress,  $\sigma_x$ , in the specimens except that for a fibre orientation of 90 degree. Further, the angle,  $\alpha$ , between the direction of cracks and the direction perpendicular to maximum specimen stress (schematically shown in Figure 2.3) changes with fibre orientation. Consistency of these observations can be explained by considering directions of principal stresses and strains in the specimens and the coating.

In coating, the directions of principal stresses and strains coincide because the coating is isotropic. Therefore, the cracks represent this common direction. However,

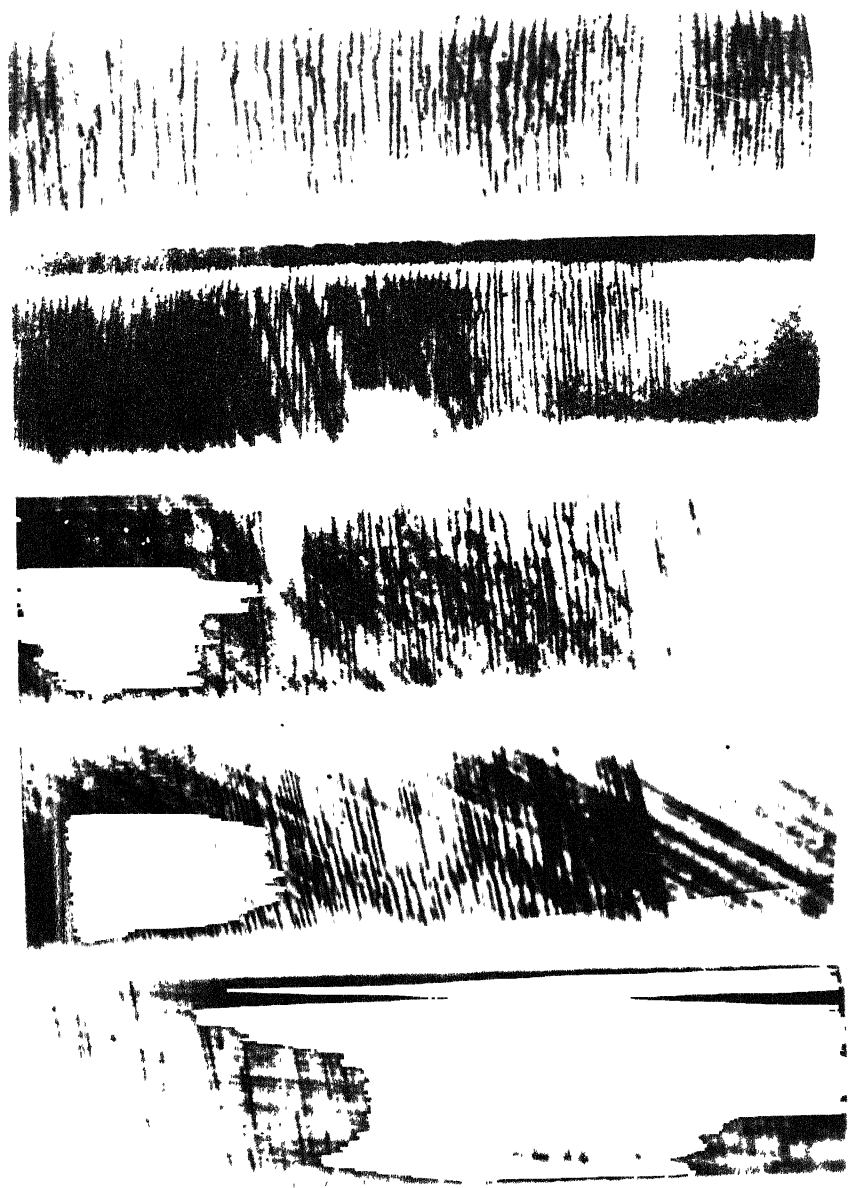


Figure 2.2 Brittle coating crack patterns on the beam specimens under uniaxial state of stress. Left to right: Fibre orientations 5, 30, 45, 75 and 90 degree.

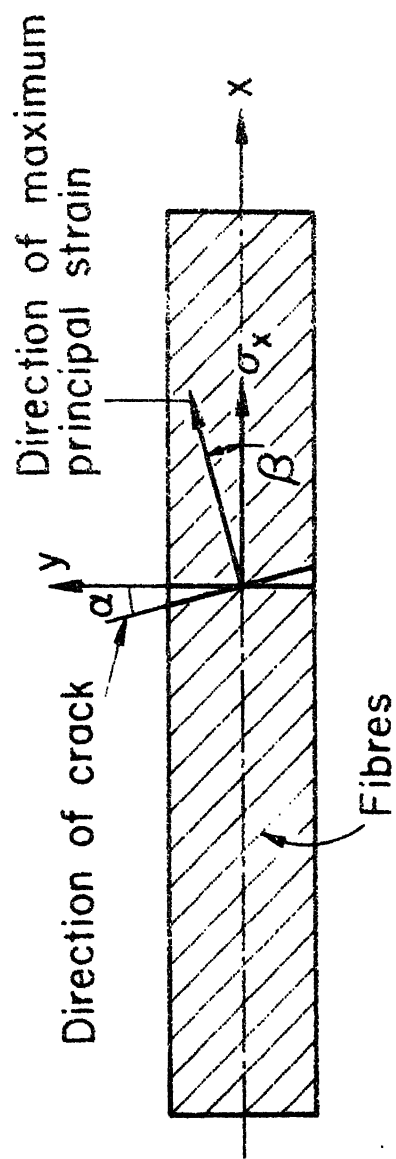


Figure 2.3 Schematic diagram showing directions of coating cracks, maximum principal stress and maximum principal strain on the beam specimen

specimens are orthotropic and the directions of principal stresses and strains are, in general, different. The direction of major principal stress is the x - direction (Figure 2.3). The directions of principal strains were experimentally obtained by strain gauge measurements. The angle,  $\beta$ , between the directions of principal stress and principal strain in the specimen has been calculated theoretically also as follows. A uniaxial stress,  $\sigma_x$ , produces the following normal and shear strains in the specimen:

$$\begin{aligned}\epsilon_x &= \frac{\sigma_x}{E_x} \\ \epsilon_y &= -\nu_{xy} \frac{\sigma_x}{E_x} \\ \gamma_{xy} &= -m_x \frac{\sigma_x}{E_L}\end{aligned}\tag{2.1}$$

where  $E_x$ ,  $\nu_{xy}$  and  $m_x$  are the elastic constants in the x - y directions and are related to  $E_L$ ,  $E_T$ ,  $G_{LT}$  and  $\nu_{LT}$  through equations given in Appendix A. It may be noted that the shear coupling coefficient,  $m_x$ , is, in general, not zero. Due to the presence of,  $m_x$ , directions of principal strains differ from the directions of principal stresses in the specimen. The angle,  $\beta$ , for the stresses and strains given by Eq. (2.1) can be shown to be

$$\beta = \frac{1}{2} \tan^{-1} \left[ \frac{m_x E_x}{E_L (1 + \nu_{xy})} \right]\tag{2.2}$$

The angles,  $\beta$ , calculated from Eq. (2.2) for different fibre orientation, and experimentally obtained from strain gauge measurements, have been compared, in Table 2.1, with the angles,  $\alpha$ , measured with the help of an optical projector (Baush and Lomb) from the brittle coating crack patterns on the corresponding specimens (The crack patterns are shown in Figure 2.2 and the angles,  $\alpha$ , and  $\beta$ , defined in Figure 2.3). It can be noted from Table 2.1 that the angles,  $\alpha$ , and  $\beta$ , have quite comparable values. It may, therefore, be concluded that the brittle coating cracks indicate the directions of principal strains in the specimen and not the directions of principal stresses. This conclusion is of particular significance for the orthotropic materials where the two directions are different. In case of isotropic specimen materials, this conclusion is redundant.

It is interesting to examine the effect of orthotropy of specimen material through a partially reinforced specimen. Figure 2.4 shows crack pattern on a specimen which contains inclined unidirectional fibres in part of its length while the rest was purely resin. The reinforced and unreinforced regions have been shown separated by a dotted line and the direction of fibres is indicated by a double arrow. The cantilever specimen was deflected by an end load. It is seen from Figure 2.4 that the cracks

Table 2.1 : Results for Coating Behaviour under Uniaxial Stress

Fibre orientation $\theta$ , degree	$\beta$ , degree		Coating crack angle, $\alpha$ , degree
	Strain gauge measurements	Theoretical calculations	
5	6.85	6.80	7.75
30	11.00	12.20	10.75
45	7.25	5.75	6.00
75	3.20	1.00	3.00
90	90.00	90.00	90.00



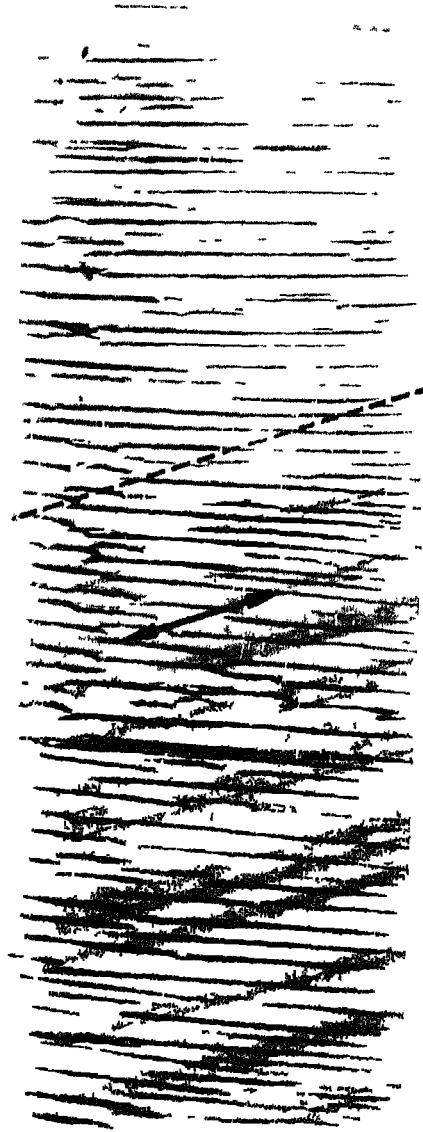


Figure 2.4 Brittle coating crack pattern on a partially reinforced beam specimen. Dotted line represents boundary of the reinforced region and the double arrow indicates fibre direction

in the unreinforced region are perpendicular to maximum principal stress whereas in the reinforced region it is not so although uniaxial state of stress exists everywhere in the specimen.

In each of the tests conducted on the specimens with different fibre orientation, the minimum strain which causes the coating cracks has also been obtained from strain gauge measurements as well as from theoretical calculations. The values, thus obtained are within 4 percent of the threshold strain obtained earlier during coating calibration. This indicates that the threshold strain or the coating sensitivity is not significantly influenced by the degree of mismatch between the Poisson's ratios of specimen material and the coating. This is also important because, in an orthotropic material, Poisson's ratio changes with the direction.

### 2.3.2 Coating Behaviour Under Biaxial Stresses

The circular disc specimens, coated with brittle coating, were compressed by two equal and diametrically opposite forces as shown schematically in Figure 2.1b. Diametral compression produces a biaxial state of stress at an interior point in the disc. Photographs of resulting crack patterns for fibre orientations of 15, 45, and 60 degree are shown in Figure 2.5. The crack pattern is

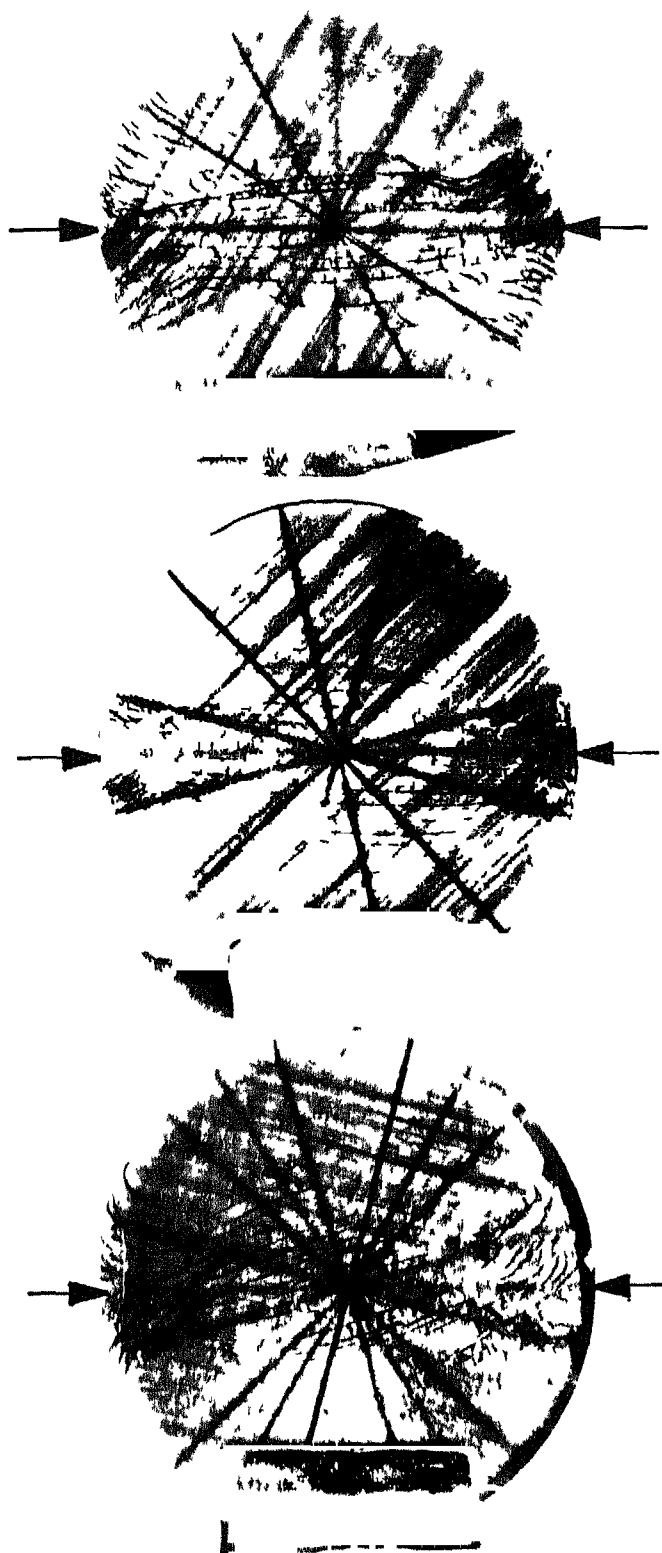


Figure 2 5 Brittle coating crack patterns on the circular disc specimens under diametral compression  
Left to right: Fibre orientations 15, 45 and 60 degree

clear throughout the disc except in the close vicinity of the points of application of load. Due to very high compressive stresses in this region, the coating peels-off the surface of the specimen.

For an interpretation of the crack patterns, it is required that the directions of principal stresses and strains be known at every point in the disc. Okubo [4] reported an analytical solution of the problem of orthotropic circular disc under diametral compression. While trying to compute the stresses in the present orthotropic disc, some obvious errors were noticed in his formulation, the most important being an inconsistency in coordinate transformation. Therefore, even after considerable efforts, it was not possible to use his results with the present findings. One may probably develop a consistent solution to this problem using Okubo's approach. However, this was not done by the author for obvious reasons. Photoelastic analysis of orthotropic disc under diametral compression has been attempted [21] . Isoclinic and isochromatic fringe patterns have been obtained but it has not been so far possible to establish the directions of principal stresses or strains. It was, therefore, decided to establish the directions of principal strains at three different points in the disc using strain gauge measurements. The three points considered are shown in Figure 2.6. They

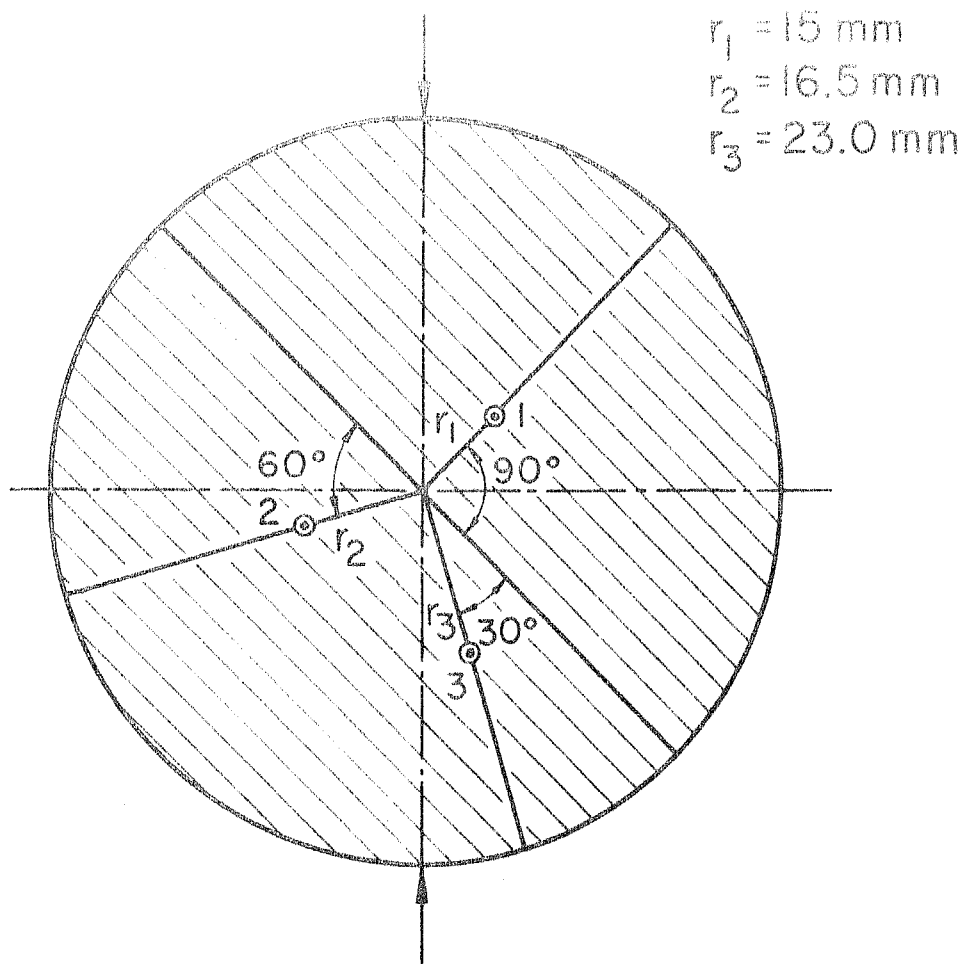


Figure 2.6 Schematic diagram showing the positions of strain gauge rosettes mounted on the circular disc specimen

were kept the same for all orientations of the disc. The strain gauge measurements provide not only the directions of principal strains but also their magnitude. Therefore, the normal and shear stresses along the directions of principal strains can be found using the following stress-strain relations [35] .

$$\begin{aligned}
 \epsilon_p &= \frac{\sigma_p}{E_p} - \nu_{qp} \frac{\sigma_q}{E_q} - m_p \frac{\tau_{pq}}{E_L} \\
 \epsilon_q &= -\nu_{pq} \frac{\sigma_p}{E_p} + \frac{\sigma_q}{E_q} - m_q \frac{\tau_{pq}}{E_L} \\
 \gamma_{pq} &= 0 = \frac{\tau_{pq}}{G_{pq}} - m_p \frac{\sigma_p}{E_L} - m_q \frac{\sigma_q}{E_L}
 \end{aligned} \tag{2.3}$$

Where the directions  $p$  and  $q$  refer to the directions of principal strains so that  $\gamma_{pq}$  vanishes. The elastic properties  $E_p$ ,  $E_q$ ,  $G_{pq}$ ,  $\nu_{pq}$ ,  $\nu_{qp}$ ,  $m_p$  and  $m_q$  of the specimen in the  $p - q$  directions can be obtained using transformation relations given in Appendix A. Eq. (2.3) can be solved for  $\sigma_p$ ,  $\sigma_q$  and  $\tau_{pq}$  from which magnitude and directions of principal stresses can be easily established.

The results of above measurements and analysis have been presented in Table 2.2 by giving angles which the maximum principal strain and maximum principal stress at a point make with the load axis. Also given in Table 2.2 are the angles which the tangents to the cracks at the corresponding points make with the direction

Table 2.2 : Results for Coating Behaviour Under Biaxial Stresses

Fibre orientation angle, $\theta$ , degree	Point under consideration	$\alpha_{\sigma}^*$ degree	$\alpha_{\epsilon}^{**}$ degree	$\alpha_{\text{crack}}^{***}$ degree
15	1	85.7	77.6	76.5
	2	88.8	85.7	85.0
	3	76.7	66.2	66.0
45	1	81.6	89.0	89.5
	2	78.0	88.4	88.5
	3	70.7	80.5	83.5
60	1	88.5	82.0	81.5
	2	86.4	83.6	83.0
	3	77.5	82.5	86.0

\*  $\alpha_{\sigma}$  = Angle between maximum principal stress and the load axis.

\*\*  $\alpha_{\epsilon}$  = Angle between maximum principal strain and the load axis.

\*\*\*  $\alpha_{\text{crack}}$  = Angle between tangent to the crack and direction perpendicular to the load axis.

perpendicular to the loading axis. It can be clearly seen from these results that the cracks represent the directions of principal strains rather than the directions of principal stresses. This observation is very significant for future application of brittle coating to the problems of stress analysis involving orthotropic materials.

## 2.4 ANALYSIS TECHNIQUE

It has been established in the preceding section that the coating cracks, produced under both uniaxial and biaxial states of stresses, represent the common directions of principal strains and principal stresses in the isotropic coating and represent the coincident principal strain directions in the orthotropic material underneath. Analysis procedure, based on these facts and aimed at evaluating specimen stresses in terms of coating stresses, has been developed in the following paragraphs.

Let  $p$ ,  $q$  be directions, normal and tangential to crack at a point so that they represent directions of principal strains in coating as well as in the specimen and also directions of principal stresses in coating. The coating strains are related to coating stresses by isotropic stress-strain relations as follows:



$$\epsilon_p^c = \frac{1}{E^c} \sigma_p^c - \nu^c \sigma_q^c \quad (2.4)$$

$$\epsilon_q^c = \frac{1}{E^c} \sigma_q^c - \nu^c \sigma_p^c$$

Specimen stresses and strains are governed by orthotropic stress-strain relations -

$$\begin{aligned} \epsilon_p^s &= \frac{\sigma_p^s}{E_p^s} - \nu_{qp}^s \frac{\sigma_q^s}{E_q^s} - \frac{m_p^s \tau_{pq}^s}{E_L^s} \\ \epsilon_q^s &= -\nu_{pq}^s \frac{\sigma_p^s}{E_p^s} + \frac{\sigma_q^s}{E_q^s} - m_q^s \frac{\tau_{pq}^s}{E_L^s} \\ \gamma_{pq}^s &= 0 = -m_p^s \frac{\sigma_p^s}{E_L^s} - m_q^s \frac{\sigma_q^s}{E_L^s} + \frac{\tau_{pq}^s}{G_{pq}^s} \end{aligned} \quad (2.5)$$

Superscripts  $c$  and  $s$  denote coating and specimen respectively. Since coating is usually very thin relative to the thickness of specimen, it is valid to assume that surface strains occurring on the specimen are transmitted to the coating without magnification or attenuation so that

$$\begin{aligned} \epsilon_p^c &= \epsilon_p^s \\ \epsilon_q^c &= \epsilon_q^s \end{aligned} \quad (2.6)$$

It is also reasonable to assume that a state of plane stress exists in both the coating and the boundary layer of the specimen.

Substitution of Eqs. (2.4) and (2.5) into Eq. (2.6) and solving for specimen stresses yields:

$$\begin{aligned}\sigma_p^s &= \frac{(A - B v^c) \sigma_p^c + (B - A v^c) \sigma_q^c}{AC - B^2} \\ \sigma_q^s &= \frac{(C - B v^c) \sigma_q^c + (B - C v^c) \sigma_p^c}{AC - B^2} \\ \tau_{pq}^s &= \frac{G_{pq}^s}{E_L^s} (m_p^s \sigma_p^s + m_q^s \sigma_q^s)\end{aligned}\quad (2.7)$$

where

$$\begin{aligned}A &= E_c \left[ \frac{1}{E_q^s} - \frac{(m_q^s)^2 G_{pq}^s}{(E_L^s)^2} \right] \\ B &= E_c \left[ \frac{v_{pq}^s}{E_p^s} + \frac{m_p^s m_q^s G_{pq}^s}{(E_L^s)^2} \right] \\ C &= E_c \left[ \frac{1}{E_p^s} - \frac{(m_p^s)^2 G_{pq}^s}{(E_L^s)^2} \right]\end{aligned}\quad (2.8)$$

It will be possible to calculate the specimen stresses from above equations provided the coating stresses  $\sigma_p^c$  and  $\sigma_q^c$  are known at a point for a given load. The coating stresses can be accurately estimated at a point only when the crack appears there. It is assumed that at the minimum load at which a crack appears, the coating stresses  $\sigma_p^c$  and  $\sigma_q^c$  at the point of appearance of crack, are

related to the ultimate strengths of the coating through a failure law. For example, when the state of stress in the specimen is unidirectional, a crack appears when the stress normal to the crack exceeds the ultimate tensile strength of the coating. Under the state of biaxial stresses, coating stresses can be estimated for any given load only after the cracks at the point under consideration have been observed in the two perpendicular directions. The estimation of coating stresses will require incorporation of a suitable failure theory and the knowledge of ultimate strengths of the coating. Some of the failure theories have been discussed in Appendix B. Also given in the Appendix B is the method of evaluating coating ultimate strength. The method of evaluating  $\sigma_p^c$  and  $\sigma_q^c$  under biaxial state of stress can be better illustrated through the following example in which Mohr theory as discussed in Appendix B has been employed to predict failure of the coating.

Let  $\sigma_p^c$  be the tensile stress at the minimum load  $P$  at which a crack first appeared at a point. To obtain information about the  $\sigma_q^c$  the following two cases should be considered:

Case 1 (  $\sigma_q^c > 0$  ): When  $\sigma_q^c$  is tensile, crack in the direction perpendicular to  $\sigma_q^c$  will appear for an

increased load  $P/\alpha^p$  ( $\alpha^p < 1$ ). According to Mohr theory

$$\sigma_p^c = \sigma_{ut}^c \quad \text{at load } P$$

$$\sigma_q^c = \sigma_{ut}^c \quad \text{at load } P/\alpha^p$$

Therefore

$$\sigma_p^c = \sigma_{ut}^c \quad \text{at load } P \quad (2.8)$$

$$\sigma_q^c = \alpha^p \sigma_{ut}^c$$

The specimen stresses at load  $P$  can now be obtained through Eq. (2.7) by substituting the above values of coating stresses.

Case 2:  $\sigma_q^c < 0$  : When  $\sigma_q^c$  is compressive, the

cracks in the perpendicular direction will not appear by increasing the load beyond  $P$ . In this case the magnitude of  $\sigma_q^c$  is obtained by the technique known as relaxation technique [36, 37]. In the relaxation technique, an uncoated specimen is subjected to a known load. The coating is applied to the specimen under load. Thus during unloading of the specimen coating stress  $\sigma_q^c$  will be tensile and  $\sigma_p^c$  will be compressive and the magnitude of stresses will be proportional to the amount of unloading. Under these conditions, the cracks will appear in the direction perpendicular to  $\sigma_q^c$  when the load has been reduced by  $\gamma^p P$ . An estimation of stresses can be made as follows.

Let the coating stresses at load  $P$  during observations of first cracks be:

$$\begin{aligned}\sigma_p^c &= \sigma_o \\ \sigma_q^c &= -\beta^p \sigma_o\end{aligned}\quad (2.9)$$

Therefore the coating stresses in the relaxation procedure when the load has been reduced by  $\gamma^p P$  will be

$$\begin{aligned}\sigma_p^c &= -\gamma^p \sigma_o \\ \sigma_q^c &= \beta^p \gamma^p \sigma_o\end{aligned}\quad (2.10)$$

where  $\beta^p$  and  $\gamma^p$  are both positive. The stress conditions indicated by Eqs. (2.9) and (2.10) will satisfy the failure conditions (B.2) of the Mohr theory so that

$$\begin{aligned}\frac{\beta^p \gamma^p \sigma_o}{\sigma_{ut}^c} + \frac{\gamma^p \sigma_o}{K \sigma_{ut}^c} &= 1 \\ \frac{\sigma_o}{\sigma_{ut}^c} + \frac{\beta^p \sigma_o}{K \sigma_{ut}^c} &= 1\end{aligned}\quad (2.11)$$

These two equations can be solved for  $\beta^p$  and  $\sigma_o$  as

$$\begin{aligned}\beta^p &= \frac{K - \gamma^p}{K \gamma^p - 1} \\ \text{and} \quad \sigma_o &= \frac{\sigma_{ut}^c}{r}\end{aligned}\quad (2.12)$$

$$\text{where } \gamma = 1 + \frac{1}{K} \frac{K - \gamma^p}{K \gamma^p - 1}$$

Thus the coating stresses at load  $P$  are:

$$\sigma_p^c = \frac{\sigma_{ut}^c}{r}$$

$$\sigma_q^c = -\frac{\beta^p}{r} \sigma_{ut}^c$$

The specimen stresses can now be obtained from Eq. (2.7).

## CHAPTER 3

### DEVELOPMENT AND CHARACTERISATION OF OPTICALLY SUPERIOR PHOTOELASTIC ORTHOTROPIC MODEL MATERIALS

#### 3.1 INTRODUCTION

The first requirement of applying the transmission photoelastic technique to the stress analysis of orthotropic materials is to have a suitable model material. A photoelastic model material should be transparent, optically homogeneous and birefringent. Glass, epoxies and polyester, which are constituents of many common orthotropic composites, are all photoelastic materials although they differ from one another in their optical properties. Therefore, glass fibre reinforced epoxy or polyester composites are natural choice for photoelastic orthotropic model materials.

First attempt to prepare photoelastic composite material seems to have been made by Horridge [16] who used a resin with refractive index close to that of glass fibres. Pih and Knight [17] produced orthotropic model materials with an epoxy resin and E - glass fibres by employing wet filament winding under vacuum. Sampson [19] used a dry filament binding of HTS glass roving followed by immersion, under vacuum, in an epoxy resin bath. Dally and Prabhakaran [20] produced large sheets of E- glass fibre/ polyester composites with unidirectional and bidirectional

reinforcement. The matrix material was blended with 30 percent styrene monomer to improve its refractive index to match it with that of fibres. The model materials used by different investigators may be characterised as 'sufficiently transparent'. They have been used to obtain isoclinic and isochromatic fringes. However, the fringes are not sharp enough to be used for accurate stress analysis purposes. Some of them have not been found adequate in sophisticated applications such as dynamic photoelasticity [31]. An improvement in the optical properties of model materials is definitely needed. This has been achieved in the present investigations first by understanding the effects of inhomogeneity through the laws of optics and then by developing scientific methods of assessing suitability of model materials to the photoelastic applications.

### 3.2 OPTICAL CONSIDERATIONS FOR A MODEL MATERIAL

A photoelastic model material should be transparent, optically homogeneous and birefringent. Glass, epoxies and polyesters are all photoelastic model materials. However, when the glass fibres are embedded in an epoxy or polyester, the resulting material is not as transparent as its constituents. Decrease in transparency occurs due to scattering of light at the fibre matrix interfaces. Transparency is very significantly affected also by entrapped air in the



composite either in the form of minute bubbles in the matrix or as a thin film at the fibre-matrix interface. Thus, transparency of photoelastic composites can be improved by minimising both the entrapped air and the scattering of light.

Optical inhomogeneity, introduced due to the presence of glass fibres in the matrix material, produces another effect which is more detrimental than the loss of transparency for photoelastic applications. Refraction at the interface of such inhomogeneities causes the path of light to deviate from its original straight line path. Moreover, in glass fibre reinforced composites the interfaces are not straight so that non uniform deviation of light occurs from different points at the interface. The effect of refraction may be illustrated by considering the path of light, according to the laws of geometrical optics, through homogeneous and inhomogeneous materials as follows.

Consider that a parallel beam of light is incident on a plane surface of a solid transparent medium (homogeneous or heterogeneous) and that the surface, out of which the light emerges, is also plane and parallel to the surface of the beam incidence. In case of a homogeneous medium (Figure 3.1 a) the emergent beam of light will also be a parallel beam travelling in the direction parallel to the incident beam. The same is true of a medium which consists

of two different materials having different refractive indices out with the interface plane and parallel to the surfaces of light incidence and emergence (Figure 3.1 b). In glass fibre reinforced materials, the glass phase is uniformly dispersed in the form of thin circular cylinders. The cross section of a composite containing a single fibre may be represented as shown in Figure 3.1 c. The parallel beam of light is shown to make a normal incidence on the material surface. It will continue to travel in the direction of incident beam until it meets the fibre-matrix interface. At the interface, due to change in refractive index, the incident ray deviates. The amount of deviation of a particular light ray will be determined by the orientation of interface and the degree of mismatch of refractive indices of the two media. Thus the parallel rays get deflected by unequal angles from different points of fibre-matrix interface resulting into diffusion of light beam. Consequently, a finite-width incident light beam will appear attenuated. The following simple experiment was performed to demonstrate the above effect.

A model was prepared by embedding a parallel row of circular rods in a plate of an epoxy resin. The influence of placing this model in the path of a directed light beam has been examined. For this purpose, light coming out of a slit source is passed through a set of two lenses

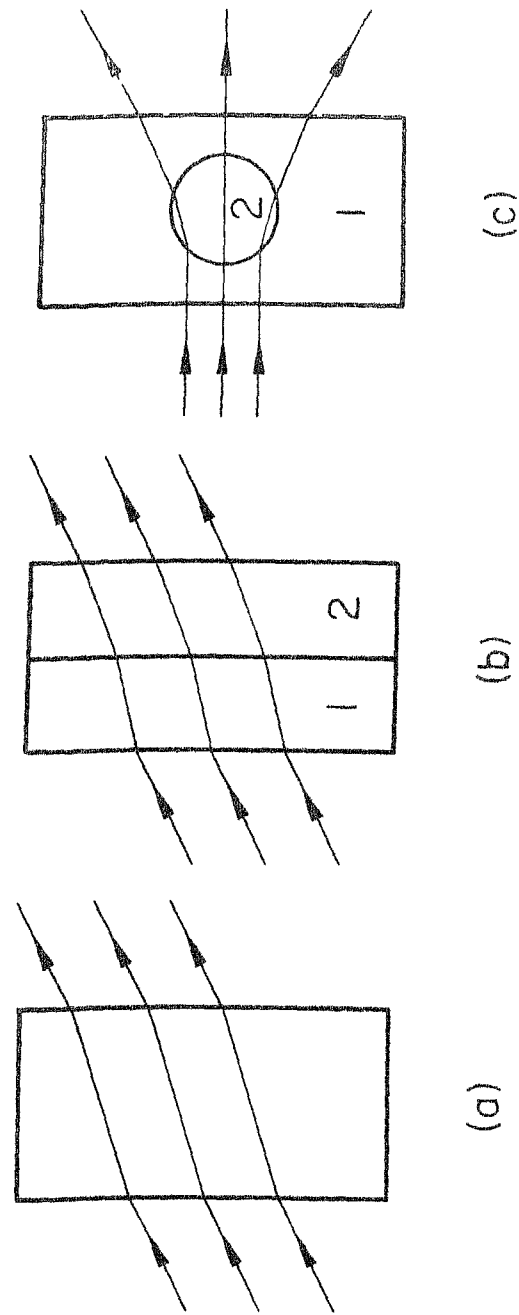
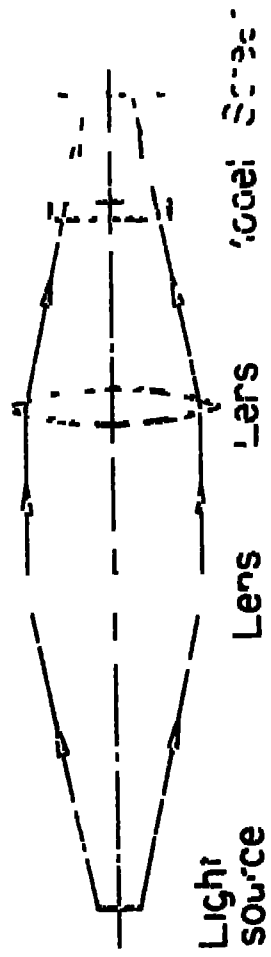


Figure 3.1 Schematic representation of path of light through  
 (a) Homogeneous solid (b) Two solid mediums with  
 a straight interface and (c) Solid medium with  
 another solid inclusion having a curved interface

so that the emerging beam is convergent one. A screen is placed at the focal plane of the second lens so that a sharp image of the slit is formed on the screen. An arrangement of the optical bench is schematically shown in Figure 3.2. When the model is placed between the second lens and the screen, a distortion in the image of the slit occurs. The direction of distortion changes with the orientation of glass rods with respect to the slit. The images of slit have been shown in Figure 3.3 a to 3.3 c for 0, 45 and 90 degree orientations and compared with the image without model (Figure 3.3 d). It may be observed that the distortions in the image are always perpendicular to the axis of the glass rods. When the model is replaced by a plate of the epoxy resin without glass rods, no distortion of the image was observed. This simple experiment demonstrates that a glass fibre reinforced material may cause smearing of directed beam of light as schematically illustrated in Figure 3.1 c.

The affects of placing a glass fibre reinforced composite model in the path of light can now be summarised as follows:

- 1) A parallel beam of light appears smeared in the direction perpendicular to the fibres.



**Figure 3 2      Arrangement of the elements in CP as lens**

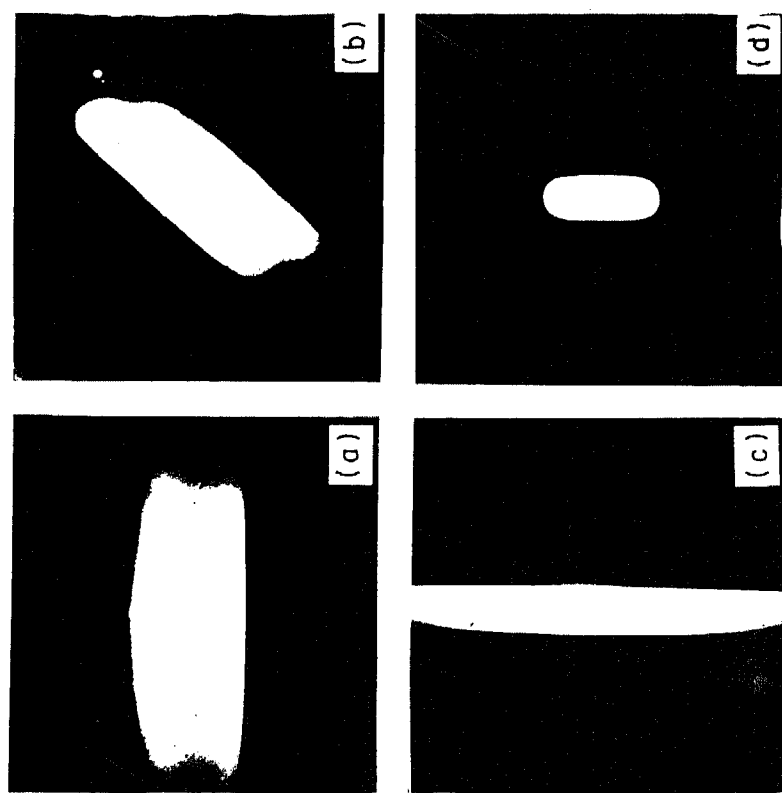


Figure 3.3 Image of slit through a glass rods reinforced epoxy model. Angle of glass rods with the slit (a)  $0^\circ$ , (b)  $45^\circ$  and (c)  $90^\circ$ , and (d) image through unreinforced epoxy model

- ii) Sharp boundaries of an object, when viewed through the model, appear smeared, again, in the direction perpendicular to the fibres. As a consequence very closely spaced straight parallel lines may not appear distinct.
- iii) White light passing through the model gets split in its colours and exhibits a double spectrum symmetrical about the centre line. This is caused because the refractive index depends upon the wavelength of colour of light. Thus, the rays of different colours deviate by unequal angles from the same point of the interface.

The above effects are undesirable for photo-elastic applications. The first two cause a reduction in the sharpness of isoclinic and isochromatic fringes. The third one will interfere in the analysis if white light is used. It is, therefore, quite clear that the effect of mismatch of refractive indices is not only to reduce the transparency but to produce above undesirable effects also. It is, therefore, suggested that the matching of refractive indices be judged by the absence of above effects and not just by visual inspection for transparency. The first two effects have been utilised in the present investigations to demonstrate optical superiority of the model materials. The third effect has been found to be very convenient for quick visual inspection of the material.

### 3.3 FABRICATION OF MATERIAL

The two most important conditions for obtaining optically superior composite model materials are:

- i. the refractive indices of the fibres and the matrix material should be matched as closely as possible and
- ii. the entrapped air in the composite should be minimised.

The model materials developed in the present study are made of E - glass fibres (a product of Fibreglass Pilkington Ltd., India) and polyester resin. The polyester resin of a low viscosity and clear casting grade (a product of Glafpster Industries, Surat, India) has been used with 0.4 per cent cobalt octate as accelerator and 1.0 percent methyl ethyl ketone peroxide (MEKP) as a catalyst. The cured resin exhibits a refractive index of 1.5532 in the white light. This refractive index can be increased by adding divinyl benzene and decreased by adding dibutylphthalate to the resin. The refractive index of glass fibres has been quoted to be  $1.549 \pm 0.003$  by the manufacturer. However, the value has not been found to be very reliable one. Moreover, the refractive index may get affected by the coupling agents and coatings applied to the surface of the fibres. Consequently, refractive index of glass



fibres in a roving is different from that of glass cloth. After trying different percentages of above additives it was found that an addition of 1.9 per cent dibutylphthalate by weight of polyester resin accurately matches its refractive index with that of the glass fibres from roving which were used for unidirectional composites. Additions of 5.0 per cent dibutylphthalate and 2.0 per cent divinyl benzene are needed to match the refractive index of resin with that of the glass cloth which was used for bidirectional composite. It may be pointed out here that the refractive index of the liquid resin is different from that of the cured resin. Hence, matching of the refractive indices has to be achieved when the resin is completely cured.

The composite plates were cast in a mould made of two plexiglass plates separated by tough rubber spacers of uniform thickness. The glass fibres were wound on a stiff, plane, rectangular frame of G.I. wire. The two ends of the fibre bundles were tied to the frame while maintaining tension in the fibres. The frame along with the fibres, gets embedded in the resin and is irretrievable. The test specimens have to be prepared from central portion of the cured plates away from the embedded frame. The resin and other chemicals were thoroughly mixed and poured into the mould after introducing the frame in it through the side opening. There are two primary sources

of air entrapped in the material prepared by this method. When the resin and other chemicals are mixed and poured into the mould, entrapment of some air is unavoidable. The air entrapped during mixing is removed by placing the mixture in a vacuum chamber for sufficient time prior to its pouring. After pouring, the mould is again placed in the vacuum chamber. Photograph in Figure 3.4 shows a mould in the vacuum chamber. This removes air entrapped during pouring and also due to improper impregnation of fibres which is the second major source of entrapped air. The improper impregnation occurs because the resin is sometimes unable to penetrate through the fibre bundles and wet all the fibres. To improve impregnation, a low viscosity resin was selected for the studies. Secondly, the fibre bundles were broken into smaller groups while winding them manually on the wire frame. This enhances resin penetration. Breaking of few fibres due to their handling in this manner may slightly reduce the ultimate strength of the composite but it does not affect the photoelastic investigations appreciably. The problem of incomplete wetting is more serious in glass cloth and twisted fibres.

For making bidirectionally reinforced composite material, glass cloth was cut into pieces of proper size and were placed in a mould one by one. For better impregnation, a small quantity of resin was poured on each layer

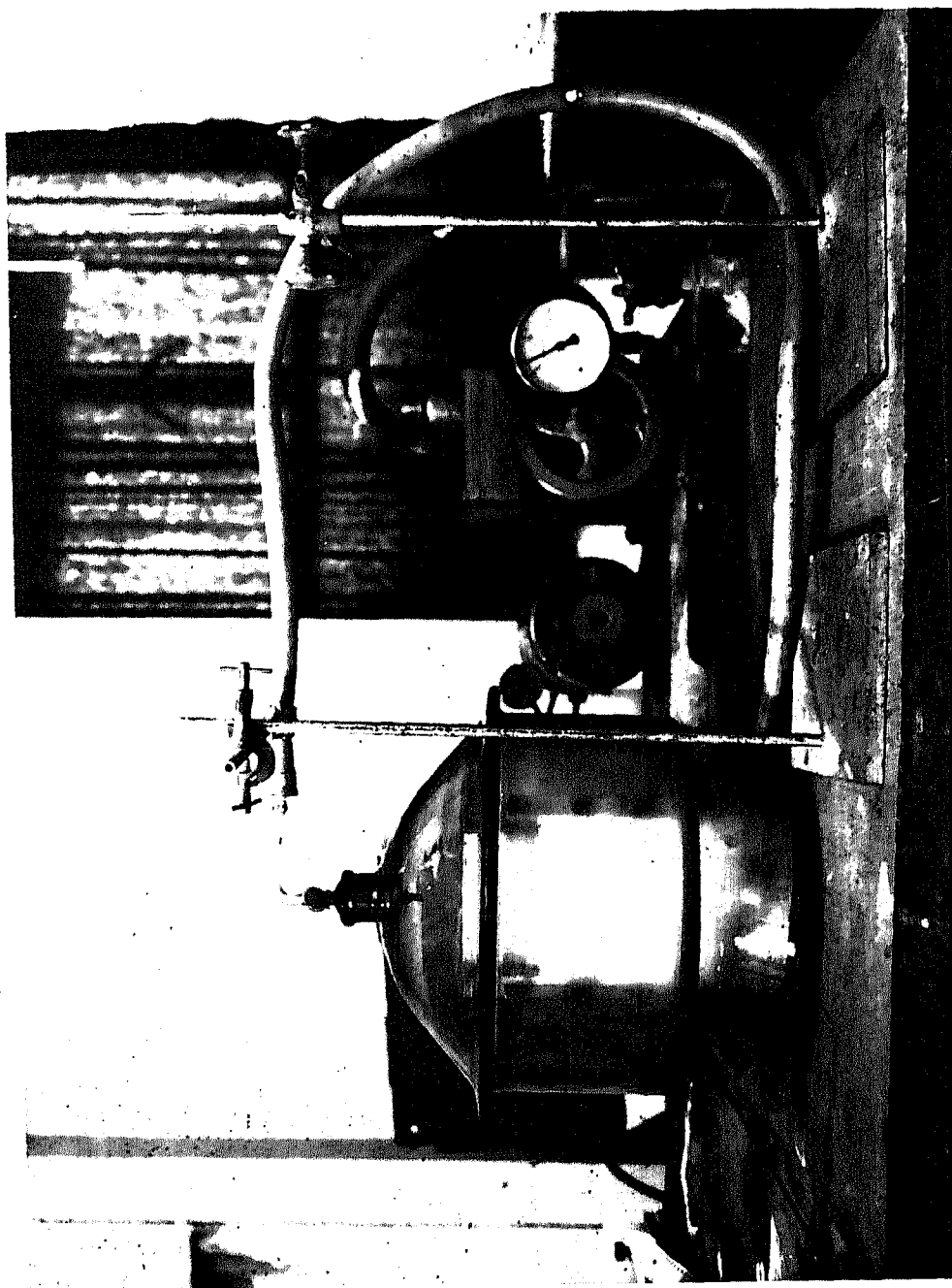


Figure 3.4 A mould in the vacuum chamber to remove entrapped air.

LIBRARY  
CENTRAL LIBRARY  
Acc. No. A 58468

and brushed. Eight layers of cloth were used in a plate. The mould was placed in a vacuum chamber to remove entrapped air.

In each case, the plates were cured in the mould at room temperature for 48 hours and post cured at 80 °C for 6 hours in a temperature controlled oven. For the purpose of studying optical properties of the materials, circular discs of 50 mm dia. were cut from each plate and machined. The discs were examined for optical properties discussed in the preceding section. The materials have been found to be adequate model materials. It may, however, be mentioned again that the proper chemical composition of the resin was arrived at after lot of trial and error. In the process, many compositions were tried and the composite plates made but later discarded due to inadequate optical properties. Some of the better materials among the discarded ones have been compared with the model materials to illustrate latter's optical superiority.

### 3.4 OPTICAL SUITABILITY OF MODEL MATERIALS

Optical properties of the unidirectional and bidirectional composite model materials have been examined to assess their suitability for photoelastic analysis and allied applications. The model materials have been tested for transparency, resolution of closely spaced lines, image

bidirectional composite indicates that it is slightly less transparent because it has higher volume fraction of glass fibres. The transmission ratios of the two composite model materials are lower than the transmission ratio of the unreinforced polyester disc of equal thickness which was found to be 0.8. However, both the materials are quite adequately transparent. Another model of glass fibre polyester composite with only marginally different resin composition (consequently, slightly bad matching of refractive indices) showed a lower transmission ratio of 0.50 when fibres were perpendicular to the slit and further reduced to 0.40 for fibres parallel to slit. A glass fibre epoxy composite, which looked adequately transparent but had a greater mismatch of refractive indices, exhibited much lower transmission ratios of 0.10 and 0.04 respectively, for fibres perpendicular and parallel to slit. This shows that a visual inspection for transparency is inadequate. A scientific method, such as the one described above, should be used for precise and quantitative measurements of transparency of materials.

### 3.4.2 Resolution of Lines Through Model Materials

It was pointed out earlier that the sharp boundaries of an object may appear smeared when viewed through a composite model whose constituents do not have well matched

refractive indices. This effect has been examined by viewing closely spaced straight and parallel lines through the models. Two sets of equispaced lines were drawn inside a circle with lines in one set being perpendicular to those in other set (Figure 3.5 a). These lines were viewed through the circular discs of unidirectional and bidirectional model materials (Figure 3.5 b and c). Direction of fibres has been indicated by arrows. It is clear from the figures that the lines are easily distinguishable from one another in either case. Another unidirectional material with a small mismatch of refractive indices shows a different behaviour (Figure 3.5 d). The lines which are perpendicular to the fibres still do not appear smeared while the lines parallel to fibres are affected to an extent that they can not be distinguished from one another.

For a quantitative measurement of the above effect, the parallel lines, with distance between two consecutive lines changing according to a logarithmic scale, were viewed through unidirectional models. The spacing between the lines varied from 0.1 mm (pitch 0.2 mm) to 1.0 mm (pitch 2.0 mm). The behaviour of model material has been compared with the other inferior material. For the superior model material the lines could be clearly distinguished from each other by naked eye even for smallest spacing. Moreover, the observation is independent of orientation of fibres with respect to lines. A slightly inferior material exhibited a limit of resolution of lines which changed with

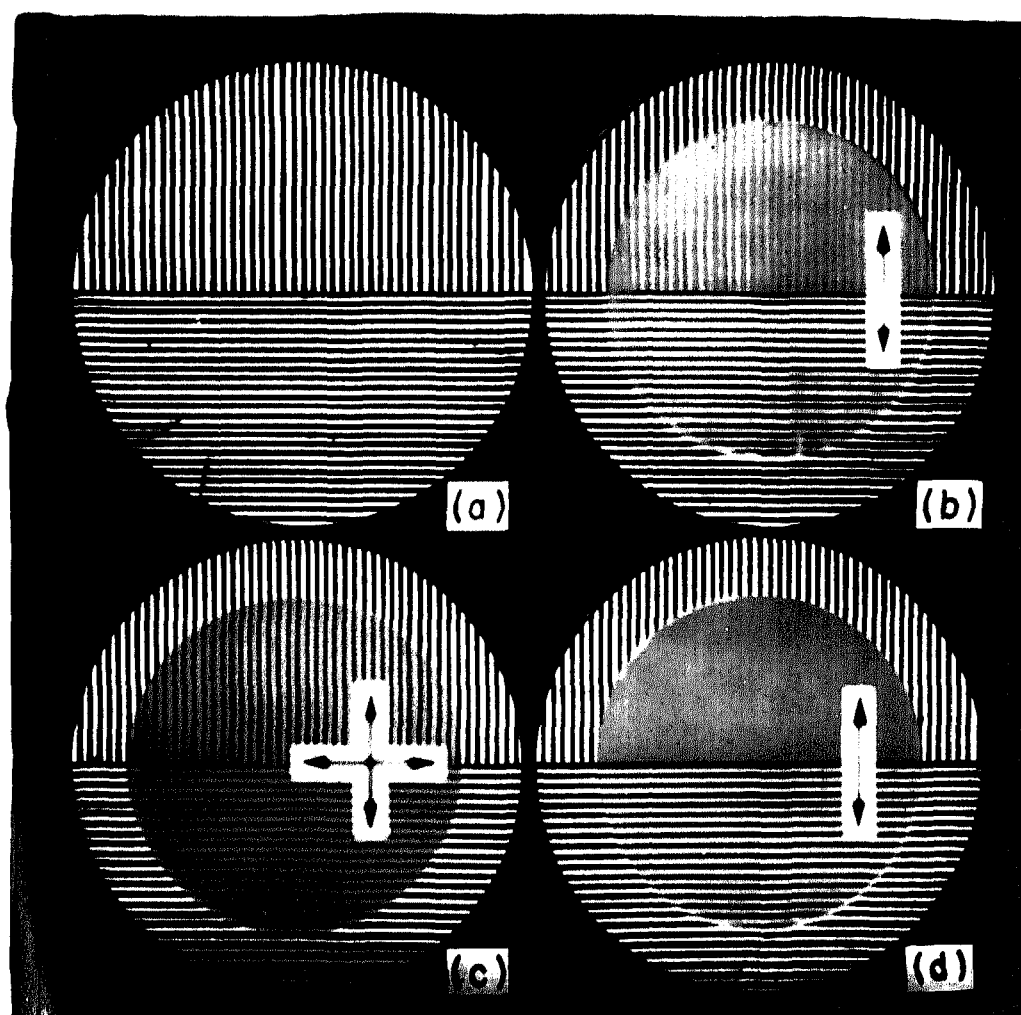


**Figure 3.5** View of parallel lines through (a) no model, (b) unidirectional model material, (c) bidirectional model material and (d) a material with small mismatch of refractive indices. Arrows indicate the direction of fibres.

the angle between the fibres and the lines. The variation in the limit of resolution of lines has been shown as a function of fibre orientation in Figure 3.6. The highest resolution of about 4 lines per mm (spacing 0.125 mm) is obtained when fibres are perpendicular to the lines. The limit of resolution markedly reduces to only one line per mm (spacing 0.5 mm) for fibres parallel to lines. The difference in resolution of lines through the two materials is due to optical inhomogeneity of the second material which arises due to the difference in refractive indices of its constituent materials.

### 3.4.3 Image Forming Characteristics

Optical inhomogeneity in the path of light causes its deflection and consequently, a directed beam of light gets deviated. As discussed earlier, optical homogeneity of the model material, which is directly related to the accuracy of matching of refractive indices of its constituents, can be examined by studying the image forming characteristics of the material. For this purpose the optical bench, shown schematically in Figure 3.2 and discussed earlier, has been used. With this arrangement of optical elements a sharp image of the slit is formed on the screen (Figure 3.3 d). The influence of placing the model between the second lens and screen is examined here.



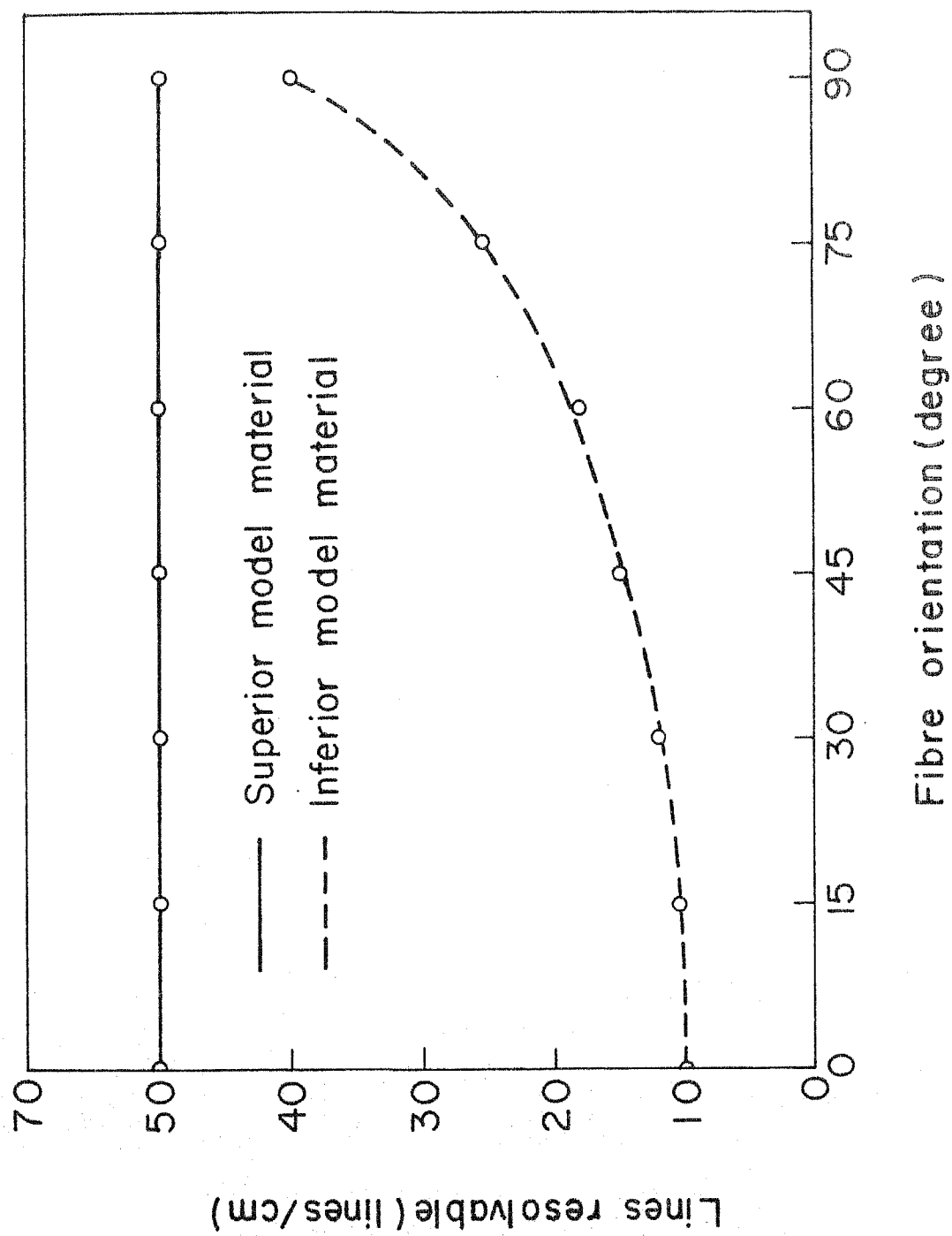


Figure 3.6 Limit of resolution of lines for unidirectional materials

Photographs in Figure 3.7 show images of the light source with models placed in position indicated in Figure 3.2. The images in Figure 3.7 a, b and c correspond to the unidirectional model material with fibres oriented at 0, 45 and 90 degree to the slit. The image in Figure 3.7 d corresponds to the bidirectional model material. It can be clearly seen that there is a negligible distortion of images when the superior model materials are placed in the path of light. The main image can be clearly distinguished from the diffused light which is observed in the direction perpendicular to fibres. This shows that the refractive indices of the glass fibres and the polyester matrix have been matched quite adequately and the materials may be regarded as optically homogeneous.

The effect of mismatch of refractive indices can be seen in Figure 3.8. Photographs in Figure 3.8 a and b correspond to a glass-polyester composite with composition of polyester only slightly different from that of superior model material. Images in Figure 3.8 c and d correspond to a glass-epoxy composite which has still larger mismatch of the refractive indices. It may be pointed out that on visual inspection all three materials look adequately transparent and may be thought of as suitable model materials for photoelastic applications. However, capability of retaining a directed light beam in its original form makes a material superior than the others.

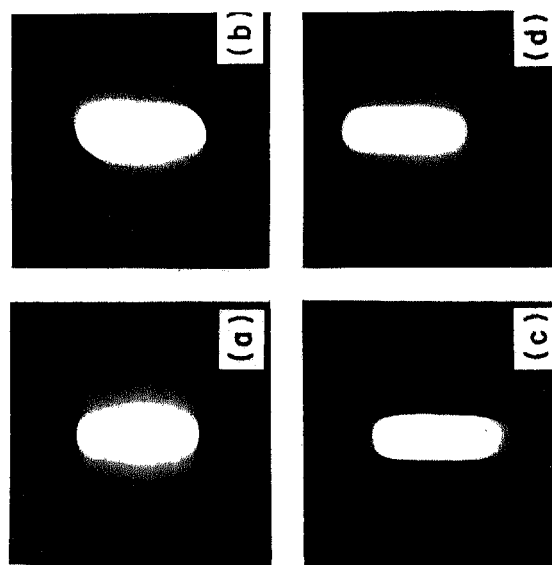


Figure 3.7 Image of slit through unidirectional model material with fibres inclined at (a)  $0^\circ$ , (b)  $45^\circ$  and (c)  $90^\circ$ ; and (d) image through bidirectional model material.

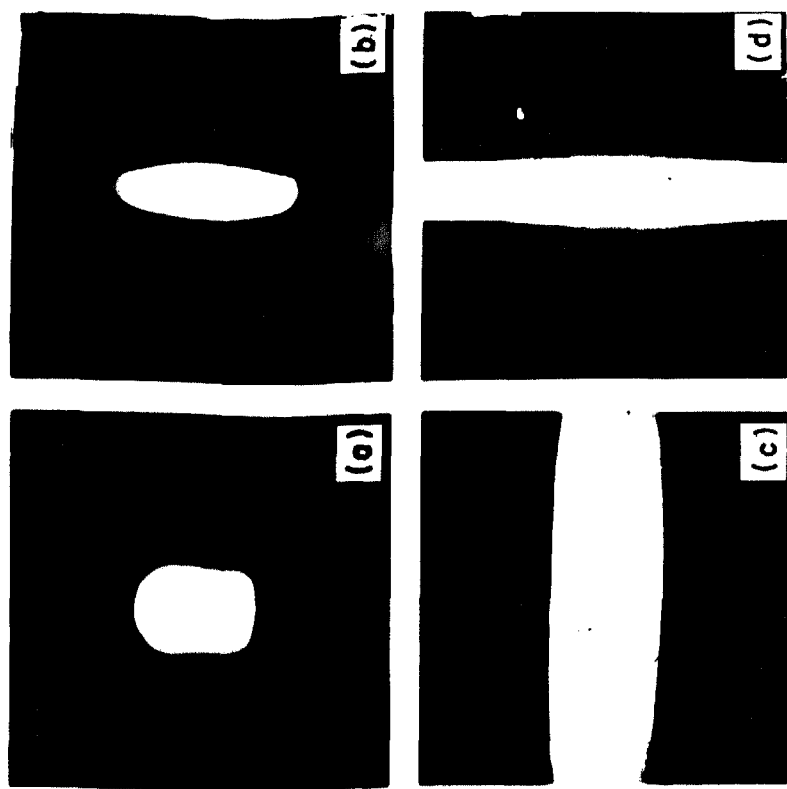


Figure 3.8 Image of slit through inferior model materials.  
(a) glass-polyester  $0^\circ$ , (b) glass-polyester  $90^\circ$   
(c) glass-epoxy  $0^\circ$  and (d) glass-epoxy  $90^\circ$ .

The effect of mismatch of refractive indices becomes more acute when the incidence of light on the material surface occurs at an oblique angle. It has been observed that the image of the straight slit becomes curved by oblique incidence on models with mismatched refractive indices of the constituents. However, no distortion of the image observed by oblique incidence on the superior model materials.

#### 3.4.4 Photoelastic Effects

The model materials have been examined for photoelastic effect by placing their circular disc models in a circular polariscope employing a diffused sodium light source. The discs were loaded in diametral compression with fibres oriented at  $45^{\circ}$  to the loading axis. The resulting isochromatic fringe patterns for unidirectional and bidirectional models have been shown in Figure 3.9 a and b respectively. The isochromatic fringe patterns for another glass-polyester composite model with slight mismatch of refractive indices and a glass-epoxy composite model with larger mismatch have been shown in Figure 3.9 c and d respectively. It can be clearly seen that the fringes for the superior model materials (Figure 3.9 a and b) are much better defined than for other materials (Figure 3.9 c and d). Some nonuniformity of fringes parallel to the fibres occurs

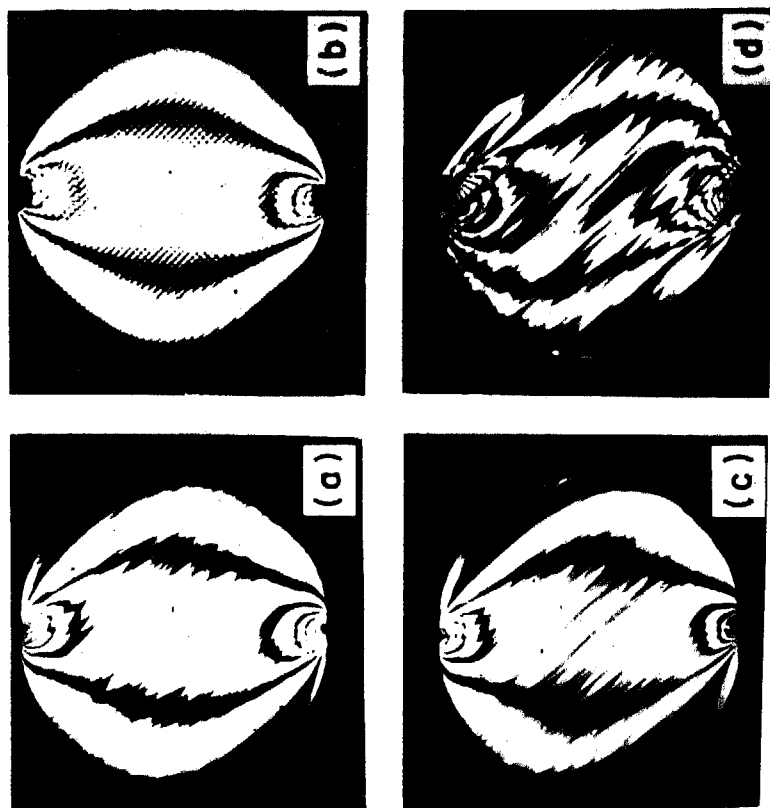


Figure 3.9 Isochromatic fringe patterns for (a) unidirectional model (b) bidirectional model (c) glass-polyester model with small mismatch and (d) glass-epoxy model with large mismatch of refractive indices.

due to nonuniform distribution of fibres so that photoelastic sensitivity of the material changes from point to point. From the fringe pattern shown in Figure 3.9 c, it may appear that the inferior glass-polyester composite is also an adequate photoelastic material but due to undesirable characteristics (Figure 3.5 d, 3.8 a and b) as a result of larger mismatch of refractive indices, this material may not be suitable for more sophisticated analyses.

### 3.5 MECHANICAL AND PHOTOELASTIC CHARACTERISATION

Mechanical and photoelastic properties of birefringent materials play an important role in their selection as model materials. The mechanical properties of orthotropic materials, which are relevant to photoelastic analyses, are the elastic moduli along the two principal material axes, shear modulus and the major Poisson's ratio. These properties were evaluated in uniaxial tension tests on specimens with different fibre orientations. The two elastic moduli and Poisson's ratio are directly determined from tests on specimens with fibres oriented at 0 and 90 degree to the load axis. The shear modulus has been indirectly determined by measuring off axis elastic modulus on a 45 degree specimen and using transformation equations given in Appendix A. All the tests were performed on an Instron machine where the load was measured by a load cell and

strains were measured by mounting electrical resistance strain gauges on the specimens. The mechanical properties of the unidirectional and bidirectional materials are given in Table 3.1. It may be observed that the ratio of the two elastic moduli is 2.7 for unidirectional material which indicates that the material possesses adequate mechanical anisotropy. Anisotropy of the material may be changed by changing volume fraction of fibres.

The property that determines the photoelastic sensitivity of a model material is the stress-fringe value or equivalently, the strain-fringe value. For an isotropic material stress-fringe value  $f_{\sigma}$  and strain fringe value  $f_{\epsilon}$  are independent of direction and are defined as

$$f_{\sigma} = \frac{\sigma_p - \sigma_q}{N}$$

$$f_{\epsilon} = \frac{\epsilon_p - \epsilon_q}{N}$$

where

$$\sigma_p - \sigma_q = \text{principal stress difference}$$

$$\epsilon_p - \epsilon_q = \text{principal strain difference}$$

$$N = \text{relative retardation or fringe order}$$

For orthotropic materials, the  $f_{\sigma}$  and  $f_{\epsilon}$  change with the direction. The theory of photoelasticity for orthotropic material will be discussed in the next two chapters but it may be mentioned here that photoelastic characterization of an orthotropic material requires three independent



photoelastic constants that is either the stress-fringe values or the strain-fringe values defined as follows

$$f_{\sigma L} = \frac{\sigma_L}{N}$$

$$f_{\sigma T} = \frac{\sigma_T}{N}$$

$$f_{\sigma LT} = \frac{2 \tau_{LT}}{N}$$

and  $f_{\epsilon L} = \frac{\epsilon_L}{N}$

$$f_{\epsilon T} = \frac{\epsilon_T}{N}$$

$$f_{\epsilon LT} = \frac{\gamma_{LT}}{N}$$

where subscripts L and T refer to the longitudinal and transverse directions in the material. The stress-fringe values,  $f_{\sigma L}$  and  $f_{\sigma T}$ , are determined by applying uniaxial stresses in the L and T directions respectively. The strain fringe values  $f_{\epsilon L}$  and  $f_{\epsilon T}$  may be determined by applying uniaxial strains in the L and T directions respectively. The  $f_{\sigma LT}$  and  $f_{\epsilon LT}$  are determined by applying the shear stress and shear strain respectively in the L and T directions. In the present studies the  $f_{\sigma L}$  and  $f_{\sigma T}$  were determined directly using tension specimens with fibres oriented at 0 and 90 degrees to the load axis. The strain-fringe values  $f_{\epsilon L}$  and  $f_{\epsilon T}$  are difficult to determine directly due to the experimental difficulties in applying the uniaxial

strains. Therefore, strain-fringe values  $f_{\epsilon_L}$ ,  $f_{\epsilon_T}$  and  $f_{\epsilon_{LT}}$  and the stress fringe value  $f_{\sigma_{LT}}$  were evaluated indirectly using theory of photo-orthotropic elasticity to be discussed in the following chapters. The values of the six photo-elastic constants for the model materials are given in Table 3.2. These values are quite comparable with the photoelastic constants of other orthotropic materials reported in literature [19, 20, 25]

Table 3.1 Elastic Properties of Model Materials

Material	$E_L$	$E_T$	$G_{LT}$	$\nu_{LT}$
	$10^6 \text{ N/m}^2$	$10^6 \text{ N/m}^2$	$10^6 \text{ N/m}^2$	
Unidirectional	15227.3	5638.8	1687.2	0.33
Bidirectional	8430.0	7734.5	1765.8	0.25

Table 3.2 Photoelastic Properties of Model Materials

Material	Stress-fringe values*			Strain-fringe values*		
	$f_{\sigma L}$	$f_{\sigma T}$	$f_{\sigma LT}$	$f_{\epsilon L}$	$f_{\epsilon T}$	$f_{\epsilon LT}$
	$10^3 \text{ N/fr-m}$	$10^3 \text{ N/fr-m}$	$10^3 \text{ N/fr-m}$	$10^{-6} \text{ m/fr}$	$10^{-6} \text{ m/fr}$	$10^{-6} \text{ m/fr}$
Unidirectional	108.0	45.8	35.1	9.565	9.060	10.402
Bidirectional	90.5	80.5	35.8	13.634	12.624	10.137

\* Wavelength of light,  $\lambda = 5893 \text{ \AA}$

## CHAPTER 4

### EXACT THEORIES OF PHOTO-ORTHOTROPIC-ELASTICITY

#### 4.1 INTRODUCTION

The second requirement for the application of transmission photoelasticity to the stress analysis of composite materials is to develop an adequate theory through which photoelastic observations can be interpreted and translated into desired stresses or strains. Microscopically, glass fibre reinforced composites are heterogeneous with each constituent being homogeneous and isotropic. On a macroscopic scale, the fibrous composites are often assumed to be homogeneous but anisotropic. Therefore, the photoelastic theories for composite materials have been developed by considering their behaviour either on microscopic or macroscopic scale. In the former case, the photoelastic response of each constituent of composite material is taken into consideration to predict the overall response of the composite. In the latter case, the behaviour of composite material is assumed to be analogous to anisotropic crystals and therefore, their photoelastic response is predicted using photoelastic theories of crystals. In this chapter some of the existing theories of photo-orthotropic-elasticity will be reviewed first. Then, an exact strain-optic law will be derived with a view that it

may be later modified to remove limitations of the existing theories of photo-orthotropic-elasticity.

#### 4.2 ASSESSMENT OF EXISTING THEORIES OF PHOTO-ORTHOTROPIC-ELASTICITY

Pih and Knight [17] were probably the first to propose a stress-optic law for orthotropic materials. Their approach was based on the distribution of stresses between the constituents of a composite. However, their theoretical predictions and experimental results did not show good agreement. Therefore, their approach was not pursued further by other investigators. Sampson [19] developed the concept of a Mohr circle of birefringence by simple analogy. He postulated that the orthotropic materials can be characterised with three principal stress-fringe values  $f_{\sigma L}$ ,  $f_{\sigma T}$ ,  $f_{\sigma LT}$ , and that the stress system  $\sigma_L$ ,  $\sigma_T$  and  $\tau_{LT}$  produces three components of birefringence as follows:

$$\begin{aligned} N_L &= \frac{\sigma_L}{f_{\sigma L}} \\ N_T &= \frac{\sigma_T}{f_{\sigma T}} \\ N_{LT} &= \frac{2 \tau_{LT}}{f_{\sigma LT}} \end{aligned} \quad (4.1)$$

where the subscripts L and T refer to the principal material axes (for example, the directions parallel and perpendicular to fibres in a unidirectional composite). The resultant

birefringence, then, is:

$$N = \left[ \left( \frac{\sigma_L}{f_{\sigma L}} - \frac{\sigma_T}{f_{\sigma T}} \right)^2 + \left( \frac{2\tau_{LT}}{f_{\sigma LT}} \right)^2 \right]^{1/2} \quad (4.2)$$

The principal stress-fringe values  $f_{\sigma L}$ ,  $f_{\sigma T}$  and  $f_{\sigma LT}$  can be experimentally determined through three independent tests to be discussed later in this chapter.

An off-axis stress-fringe value,  $f_{\sigma\theta}$ , under uniaxial state of stress, may be defined as :

$$f_{\sigma\theta} = \frac{\sigma_\theta}{N} \quad (4.3)$$

where  $\sigma_\theta$  is the uniaxial stress applied at an angle,  $\theta$ , to the longitudinal direction. Using the laws of stress transformation,  $f_{\sigma\theta}$  may be obtained in terms of  $f_{\sigma L}$ ,  $f_{\sigma T}$  and  $f_{\sigma LT}$  as:

$$f_{\sigma\theta} = f_{\sigma L} \left[ \left( \cos^2 \theta - \frac{f_{\sigma L}}{f_{\sigma T}} \sin^2 \theta \right)^2 + \frac{f_{\sigma L}^2}{f_{\sigma LT}^2} \sin^2 2\theta \right]^{-1/2} \quad (4.4)$$

The optical isoclinic parameter,  $\phi$  (that is, angle that an isoclinic fringe makes with the fibre direction) can be computed as a function of principal stress direction,  $\theta$ , for uniaxial stress:

$$\tan 2\phi = \frac{f_{\sigma L} \sin 2\theta}{f_{\sigma LT} (\cos^2 \theta - f_{\sigma L}/f_{\sigma T} \cdot \sin^2 \theta)} \quad (4.5)$$

Sampson [19] supported his theory by limited experimental results which were obtained by testing unidirectional

composites under uniaxial state of stress.

Dally and Prabhakaran [20], like Sampson [19], assumed that the photoelastic response of orthotropic materials can be predicted through three independent stress-fringe values. They derived a stress-optic law for uniaxial state of stress. Conceptually, their approach is based on the finding out the stresses, and hence the contributing birefringence in each constituent. The net birefringence is an algebraic sum of the contributions by each constituent. The accuracy of results is greatly influenced by the accuracy with which the stresses in constituents can be evaluated. This becomes a limitation of the approach particularly because it is very difficult to predict transverse stresses accurately. Moreover, they did not discuss the interpretation of isoclinics in orthotropic birefringent materials. Experimental and theoretical results of Dally and Prabhakaran closely agreed with the stress-optic law formulated by Sampson.

Bert [22] modelled fibrous composites by orthorhombic crystalline system and applied the theory of photoelasticity for anisotropic crystals which was initially propounded by Pockels [23] and later modified by Bhagavantam [24]. According to this theory the symmetric second order birefringence tensor is related to stress or strain tensor through a fourth order photoelastic-property tensor. Using this theory Bert derived a stress-optic law for orthotropic

materials subjected to plane stress and showed that the concept of Mohr circle of birefringence, as proposed intuitively by Sampson [19], is a direct result of tensorial nature of birefringence. The interpretation that the isoclinic angle represents principal birefringence direction, is also consistent. More recently Knight and Pih[ 25] using Bhagavantam-Pockels theory derived a general stress-optic law and then simplified it to a two dimensional case. Their formulation is general and accounts also for initial birefringence which is usually present in two-phase materials. However, their simplified equations are of the same form as those of Sampson[ 19] and Bert [22].

It is clear from the above discussion that most of the existing theories of photo-orthotropic-elasticity lead to stress-optic law of the form proposed by Sampson. Some experimental results reported in the literature indicate that the photoelastic response of orthotropic materials can be accurately predicted through three independent photoelastic constants. It was, however, decided to assess this form of stress-optic law through the experiments conducted on superior orthotropic model materials whose development has been discussed in the previous chapter.

Photoelastic response of model materials was studied on tensile specimens of unidirectionally and bidirectionally reinforced materials. The fibre orientations were



kept at 0, 15, 30, 45, 60, 75 and 90 degree to the longitudinal edge of the specimens. The specimens were gradually loaded in uniaxial tension and observed in a transmission polariscope for isoclinic and isochromatic measurements. The resulting isoclinic parameter and isochromatic fringe order was noted down for each increment of load. The stress-fringe value of a specimen was obtained by measuring slope of the plot of the fringe order ( $N$ ) as a function of applied stress. A typical fringe order vs stress curve is shown in Figure 4.1 for the specimen with fibre orientation of 30 degree. The value of  $f_{\sigma LT}$  was determined using an indirect procedure in which an off-axis stress-fringe value is measured and the value of  $f_{\sigma LT}$  is calculated from Eq. (4.4). In general any off axis specimen can be chosen for the purpose but the effect of errors, which might have been made in the measurements of  $f_{\sigma L}$  and  $f_{\sigma T}$ , can be minimised, if not completely eliminated, through proper selection of off-axis specimens. It can be seen from the Eq. (4.4) that  $f_{\sigma LT}$  will be related to only  $f_{\sigma \theta}$  provided the term in parenthesis is zero. When this is achieved  $f_{\sigma LT}$  becomes:

$$f_{\sigma LT} = f_{\sigma \theta_0} \sin 2 \theta_0$$

wher  $\tan^2 \theta_0 = \frac{f_{\sigma T}}{f_{\sigma L}}$  (4.6)

Angles  $\theta_0$  for the unidirectional and bidirectional materials were found to be 33 and 43 degrees respectively.

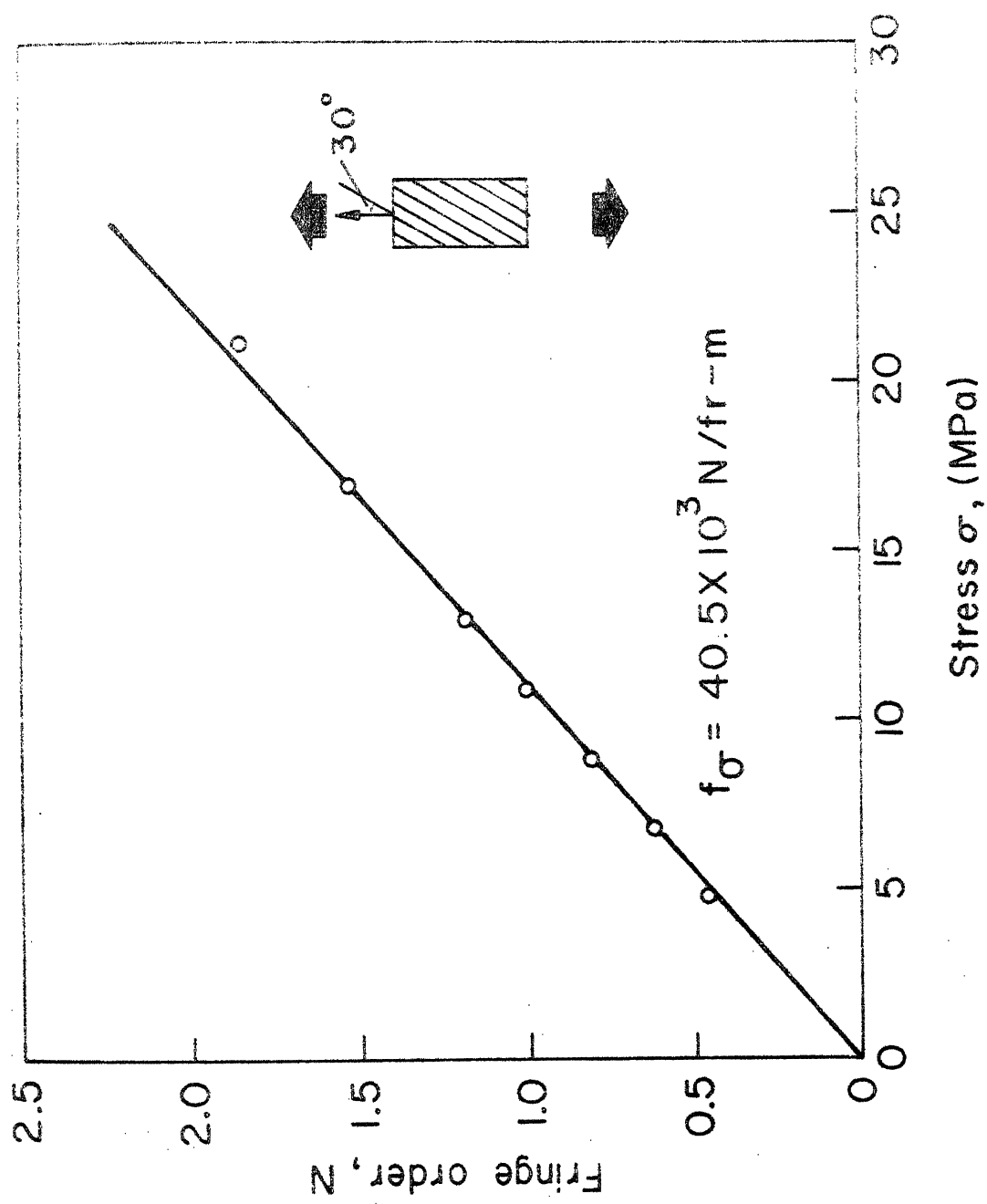


Figure 4.1 Evaluation of off-axis stress-fringe value

In the present case  $f_{\sigma LT}$  was, therefore, calculated from a 30 degree specimen for unidirectional material and from 45 degree specimen for bidirectional material.

The stress-fringe value has been plotted as a function of fibre orientation,  $\theta$ , in Figure 4.2 for both model materials. The difference observed in the values of  $f_{\sigma L}$  and  $f_{\sigma T}$  for bidirectional material is expected because the amount of reinforcement in the two directions is not equal. Also shown in Figure 4.2 are the theoretical predictions based upon Eq. (4.4). It is very clear that the experimental results agree very well with the theoretical predictions. Isoclinic angle,  $\phi_{\sigma}$ , as measured from the direction of load, has been plotted as a function of fibre orientation,  $\theta$ , in Figures 4.3 and 4.4 for unidirectional and bidirectional model materials respectively. Isoclinic angles predicted by Eq. (4.5) have also been plotted. It may be mentioned that Eq. (4.5) gives angle from the fibre direction where as the angles plotted in Figures 4.3 and 4.4 have the load direction as the reference. Also shown in the figure are the directions of principal stresses and principal strains. It is observed that the experimentally measured values of isoclinic angles are in good agreement with the theoretical predictions. Further, the isoclinics do not coincide with either the directions of principal stresses or strains which means that the principal

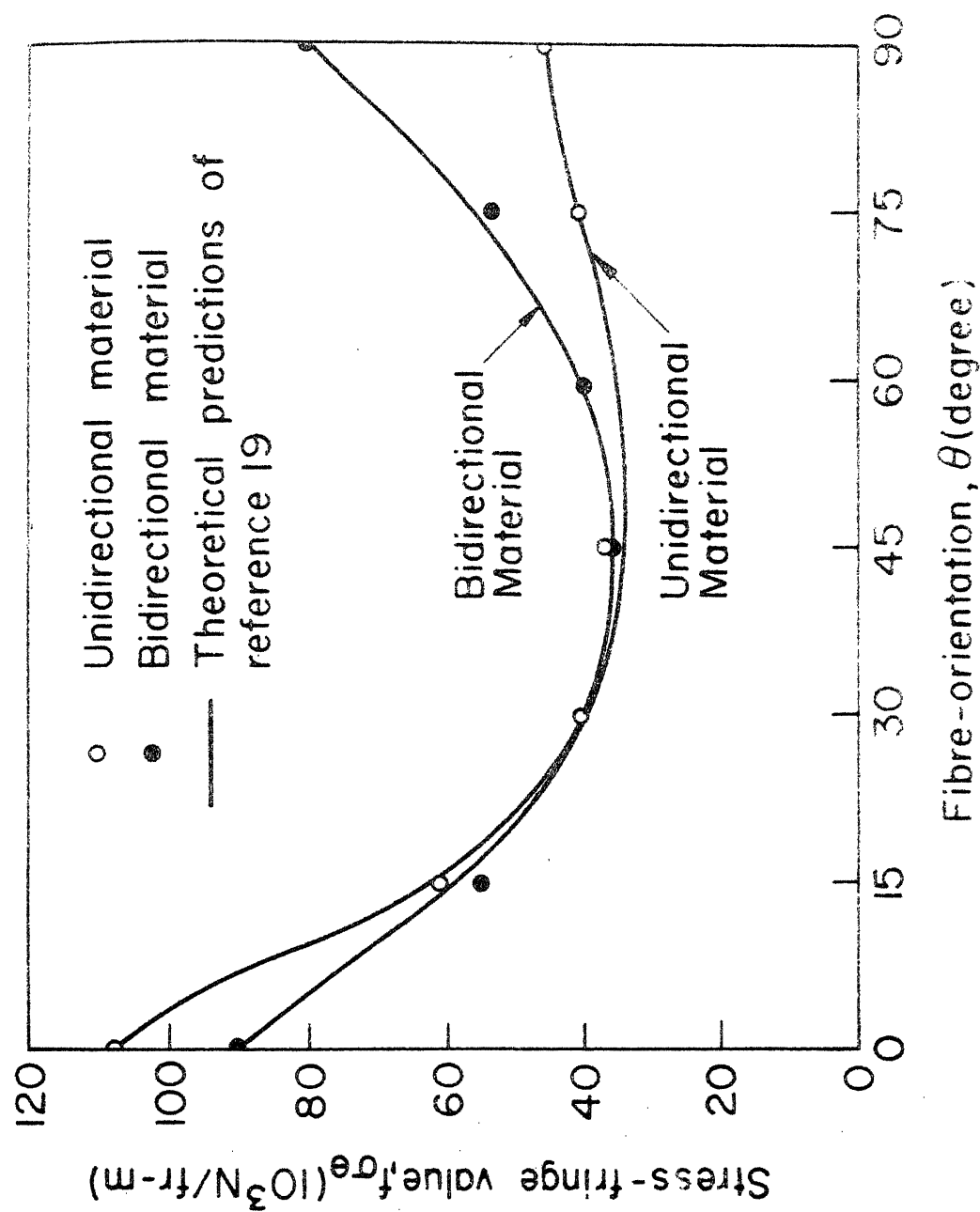


Figure 4.2 Stress-fringe value as a function of the fibre orientation for uniaxial loading of tensile specimens.

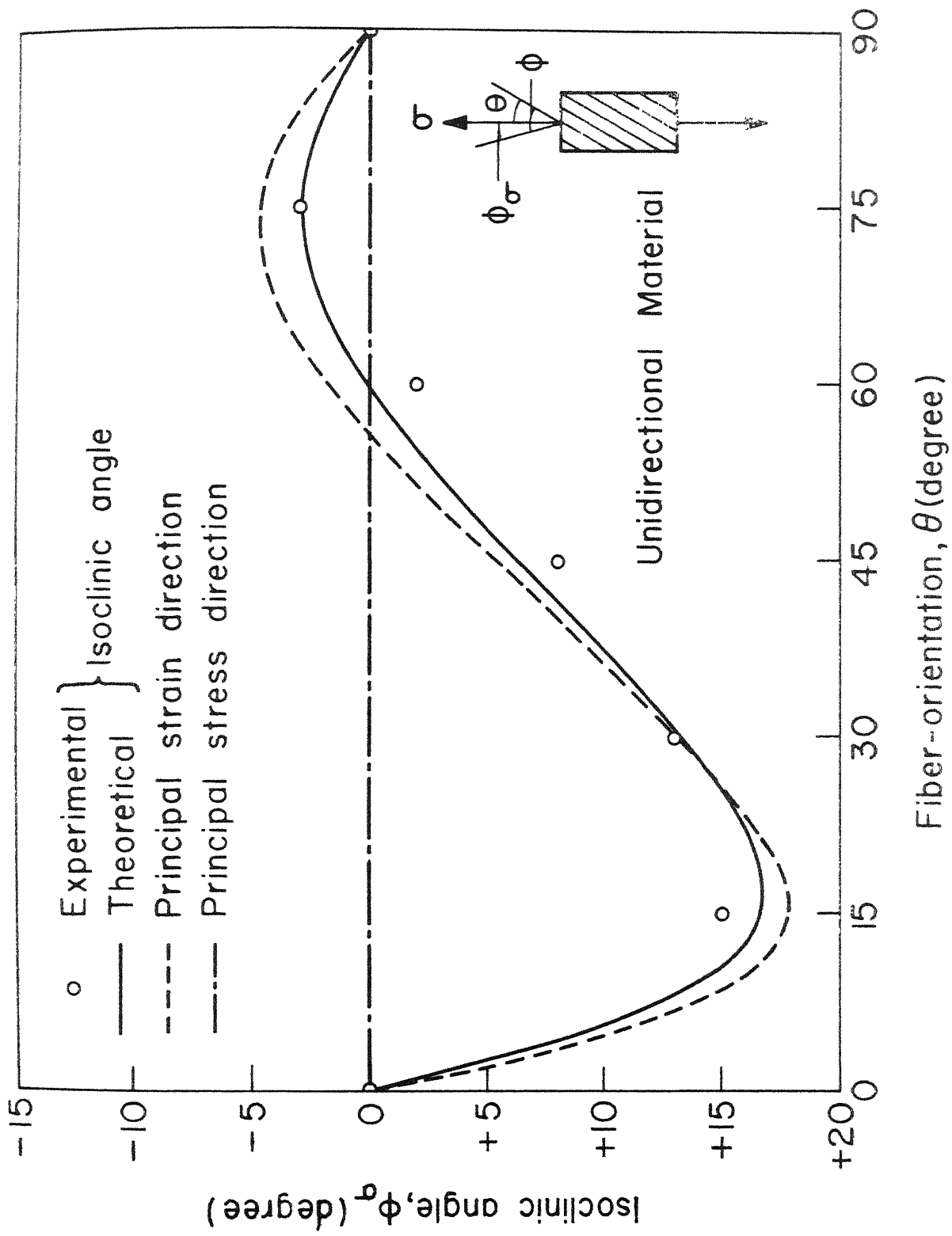


Figure 4.3 Isoclinic angle as a function of the fibre orientation for uniaxial loading of tensile specimens

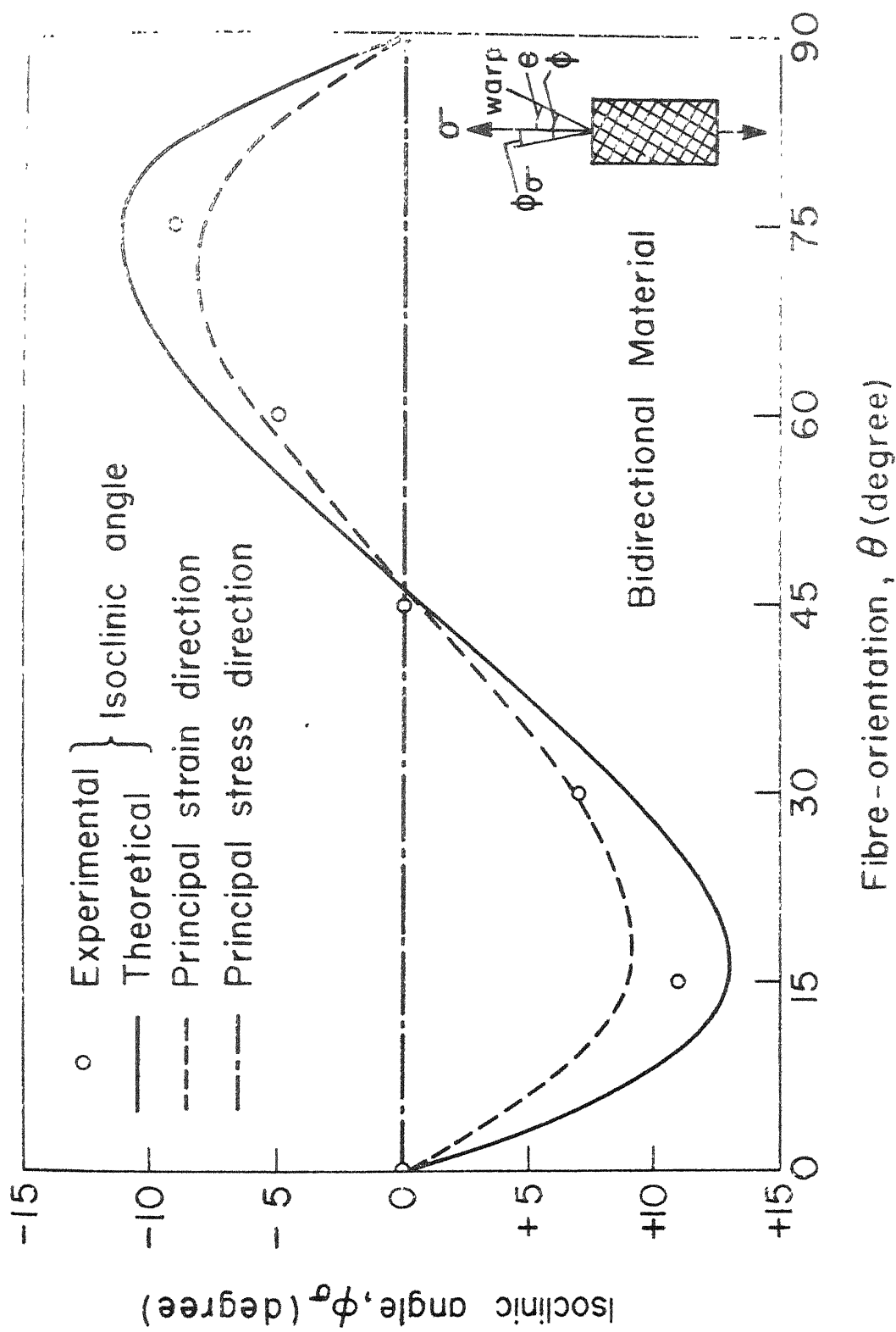


Figure 4.4 Isoclinic angle as a function of the fibre orientation for uniaxial loading of tensile specimens.

birefringence directions in orthotropic material are, in general, not the same as the principal stress or strain directions. However, the isoclinics are closer to the directions of principal strains than the principal stresses. Also, the directions of principal strains show the similar variation as the isoclinics for both the materials. It may be mentioned that the initial birefringence in orthotropic materials will influence the isoclinic angle. In the present case, however, the initial birefringence was very small in magnitude. And its influence was further minimised by measuring the isoclinic angle at higher stresses when the isoclinic angle becomes practically constant.

It is now quite clear from the above discussion that photoelastic response of orthotropic materials can be accurately predicted through three independent photoelastic constants. It is, however, not possible to evaluate, through the existing stress-optic laws, the individual stress or strain components or the difference between their principal values from the birefringence measured in a polariscope. Similarly it is possible to predict the optical isoclinic angle for a known state of stress but it is not possible to predict the direction of principal stress or strain from the measured optical isoclinic angle. Thus the existing theories of photo-orthotropic-elasticity are not capable of translating photoelastic measurements into

desired stresses or strains. This has been the aim of present investigations to develop a theory of photo-orthotropic-elasticity which will overcome the above limitations in the applications of transmission photoelasticity to the problems of stress analysis of orthotropic materials.

Some approximate laws have been proposed by investigators to overcome the limitations of theories of photo-orthotropic-elasticity discussed above. Pipes and Rose [26] proposed the use of strain-optic law in place of stress-optic law. They assumed that isotropic strain-optic law (with a single strain-fringe value) is applicable for low fibre-volume-fraction composites where the matrix dominates the optical response of the material. They reasonably verified this assumption for composite with low fibre-volume-fraction. However, usefulness of their work is limited because the real composites often have high fibre volume content and because they did not indicate the magnitude of error that may arise due to the simplifying assumptions. Their work did show a new direction in which efforts could be made to make transmission photoelasticity more useful. Prabhakaran [27] proposed a strain-optic law with three principal strain-fringe values and hence it has the same drawbacks as the stress-optic laws discussed earlier. In the same paper Prabhakaran has proposed a simplified strain-optic law with a single strain-fringe value which is taken



to be the arithmetic average of the three principal strain-fringe values. The approaches of Pipes and Rose and of Prabhakaran are really some kind of ad hoc approaches in which the strain-fringe values are calculated from the stress-fringe values through the composite stress-strain relations. The derivations have neither mathematical rigour nor a fundamental basis of the material behaviour. Their formulations failed to provide a method of taking the errors into account due to approximations involved.

In the present investigations it was decided to develop an approximate strain-optic law. The motivation behind picking up the strain-optic law and not the stress-optic law for approximations was that in orthotropic materials, the optical isoclinic angles are closer to the directions of principal strains than the principal stresses. Secondly there are some indications that the orthotropic materials exhibit lower degree of orthotropy with respect to strain-optic behaviour than that with respect to stress-optic behaviour. The approximate strain-optic law was derived from an exact strain-optic law which in turn was derived from the Bhagavantam - Pockels theory of photoelasticity of crystals. The approximations have been made in a manner which minimises the error. Moreover, a method has been developed to estimate the error with a reasonable degree of accuracy.

### 4.3 EXACT STRAIN-OPTIC LAW

It is generally agreed that macroscopic behaviour of fibrous composites can be accurately predicted using theory of anisotropic elasticity. It, therefore, seems appropriate to assume that the photoelastic behaviour of composites is analogous to that of anisotropic crystals. The theory of photoelasticity of crystals was first proposed by Fockels [23]. Later on Bhagavantam [41] corrected certain errors in it. In the established theory of crystalline photoelasticity [24], birefringence is shown to be a symmetric second order tensor like stress or strain. The birefringence tensor  $N_{ij}$  is related to the strain tensor  $(\epsilon_{kl})$  through the following relation:

$$N_{ij} = P_{ijkl} \epsilon_{kl} \quad (i, j = 1, 2, 3) \quad (4.7)$$

where  $P_{ijkl}$  is a fourth order strain-optic property tensor like the elastic coefficient tensor. However, unlike the elastic coefficient tensor, the strain-optic property tensor is generally unsymmetric. The tensor,  $P_{ijkl}$ , in general, consists of 36 independent strain-optic coefficients for a three dimensional anisotropic birefringent material.

For simplicity Eq. (4.7) may be written in the contracted notations as:

$$N_q = P_{qr} \epsilon_r \quad (q, r = 1, 2, \dots 6) \quad (4.8)$$

Behaviour of an orthotropic material, such as fibrous composite, can be considered analogous to that of an orthorhombic crystal having three principal material symmetry axes. For orthorhombic system the strain-optic relation, Eq. (4.8) takes the following form when written in the matrix notation:

$$\begin{bmatrix} N_1 \\ N_2 \\ N_3 \\ N_4 \\ N_5 \\ N_6 \end{bmatrix} = \begin{bmatrix} P_{11} & P_{12} & P_{13} & 0 & 0 & 0 \\ P_{21} & P_{22} & P_{23} & 0 & 0 & 0 \\ P_{31} & P_{32} & P_{33} & 0 & 0 & 0 \\ 0 & 0 & 0 & P_{44} & 0 & 0 \\ 0 & 0 & 0 & 0 & P_{55} & 0 \\ 0 & 0 & 0 & 0 & 0 & P_{66} \end{bmatrix} \begin{bmatrix} \epsilon_1 \\ \epsilon_2 \\ \epsilon_3 \\ \epsilon_4^* \\ \epsilon_5^* \\ \epsilon_6^* \end{bmatrix} \quad (4.9)$$

It may be noted that there are 12 independent strain-optic coefficients for an orthotropic material compared to only 9 elastic constants. .

Using the same reasoning as used for the analysis of mechanical behaviour of fibrous composites [35], it can be assumed that the unidirectional material, on a macroscopic scale, is transversely isotropic, with the plane of isotropy being normal to the fibres. If the fibre direction is taken as axis 1, Eq. (4.9) becomes:

---

\*Here onwards  $\epsilon_4$ ,  $\epsilon_5$  and  $\epsilon_6$  will be denoted in terms of shear strains as  $\gamma_{23}$ ,  $\gamma_{31}$  and  $\gamma_{12}$  .

$$\begin{bmatrix} N_1 \\ N_2 \\ N_3 \\ N_4 \\ N_5 \\ N_6 \end{bmatrix} = \begin{bmatrix} P_{11} & P_{12} & P_{12} & 0 & 0 & 0 \\ P_{21} & P_{22} & P_{23} & 0 & 0 & 0 \\ P_{21} & P_{23} & P_{22} & 0 & 0 & 0 \\ 0 & 0 & 0 & \frac{P_{22}-P_{23}}{2} & 0 & 0 \\ 0 & 0 & 0 & 0 & P_{66} & 0 \\ 0 & 0 & 0 & 0 & 0 & P_{66} \end{bmatrix} \begin{bmatrix} \epsilon_1 \\ \epsilon_2 \\ \epsilon_3 \\ \gamma_{23} \\ \gamma_{13} \\ \gamma_{12} \end{bmatrix} \quad (4.10)$$

A large number of real-life problems are idealised to be plane stress problems. The strain-optic relation for plane-stress becomes:

$$\begin{bmatrix} N_1 \\ N_2 \\ N_3 \\ N_6 \end{bmatrix} = \begin{bmatrix} P_{11} & P_{12} & P_{12} & 0 \\ P_{21} & P_{22} & P_{23} & 0 \\ P_{21} & P_{23} & P_{22} & 0 \\ 0 & 0 & 0 & P_{66} \end{bmatrix} \begin{bmatrix} \epsilon_1 \\ \epsilon_2 \\ \epsilon_3 \\ \gamma_{12} \end{bmatrix} \quad (4.11)$$

It may be noted that, for a plane stress case, the out-of-plane strain,  $\epsilon_3$ , is, in general, not zero and will affect the in-plane birefringence. Therefore, the terms in the third row and third column of the matrix in Eq. (4.10) can not be dropped. However, for a plane stress case of transversely isotropic composite, the strain,  $\epsilon_3$ , normal to the plane of composite lamina can be written in terms of in-plane strains,  $\epsilon_1$ , and,  $\epsilon_2$ , as follows:

$$\epsilon_3 = - \frac{1}{1 - \nu_{12} \nu_{21}} [\nu_{12} (1 + \nu_{23}) \epsilon_1 + (\nu_{23} + \nu_{12} \nu_{21}) \epsilon_2] \quad (4.12)$$

or

$$\epsilon_3 = - K_1 \epsilon_1 - K_2 \epsilon_2 \quad (4.13)$$

where

$$K_1 = \frac{\nu_{12} (1 + \nu_{23})}{1 - \nu_{12} \nu_{21}} \quad (4.14)$$

$$K_2 = \frac{\nu_{23} + \nu_{12} \nu_{21}}{1 - \nu_{12} \nu_{21}}$$

The birefringence components in the plane 1 - 2 can be written in terms of strain components from Eq. (4.11) as follows:

$$N_1 - N_2 = (P_{11} - P_{21}) \epsilon_1 - (P_{22} - P_{12}) \epsilon_2 + (P_{12} - P_{23}) \epsilon_3$$

$$N_6 = P_{66} \gamma_{12} \quad (4.15)$$

Now, by substituting Eq. (4.13) into Eqs. (4.15), the in-plane birefringence components can be written in terms of the in-plane strains only as:

$$N_1 - N_2 = b_1 \epsilon_1 - b_2 \epsilon_2$$

$$N_6 = b_3 \gamma_{12} \quad (4.16)$$

where

$$b_1 = (P_{11} - P_{21}) - K_1 (P_{12} - P_{23})$$

$$b_2 = (P_{22} - P_{12}) + K_2 (P_{12} - P_{23})$$

$$b_3 = P_{66} \quad (4.17)$$

The quantities observed in a polariscope are the resultant birefringence and the direction of principal birefringence. The resultant birefringence is the difference between the principal components of birefringence. The resultant birefringence represents relative retardation and is measured through the isochromatics which are lines of constant relative retardation. The direction of principal birefringence is represented through the angle it makes with a fixed reference axis. The angle is called isoclinic angle and the lines of constant isoclinic angles are called isoclinics.

Birefringence components in an arbitrary direction can be obtained from known magnitude and direction of principal birefringence components through the second-order tensor transformations. It can be easily shown that the birefringence components given in Eq. (4.16) can be written in terms of resultant birefringence,  $N$  (the difference of principal birefringence components  $N_p$  and  $N_q$ ), and the isoclinic angle,  $\emptyset$ , measured from the fibre direction, as follows:

$$\begin{aligned} N_1 - N_2 &= N \cos 2 \emptyset = b_1 \epsilon_1 - b_2 \epsilon_2 \\ 2 N_6 &= N \sin 2 \emptyset = 2 b_3 \gamma_{12} \end{aligned} \quad (4.18)$$

The desired strain-optic law can now be written by separating the resultant birefringence and isoclinic angle:

$$N = \left[ (b_1 \epsilon_1 - b_2 \epsilon_2)^2 + (2 b_3 \gamma_{12})^2 \right]^{1/2} \quad (4.19)$$

$$\tan 2 \phi = \frac{2 b_3 \gamma_{12}}{b_1 \epsilon_1 - b_2 \epsilon_2} \quad (4.20)$$

Thus the photoelastic response of orthotropic materials can be predicted through the exact strain-optic law given by Eqs. (4.19). One may note that although there are six independent strain-optic coefficients (that is,  $P_{11}$ ,  $P_{12}$ ,  $P_{21}$ ,  $P_{22}$ ,  $P_{23}$  and  $P_{66}$ ) involved in the exact formulation of strain-optic law, they appear in groups such that only three constants are sufficient to predict the photoelastic response of material. The three constants  $b_1$ ,  $b_2$  and  $b_3$ , can be experimentally determined and related to the familiar strain-fringe values as follows:

- (i)  $b_1$  can be determined when,  $\epsilon_L$ , is the only non zero in-plane strain acting on the material. Under these conditions:

$$b_1 = \frac{1}{f_{\epsilon_L}} = \frac{N}{\epsilon_L} \quad (4.21)$$

where,  $f_{\epsilon_L}$ , is known as the longitudinal, normal strain-fringe value.

- (ii)  $b_2$  can be determined when,  $\epsilon_T$ , is the only non zero in-plane strain acting on the material. Under these conditions:

$$b_2 = \frac{1}{f_{\epsilon_T}} = \frac{N}{\epsilon_T} \quad (4.22)$$

where,  $f_{\epsilon_T}$ , is known as the transverse normal strain-fringe value.

- (iii)  $b_3$  can be determined when only pure shear strain,  $\gamma_{LT}$ , is acting on the material. Under these conditions:

$$b_3 = \frac{1}{2 f_{\epsilon_{LT}}} = \frac{N}{\gamma_{LT}} \quad (4.23)$$

With the definitions of strain-fringe values given by Eqs. (4.21), (4.22) and (4.23), the strain-optic law can be written in a more familiar form as:

$$N = \left[ \left( \frac{\epsilon_L}{f_{\epsilon_L}} - \frac{\epsilon_T}{f_{\epsilon_T}} \right)^2 + \left( \frac{\gamma_{LT}}{f_{\epsilon_{LT}}} \right)^2 \right]^{1/2} \quad (4.24)$$

and the isoclinic parameter,  $\phi$ , becomes:

$$\phi = \frac{1}{2} \tan^{-1} \frac{\frac{\gamma_{LT}}{f_{\epsilon_{LT}}}}{\frac{\epsilon_L}{f_{\epsilon_L}} - \frac{\epsilon_T}{f_{\epsilon_T}}} \quad (4.25)$$

The above form of strain-optic law is convenient when strains acting along material symmetry axes are under considerations. In many stress analysis problems, it may be necessary to consider the principal strains and their orientations. If the principal strains are denoted by  $\epsilon_p$  and  $\epsilon_q$  where the direction of,  $\epsilon_p$ , makes an angle,  $\theta$ , with the fibre direction, the strains along L and T directions can be obtained by transformation as:



$$\begin{aligned}
\epsilon_L &= \epsilon_p \cos^2 \theta + \epsilon_q \sin^2 \theta \\
\epsilon_T &= \epsilon_p \sin^2 \theta + \epsilon_q \cos^2 \theta \\
\gamma_{LT} &= (\epsilon_p - \epsilon_q) \sin 2\theta
\end{aligned} \tag{4.26}$$

Eqs. (4.26) and (4.24) can be combined to obtain a general strain-optic law for biaxial strain-field as:

$$\begin{aligned}
N &= \frac{\epsilon_p}{f_{\epsilon L}} \left\{ \left[ (\cos^2 \theta + \frac{\epsilon_q}{\epsilon_p} \sin^2 \theta) - (\sin^2 \theta + \frac{\epsilon_q}{\epsilon_p} \cos^2 \theta) \right. \right. \\
&\quad \left. \left. \frac{f_{\epsilon L}}{f_{\epsilon T}} \right]^2 + \left[ \left( 1 - \frac{\epsilon_q}{\epsilon_p} \right) \frac{f_{\epsilon L}}{f_{\epsilon LT}} \sin 2\theta \right]^2 \right\}^{1/2}
\end{aligned} \tag{4.27}$$

The expression for isoclinic parameter,  $\emptyset$ , becomes:

$$\emptyset = \frac{1}{2} \tan^{-1} \frac{\left( 1 - \frac{\epsilon_q}{\epsilon_p} \right) \frac{\sin 2\theta}{f_{\epsilon LT}}}{\frac{\cos^2 \theta}{f_{\epsilon L}} - \frac{\sin^2 \theta}{f_{\epsilon T}} + \frac{\epsilon_q}{\epsilon_p} \left( \frac{\sin^2 \theta}{f_{\epsilon L}} - \frac{\cos^2 \theta}{f_{\epsilon T}} \right)} \tag{4.28}$$

It may be pointed out that the strain-optic law proposed intuitively by Prabhakaran [27] is in agreement with the exact strain-optic law given by Eqs. (4.24) or (4.27).

However, it was not clear in Prabhakaran's approach if and how the effect of out-of-plane normal strain,  $\epsilon_3$ , is taken into account. The exact strain-optic law is also of the same form as the stress-optic laws formulated by Sampson [19], Bert [22] and Knight and Pih [25] all of which also involve three stress-fringe values.

## (b) Strain-optic law for uniaxial strain

In the case of uniaxial strain (i.e.,  $\epsilon_q = 0$ ), an off-axis strain-fringe value  $f'_{\epsilon\theta}$  may be defined as:

$$f'_{\epsilon\theta} = \frac{\epsilon_p}{N} \quad (4.33)$$

The following expressions for,  $f'_{\epsilon\theta}$ , and  $\phi$ , may be obtained by combining Eqs. (4.27), (4.28) and (4.33) and substituting  $\epsilon_q = 0$ :

$$f'_{\epsilon\theta} = \left[ \left( \frac{\cos^2 \theta}{f_{\epsilon L}} - \frac{\sin^2 \theta}{f_{\epsilon T}} \right)^2 + \left( \frac{\sin 2\theta}{f_{\epsilon LT}} \right)^2 \right]^{-1/2} \quad (4.34)$$

$$\phi = \frac{1}{2} \tan^{-1} \frac{\frac{\sin^2 \theta}{f_{\epsilon LT}}}{\frac{\cos^2 \theta}{f_{\epsilon L}} - \frac{\sin^2 \theta}{f_{\epsilon T}}} \quad (4.35)$$

It may be pointed out that although the expression (Eq. 4.34) for off-axis strain-fringe value is similar to that of off-axis stress-fringe value (Eq. 4.4), the direct determination of,  $f'_{\epsilon\theta}$ , is considerably more difficult than that of  $f_{\sigma\theta}$ . In order to obtain a uniaxial strain-field the material has to be subjected to a biaxial stress-field. Moreover, the ratio of stresses in the two directions has to be adjusted precisely to compensate for the Poisson's effect.

#### 4.3.1 Experimental Determination of Principal Strain-Fringe Values

Application of the strain-optic law derived in the previous section requires three principal strain-fringe values which have to be determined experimentally. As discussed earlier, their direct determination will require the application of biaxial stresses on the specimen. It was therefore decided to follow an indirect approach for their determination by applying uniaxial stress only. Following are the steps followed in the determination of the strain-fringe values.

- (i) A uniaxial stress,  $\sigma_L$ , along fibre direction produces the principal strains along directions (1 - 2) as follows:

$$\begin{aligned}\epsilon_1 &= \epsilon_L \\ \epsilon_2 &= -\nu_{LT} \epsilon_L\end{aligned}\tag{4.36}$$

The isochromatic and isoclinic response can be obtained from Eqs. (4.19) and (4.20):

$$\begin{aligned}N &= (b_1 + b_2 \nu_{LT}) \epsilon_L \\ \phi &= 0\end{aligned}\tag{4.37}$$

The strain can be calculated from the known longitudinal stress and elastic properties or may be directly measured by fixing electrical resistance strain gauges on the specimen. A plot of isochromatic fringe

order as a function of longitudinal strain is shown in Figure 4.5. The straight line thus obtained has a slope,  $S_1$ , given by:

$$S_1 = b_1 + b_2 \nu_{LT} \quad (4.38)$$

(ii) A uniaxial stress,  $\sigma_T$ , in the transverse direction will produce the following principal strains:

$$\begin{aligned} \epsilon_1 &= -\nu_{TL} \epsilon_T \\ \epsilon_2 &= \epsilon_T \end{aligned} \quad (4.39)$$

The isochromatic and isoclinic response can be obtained from Eqs. (4.19) and (4.20):

$$\begin{aligned} N &= (b_1 \nu_{TL} + b_2) \epsilon_T \\ \theta &= \pi/2 \end{aligned} \quad (4.40)$$

A plot of isochromatic fringe order as a function of  $\epsilon_T$  is shown in Figure 4.6. The straight line thus obtained has a slope,  $S_2$ , given by:

$$S_2 = b_1 \nu_{TL} + b_2 \quad (4.41)$$

The Eqs. (4.38) and (4.41) can be solved for  $b_1$  and  $b_2$  as:

$$\begin{aligned} b_1 &= \frac{S_1 - S_2 \nu_{LT}}{1 - \nu_{LT} \nu_{TL}} \\ b_2 &= \frac{S_2 - S_1 \nu_{TL}}{1 - \nu_{LT} \nu_{TL}} \end{aligned} \quad (4.42)$$

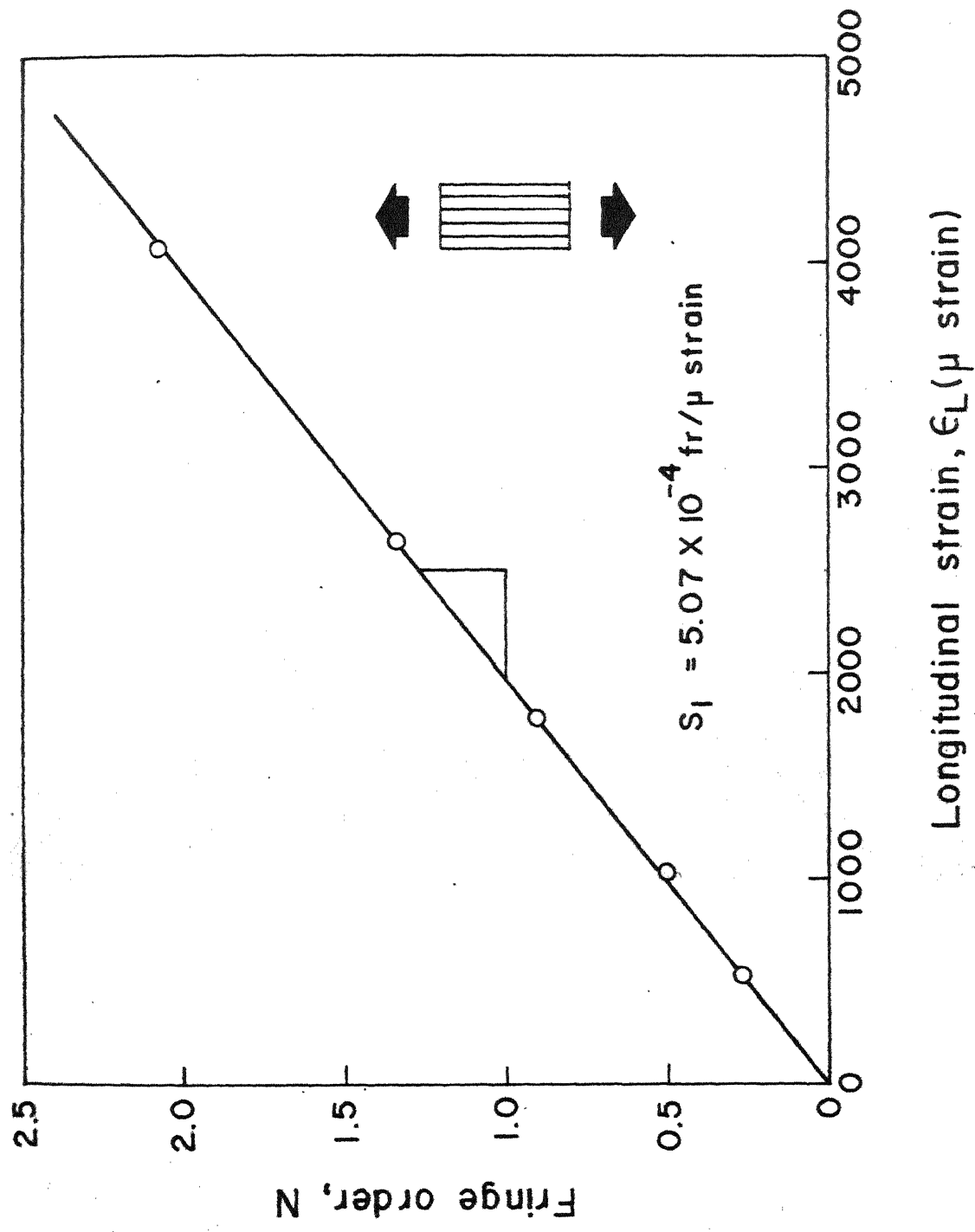
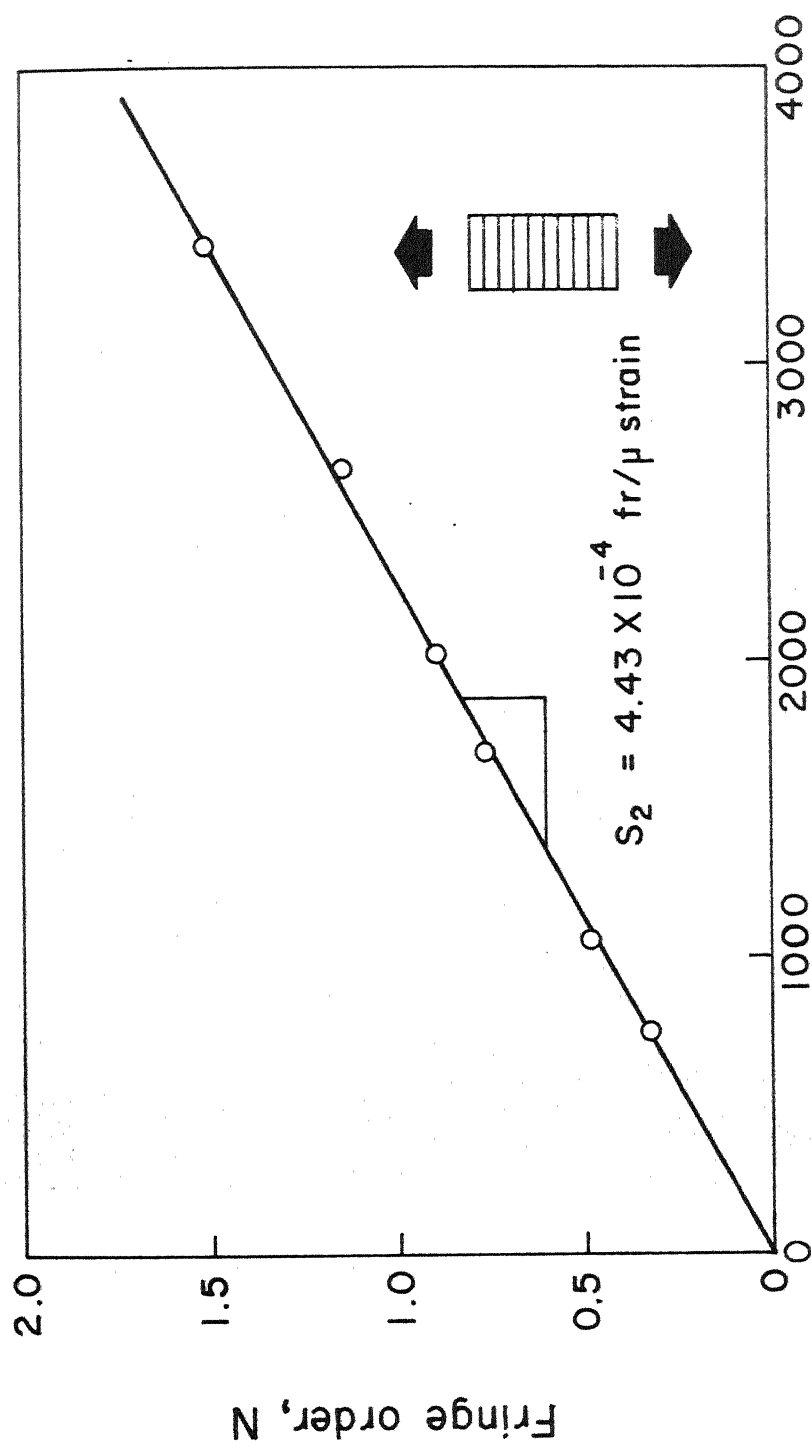


Fig. 4.5 Photoelastic characterisation - 0-degree test



Transverse strain,  $\epsilon_T$  ( $\mu$  strain)

Figure 4.6 Photoelastic characterisation - 90-degree test

The principal strain-fringe values are given in terms of  $b_1$  and  $b_2$  by Eqa. (4.21) and (4.22). Therefore, the,  $f_{\epsilon_L}$  and  $f_{\epsilon_T}$  become:

$$\begin{aligned} f_{\epsilon_L} &= \frac{1 - \nu_{LT} \nu_{TL}}{S_1 - S_2 \nu_{LT}} \\ f_{\epsilon_T} &= \frac{1 - \nu_{LT} \nu_{TL}}{S_2 - S_1 \nu_{TL}} \end{aligned} \quad (4.43)$$

- (iii) The direct determination of,  $b_3$ , or the shear strain-fringe value,  $f_{\epsilon_{LT}}$ , will require application of pure shear strain or equivalently pure shear stress. In an indirect method if the off-axis strain-fringe value,  $f'_{\epsilon_0}$ , can be determined, the  $f_{\epsilon_{LT}}$ , can be calculated from Eq. (4.34). However, due to the difficulties in applying a uniaxial strain, it was decided to calculate the shear strain-fringe value from the measured shear stress-fringe value. In view of definitions of  $f_{\epsilon_{LT}}$  and  $f_{\sigma_{LT}}$  and the relation between shear stress and strain, the relation between  $f_{\epsilon_{LT}}$  and  $f_{\sigma_{LT}}$  can be shown to be:

$$f_{\epsilon_{LT}} = \frac{f_{\sigma_{LT}}}{2 G_{LT}} \quad (4.44)$$

The method of obtaining  $f_{\sigma_{LT}}$  has already been discussed. The constant,  $b_3$ , is the reciprocal of,  $f_{\epsilon_{LT}}$ , as given by Eq. (4.23). So that:

$$b_3 = \frac{2 G_{LT}}{f_{\sigma_{LT}}} \quad (4.45)$$

The relations between the normal strain-fringe values and the normal stress-fringe values can also be obtained as:

$$f_{\epsilon L} = \frac{1 - \nu_{LT} \nu_{TL}}{\frac{E_L}{f_{\sigma L}} - \frac{E_T}{f_{\sigma T}} \nu_{LT}}$$

$$f_{\epsilon T} = \frac{1 - \nu_{LT} \nu_{TL}}{\frac{E_T}{f_{\sigma T}} - \frac{E_L}{f_{\sigma L}} \nu_{TL}} \quad (4.46)$$

The strain-fringe values and stress-fringe values for the superior, unidirectional model material have been given in Table 4.1. Some important observations on them as well as on the photoelastic constants reported by other investigators will be made in the next section.

#### 4.4. SOME IMPORTANT OBSERVATIONS

In view of the results and discussion presented in the previous section the following important observations can be made:

- (i) The variation in the strain-fringe values,  $f_{\epsilon \theta}$ , for a uniaxial stress and,  $f'_{\epsilon \theta}$ , for a uniaxial strain as shown in Figure 4.7 is less than  $\pm 10$  percent of their respective average values. This variation is much smaller compared to that in the stress-fringe value  $f_{\sigma \theta}$ , (Figure 4.2), which is nearly 100 per cent for a particular fibre orientation.



Table 4.1 Comparison of Photoelastic Properties and Anisotropic Ratios of Different Model Materials

Material	$f_{\sigma L}$ $10^3 \text{ N/}$ $\text{fr-m}$	$f_{\sigma T}$ $10^3 \text{ N/}$ $\text{fr-m}$	$f_{\sigma LT}$ $10^3 \text{ N/}$ $\text{fr-m}$	$f_{\epsilon L}$ $10^{-6} \text{ m/}$ $\text{fr}$	$f_{\epsilon T}$ $10^{-6} \text{ m/}$ $\text{fr}$	$f_{\epsilon LT}$ $10^{-6} \text{ m/}$ $\text{fr}$	$\frac{f_{\sigma L}}{f_{\sigma T}}$	$\frac{f_{\sigma T}}{f_{\sigma LT}}$	$\frac{f_{\epsilon L}}{f_{\epsilon T}}$	$\frac{f_{\epsilon T}}{f_{\epsilon LT}}$
S-glass epoxy (Ref. 26)	17.50	10.50	6.95	8.814	9.120	8.915	1.670	1.520	0.966	1.023
E-glass polyester (Ref. 27)	155.90	77.95	69.20	6.477	9.906	10.033	2.000	1.126	0.654	0.987
E-glass polyester (Present work)	108.00	45.80	35.10	9.565	9.060	10.402	2.360	1.300	1.060	0.830

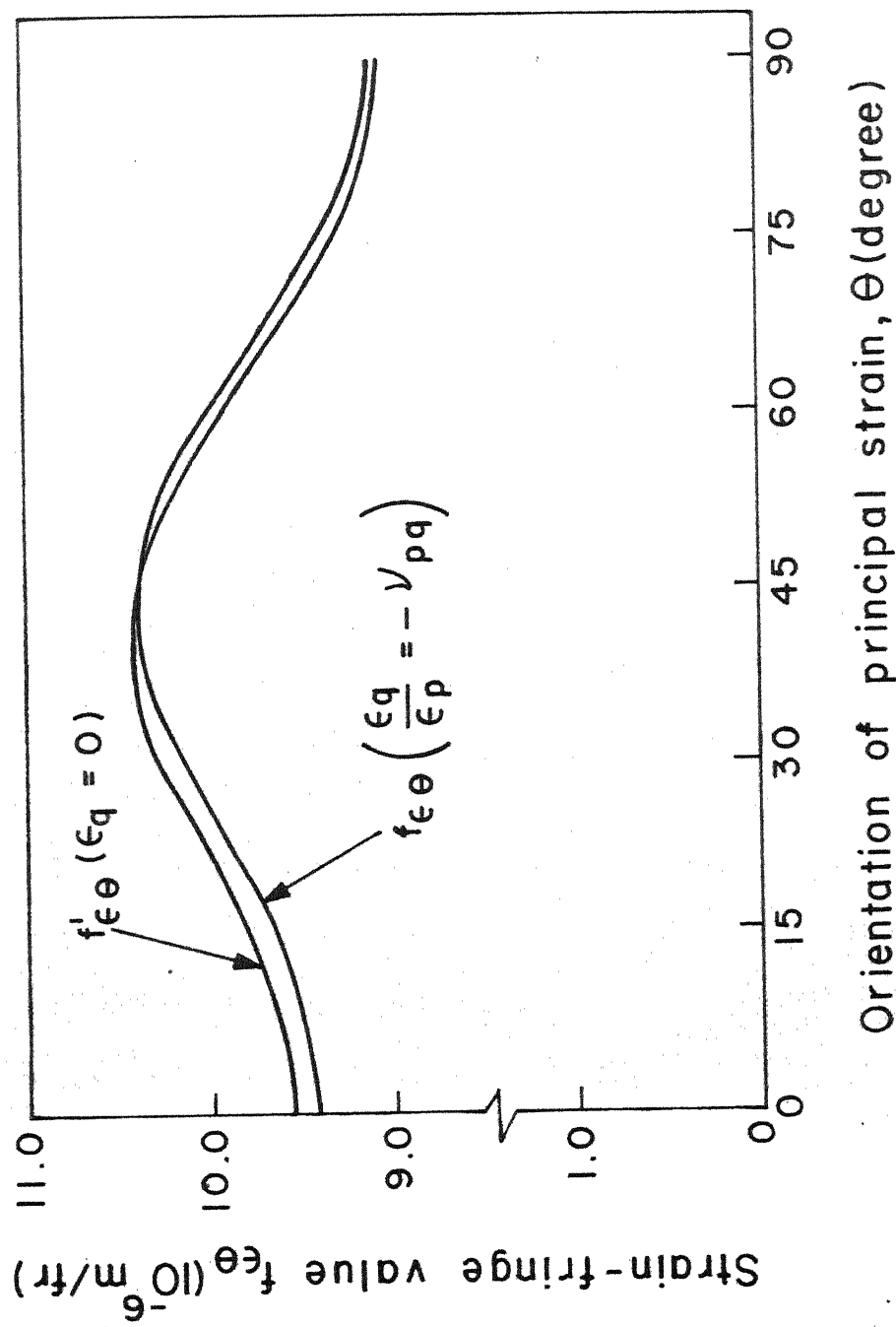


Figure 4.7 Variation of strain-fringe values with fibre orientation for unidirectional model material

- (ii) The principal strain-fringe values and stress-fringe values and their ratios have been given in Table 4.1 for the superior unidirectional model material as well as for some other materials reported in the literature. The strain-fringe values for the materials of other investigators have been calculated from the reported stress-fringe values and elastic constants using Eqs. (4.44) and (4.46). The strain-fringe values directly reported by the investigators may not be in agreement with the values calculated in this manner because of the difference in strain-optic laws. The ratios  $f_{\epsilon L}/f_{\epsilon T}$  and  $f_{\epsilon T}/f_{\epsilon LT}$  are indicative of the anisotropy with respect to strain-optic behaviour of materials, whereas the ratios  $f_{\sigma L}/f_{\sigma T}$  and  $f_{\sigma T}/f_{\sigma LT}$  are indicative of material anisotropy with respect to stress-optic behaviour. It is observed that the ratios  $f_{\epsilon L}/f_{\epsilon T}$  and  $f_{\epsilon T}/f_{\epsilon LT}$  are closer to 1.0 than the ratios  $f_{\sigma L}/f_{\sigma T}$  and  $f_{\sigma T}/f_{\sigma LT}$ . This indicates that the degree of orthotropy of materials with respect to strain-optic properties is considerably smaller than that with respect to stress-optic properties.
- (iii) In view of results shown in Figures 4.3 and 4.4, it is observed that the directions of principal birefringence (directions of isoclinics) are much

closer to the directions of principal strains than the principal stresses. The maximum angle between the principal birefringence direction and the principal strain direction is less than 5 degree where as the maximum angle between the principal birefringence direction and principal stress direction is more than 15 degree. Moreover, the variation in principal strain direction with fibre orientation is qualitatively also similar to that in the isoclinic angle.

The above observations strongly suggest that an approximate strain-optic law can be developed through which photoelastic observations can be interpreted without loosing much accuracy. An approximate strain-optic law has been developed in the next chapter.

## CHAPTER 5

### AN APPROXIMATE THEORY OF PHOTO-ORTHOTROPIC-ELASTICITY

#### 5.1 INTRODUCTION

Exact theories of photo-orthotropic-elasticity have been discussed in Chapter 4. It has been established that the photoelastic response of orthotropic composites can be accurately predicted using exact stress-optic or strain-optic laws. The exact laws require three photoelastic constants for the material which are determined experimentally. It was, however, pointed out that the exact laws are inadequate to interpret the photoelastic observations and translate them into the desired stresses or strains. An approximate strain-optic law will be derived in this chapter. A method of applying a correction to the approximate strains will also be developed which reduces the error significantly. The reasons for picking up the strain-optic law and not the stress-optic law for approximations are based on the observations made in Chapter 4. It has been observed that the birefringent composite materials exhibit a smaller degree of orthotropy with respect to strain-optic behaviour than with respect to stress-optic behaviour. It has also been observed that the directions of optical isoclinics are much closer to the principal strain directions than the principal stress directions.

Before going into the process of approximation, it will be appropriate, at this point, to examine the concept of anisotropy. Anisotropy literally means deviation from isotropic behaviour. Isotropy and anisotropy are not general properties of a material but they refer to the material behaviour with respect to a specific property only. Anisotropy of a material with respect to a particular property does not necessarily imply that the material will be anisotropic to the same degree with respect to any other property. It is in this context that the photoelastic composites are observed to be anisotropic to a smaller degree with respect to strain-optic behaviour than with respect to stress-optic behaviour. The degree of anisotropy with respect to strain-optic behaviour, as observed in Chapter 4, is small enough to justify representation of strain-optic properties by an isotropic property tensor.

## 5.2 APPROXIMATE STRAIN-OPTIC LAW

To device an approximate strain-optic law it is assumed that the fourth-order strain-optic property tensor is isotropic having only two independent strain-optic coefficients. These two constants are analogous to the two independent elastic constants for mechanically isotropic materials. The independent photoelastic constants are calculated from the constants of exact strain-

optic property tensor such that the error between the exact and approximate property tensor is minimum. This has been achieved by following the approach of Fedorov [ 38 ] used in the simplification of the study of stress waves propagation in crystals.

The approximate strain-optic property tensor,  $P_{ijkl}^0$ , is assumed to be the following most general fourth-order isotropic tensor:

$$P_{ijkl}^0 = c \delta_{ij} \delta_{kl} + a ( \delta_{ik} \delta_{jl} + \delta_{il} \delta_{jk} ) \quad (5.1)$$

where  $\delta_{ij}$  is the Kronecker delta and  $a$  and  $c$  are the independent strain-optic coefficients. The square error,  $E$ , between the approximate property tensor given by Eq. (5.1) and the exact one given by Eq. (4.7) is:

$$E = ( P_{ijkl} - P_{ijkl}^0 ) ( P_{ijkl} - P_{ijkl}^0 ) \quad (5.2)$$

The constants  $a$  and  $c$  are obtained by imposing the following conditions to minimise the error  $E$ :

$$\begin{aligned} \frac{\partial E}{\partial c} &= 0 \\ \frac{\partial E}{\partial a} &= 0 \end{aligned} \quad (5.3)$$

Substitution of Eqs. (5.1) and (5.2) into Eq. (5.3) and solving for  $a$  and  $c$  yields:

$$c = \frac{1}{15} (2 P_{iijj} - P_{ijij}) \quad (5.4)$$

$$a = \frac{1}{30} (3 P_{ijij} - P_{iijj})$$

The coefficients  $P_{ijkl}$  in Eq. (5.4) can be written in the following contracted notations consistent with those used in the Chapter 4 for transversely isotropic composite as:

$$\begin{aligned} c &= \frac{1}{15} (P_{11} + P_{22} + 4 P_{12} + 4 P_{21} + 5 P_{23} - 4 P_{66}) \\ a &= \frac{1}{30} \left[ 2 (P_{11} - P_{21}) + 2 (P_{22} - P_{12}) + 12 P_{66} \right. \\ &\quad \left. + 5 (P_{22} - P_{23}) \right] \end{aligned} \quad (5.5)$$

Approximate strain-optic relation for a plane stress case can be written in terms of  $a$  and  $c$  as follows:

$$\begin{bmatrix} N_1 \\ N_2 \\ N_3 \\ N_6 \end{bmatrix} = \begin{bmatrix} 2a+c & c & c & 0 \\ c & 2a+c & c & 0 \\ c & c & 2a+c & 0 \\ 0 & 0 & 0 & a \end{bmatrix} \begin{bmatrix} \epsilon_1 \\ \epsilon_2 \\ \epsilon_3 \\ \gamma_{12} \end{bmatrix} \quad (5.6)$$

The in-plane birefringence components can now be obtained from Eq. (5.6) and written, as follows, in terms of the resultant birefringence and birefringence direction or isoclinic angle,  $\phi$ , as was done in previous chapter:



$$N_1 - N_2 = N \cos 2\phi = 2a(\epsilon_1 - \epsilon_2) \quad (5.7)$$

$$2N_6 = N \sin 2\phi = 2a\gamma_{12}$$

The resultant birefringence and isoclinic angle can be separated as:

$$N = 2a[(\epsilon_1 - \epsilon_2)^2 + (\gamma_{12})^2]^{1/2} \quad (5.8)$$

$$\tan 2\phi = \frac{\gamma_{12}}{\epsilon_1 - \epsilon_2} \quad (5.9)$$

It may be recognised that the square root term in the Eq. (5.8) represents the difference in the in-plane principal strains. Representing the principal strain difference by  $(\epsilon_p - \epsilon_q)$ , the approximate strain-optic law may be written as:

$$\epsilon_p - \epsilon_q = N f_\epsilon \quad (5.10)$$

where  $f_\epsilon$  is the strain-fringe value of the approximating body and is equal to  $1/(2a)$ . The Eq. (5.9) implies that the directions of principal birefringence coincide with the directions of principal strains. In other words the isoclinic angle is the same as the angle between principal strain and the reference axis. This is very significant observation and, along with the approximate strain-optic law (Eq. 5.10), this will significantly simplify the problem of obtaining individual strain components.

The approximate strain-optic law, given by Eq. (5.10), contains only one photoelastic constant. Its value should be calculated from Eqs. (5.5) so that the error between approximate and exact theory is minimum. The Eqs. (5.5) gives the value 'a' (or equivalently  $\frac{1}{2f_\epsilon}$ ) in terms of six fundamental strain-optic constants namely  $P_{11}$ ,  $P_{12}$ ,  $P_{21}$ ,  $P_{22}$ ,  $P_{23}$  and  $P_{66}$ . The strain-fringe value,  $f_\epsilon$ , can be calculated if the six constants are known or if the values of their four groups as indicated in Eqs. (5.5) are known. By regrouping constants on the right hand side of Eqs. (4.17), it can be easily shown that the four groups of constants namely  $(P_{11} - P_{21})$ ,  $(P_{22} - P_{12})$ ,  $P_{66}$  and  $(P_{22} - P_{23})$  are common to Eqs. (4.17) and Eqs. (5.5). Thus Eqs. (4.17) will be quite helpful in calculating the values of these four groups. However, Eqs. (4.17) is set of only three independent equations and can be used to calculate only three groups. Therefore, an additional equation is needed to evaluate one of the groups or a combination of them. To this end attention has been focussed on the group  $(P_{22} - P_{23})$ .

It follows from Eqs. (4.11) that the term  $(P_{22} - P_{23})$  can be evaluated through an experiment in which the model is a thin 2 - 3 plane so that the birefringence  $(N_2 - N_3)$  is measured and related to strains in the 2 - 3 plane. However, a number of practical difficulties are

likely to be encountered in carrying out such an experiment due to inhomogeneity of the material (glass fibres being discrete units). It was, therefore, decided to evaluate the term  $(P_{22} - P_{23})$  through theoretical calculations. It is realised that the 2 - 3 plane behaves as an isotropic plane to in-plane loads so that a theory applicable to microscopically heterogeneous but macroscopically isotropic material can be applied to this case also. Richard and Young [39] using a self consistent approach, developed a theory for and demonstrated its applicability to an isotropic composite namely glass beads reinforced polyester resin with varying glass content. Therefore, it seems reasonable to use this theory for calculating  $(P_{22} - P_{23})$ . Following the theory, it can be shown (refer to Appendix C) that:

$$P_{22} - P_{23} = \frac{E_T}{1 + \nu_{23}} \left( X_g \frac{V_g}{f_{\sigma g}} + X_m \frac{1 - V_g}{f_{\sigma m}} \right) \quad (5.11)$$

where  $V_g$  is glass content or volume fraction;  $f_{\sigma g}$  and  $f_{\sigma m}$  are the stress-fringe values for glass and matrix material respectively;  $X_g$  and  $X_m$  are respectively the ratios of principal stress difference in glass and matrix to that in the composite. These ratios  $X_g$  and  $X_m$  can be evaluated in terms of elastic constants by following the approach of Richard and Young. The elastic constants of the isotropic composite can be determined experimentally

or estimated through self consistent approach adopted by Richard [40] . Expressions for  $X_g$  and  $X_m$  and other details concerning derivation of Eq.(5.11) have been given in Appendix C. Now, that the group  $(P_{22} - P_{23})$  is known the other groups required to calculate strain-fringe value,  $f_\epsilon$  , can be calculated using Eq. (4.17). In this manner the strain fringe value was found to be:

$$f_\epsilon = 9.90 \times 10^{-6} \text{ m/fr} \quad (5.12)$$

### 5.3 ASSESSMENT OF STRAIN-OPTIC LAWS

Photoelastic response of a material to any state of strain can now be predicted using exact or approximate strain-optic law. Predictions have been made for the superior unidirectional model material developed for photoelastic applications and whose photoelastic properties are given in Table 4.1. Wherever possible, calculations have been made for other materials reported in the literature. For the purpose of calculations it has been assumed that  $\epsilon_p$  and  $\epsilon_q$  denote maximum and minimum principal strains so that the ratio  $\epsilon_q/\epsilon_p$  can vary from  $-\infty$  to 1.

Predictions concerning isoclinic angles have been shown in Figure 5.1. Since approximate law predicts that the direction of principal birefringence coincides with that of principal strain, a plot of isoclinic angle as a function of orientation of principal strain is a

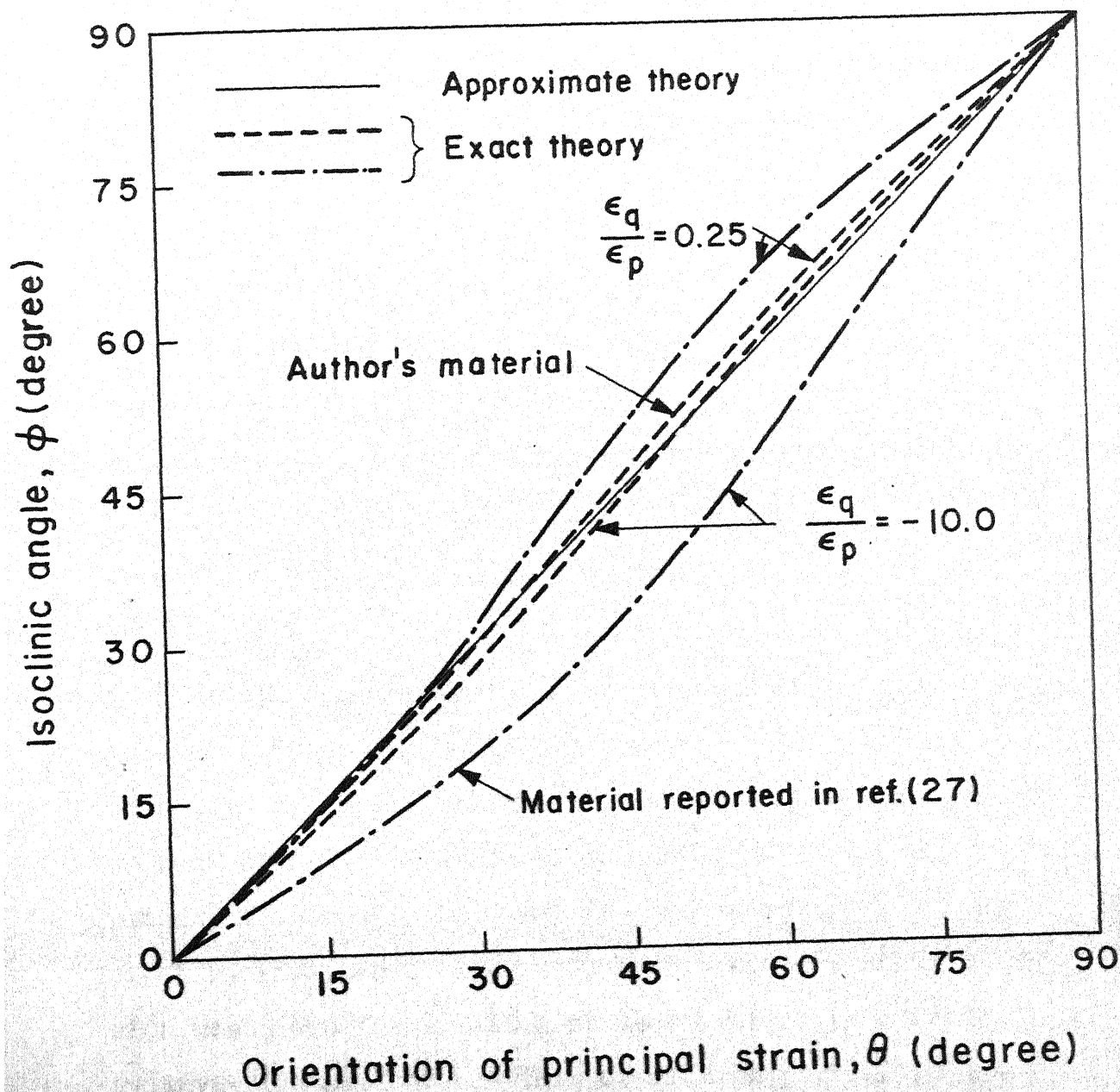


Figure 5.1 Predictions of isoclinic angle from exact and approximate theories.

straight line at 45 degree. This is true for all materials and any state of strain. However, isoclinic angle predicted by exact law depends upon both the material properties and state of strain. Isoclinic angles for two materials subjected to two widely different biaxial states of strain have been shown in Figure 5.1. It may be noted that the predictions of exact and approximate laws are very close to each other for the present material. The predictions for the material (Ref. 27) are not as good but they appear to be within permissible limits of experimental error.

Orientation of principal birefringence has been compared with the orientation of principal stress for different biaxial states of strain in Figure 5.2. In this figure all angles were measured with reference to the direction of maximum principal strain. As observed in Figure 5.1, the predictions of exact and approximate laws for principal birefringence direction are quite close to each other. It may be noted that the direction of principal stress is far away from the directions of principal birefringence or principal strain. A similar conclusion was drawn for uniaxial state of stress in a study by investigators [18]. This conclusion partially justifies the development of approximate strain-optic law and not the stress-optic law.

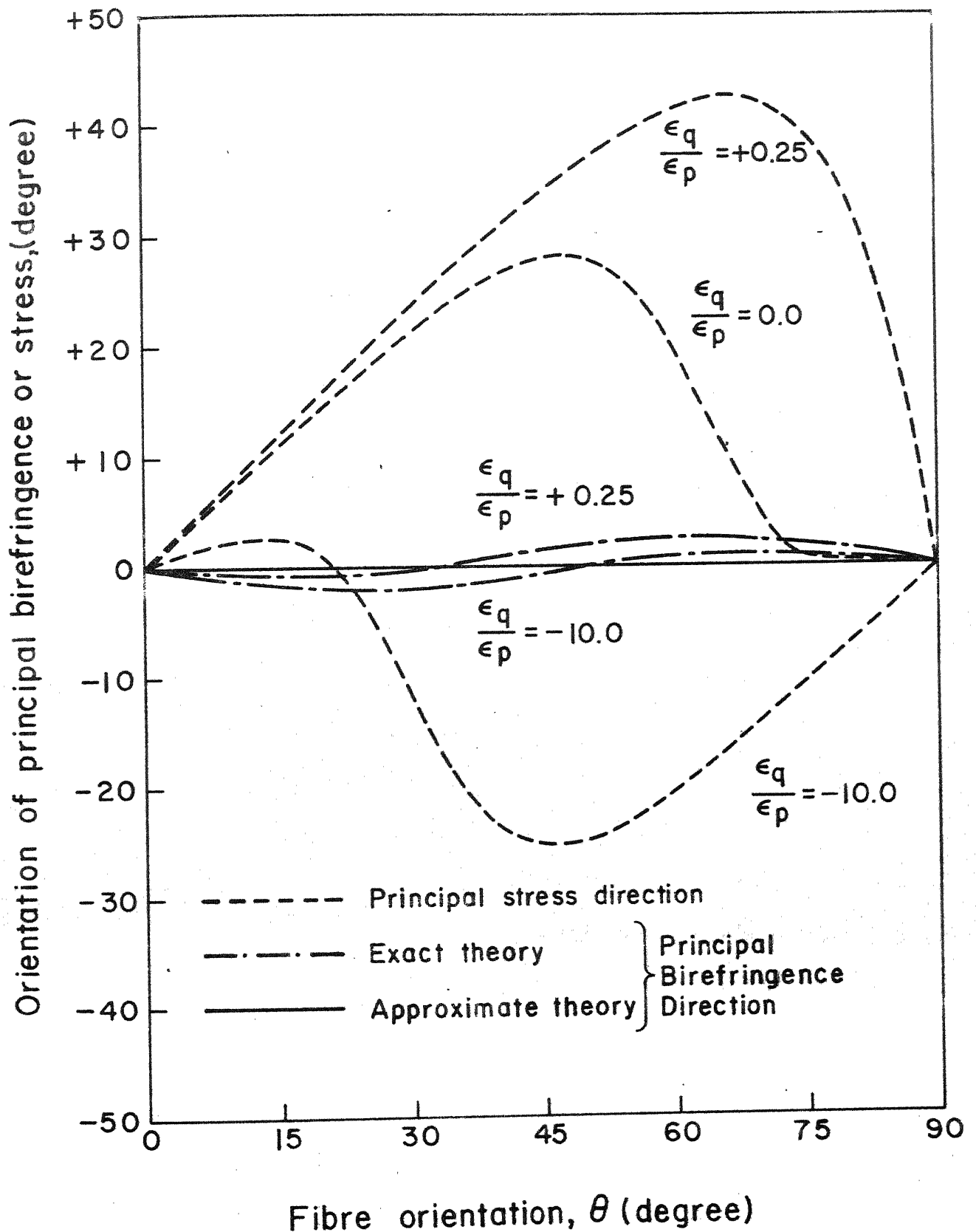


Figure 5.2 Variations in directions of principal birefringence and stress as a function of fibre orientation for different biaxial states of strain.

Predictions of the two laws regarding isochromatic fringe order have been shown in Figures 5.3 and 5.4 for four different states of strain. The approximate law predicts that the fringe order depends only on the difference in principal strains and not the orientation of principal strain with respect to the fibre direction. Variation in fringe order with fibre orientation is predicted by the exact law. It is observed that in each case the maximum difference between the predictions of the two laws is less than 10 percent. In view of the simplification that is obtained through the use of approximate law, the error may be permissible, particularly for preliminary stress analysis problems.

#### 5.4 ERROR ESTIMATION, CORRECTION AND ITS EXPERIMENTAL VERIFICATION

From the discussion in the thesis so far, it is quite clear that the photoelastic response (isochromatic fringe order and isoclinic angle) of an orthotropic material to a known state of strain can be predicted using exact and approximate strain-optic laws. It was observed in the previous section that the values of isochromatic fringe order and isoclinic angle predicted by two laws do not, in general, coincide. The difference arises because, it is implicit in the approximate law that the photoelastic response is independent of directions of principal strains.



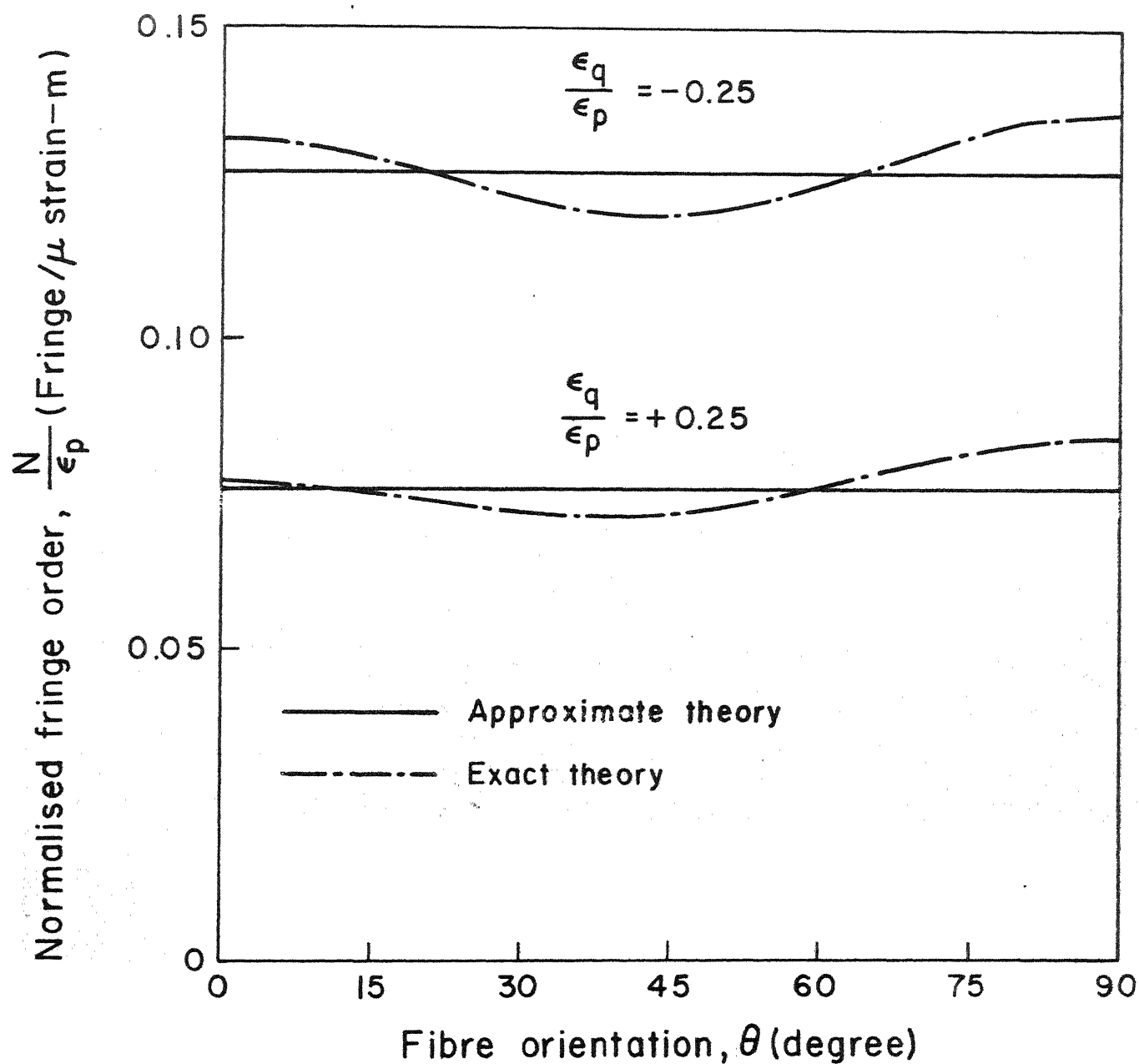


Figure 5.3 Prediction of birefringence from exact and approximate theories for principal strain ratios of  $-0.25$  and  $+0.25$

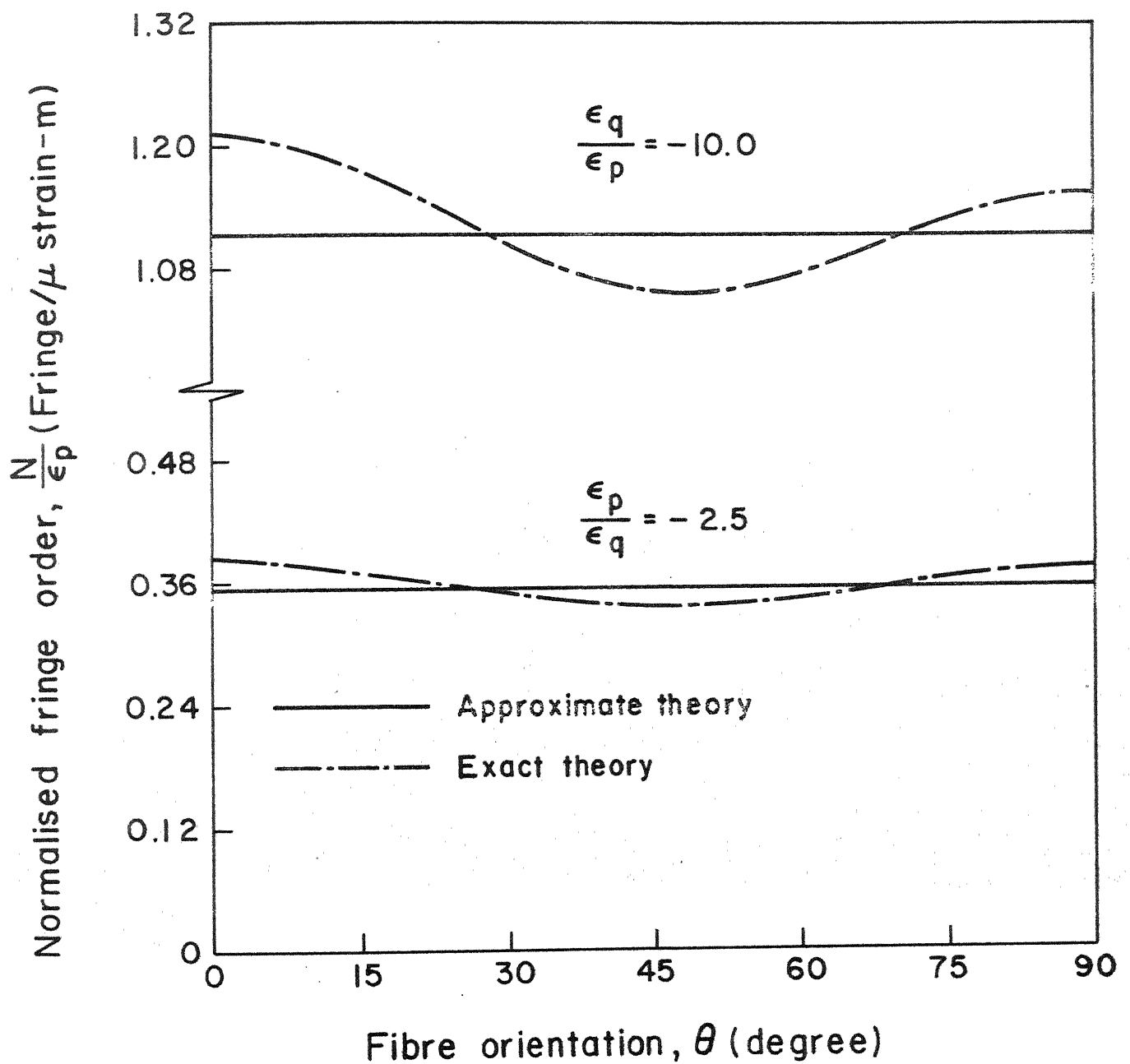


Figure 5.4 Prediction of birefringence from exact and approximate theories for principal strain ratios of -2.5 and -10.0

It is, therefore, expected that when approximate strain-optic law is used to predict magnitude and directions of principal strains from the measured values of fringe order and isoclinic angle, both the magnitude and directions of principal strains will be in error. However, it has been observed in the previous section that the maximum error in the directions of principal strains is limited to only about 5 degree and hence a correction for the same may not be essential. It will, therefore, be very desirable if a method of estimating error in the magnitudes of principal strains can be evolved.

It was intuitively felt that the exact strain-optic law and a state of strain predicted by the approximate strain-optic law may be combined to extract some useful information. In particular, it was hypothesised that the ratio of exact fringe order to approximate fringe order (calculated by substituting approximate strains in the exact strain-optic law) is same as the ratio of exact and approximate principal strain-difference. Experimental verification of the hypothesis along with other details and the procedure to be followed in the stress analysis problems has been discussed in this section.

A procedure of determining exact principal strain-difference according to the hypothesis, qualitatively stated above, really consists of the following steps:

- (i) Measure isochromatic fringe order,  $N$ , and isoclinic angle,  $\theta$ , at a point in the model for a known load.
- (ii) Using approximate strain-optic law (Eq. 5.10), approximate principal strain-difference,  $(\epsilon_p - \epsilon_q)_{ap}$  can be obtained as:

$$(\epsilon_p - \epsilon_q)_{ap} = N f_\epsilon \quad (5.13)$$

where  $N$  has been measured in step (i) and  $f_\epsilon$  is the strain-fringe value as obtained in an earlier section.

- (iii) According to approximate strain-optic law the direction of major principal strain coincides with the isoclinic so that:

$$\theta_{ap} = \theta \quad (5.14)$$

- (iv) The exact strain-optic law (Eq. 4.27) can be written in the following form:

$$N = \frac{1}{f_{\epsilon L}} \left\{ \left[ (\epsilon_p - \epsilon_q) \frac{f_{\epsilon L}}{f_{\epsilon T}} \right] - \sin^2 \theta \right. \\ \left. (\epsilon_p - \epsilon_q) \left( 1 + \frac{f_{\epsilon L}}{f_{\epsilon T}} \right)^2 \right. \\ \left. + \left[ (\epsilon_p - \epsilon_q) \frac{f_{\epsilon L}}{f_{\epsilon LT}} \sin 2 \theta \right]^2 \right\}^{1/2} \quad (5.15)$$

It is noted that in Eq. (5.15) the principal strains appear only as the difference except in one term where  $\epsilon_q$  is multiplied by the ratio  $f_{\epsilon L}/f_{\epsilon T}$ . As an approximation this term may also be assumed to be equal to the

principal strain-difference. The error introduced by this assumption will be small because the ratio  $f_{\epsilon_L}/f_{\epsilon_T}$  is close to 1. Therefore Eq. (5.15) can be written as:

$$N = \frac{\epsilon_p - \epsilon_q}{f_{\epsilon_L}} \left\{ \left[ 1 - \sin^2 \theta \left( 1 + \frac{f_{\epsilon_L}}{f_{\epsilon_T}} \right) \right]^2 + \left[ \frac{f_{\epsilon_L}}{f_{\epsilon_{LT}}} \sin 2\theta \right]^2 \right\}^{1/2} \quad (5.16)$$

It may be pointed out that if the ratios  $f_{\epsilon_L}/f_{\epsilon_T}$  and  $f_{\epsilon_L}/f_{\epsilon_{LT}}$  are approximated to 1, Eq. (5.16) will reduce to the approximate strain-optic law. By retaining the ratios  $f_{\epsilon_L}/f_{\epsilon_T}$  and  $f_{\epsilon_L}/f_{\epsilon_{LT}}$  at all places except one, Eq. (5.16) is still quite close to the exact strain-optic law.

(v) Calculate approximate fringe order,  $N_{ap}$ , by substituting  $(\epsilon_p - \epsilon_q)_{ap}$  and  $\theta_{ap}$  in Eq. (5.16).

(vi) Obtain the corrected principal strain-difference,  $(\epsilon_p - \epsilon_q)_{cr}$ , from the following relation:

$$(\epsilon_p - \epsilon_q)_{cr} = \frac{N}{N_{ap}} (\epsilon_p - \epsilon_q)_{ap} \quad (5.17)$$

Experimental verification of the hypothesis, that the  $(\epsilon_p - \epsilon_q)_{cr}$  is closer to the exact principal strain difference,  $(\epsilon_p - \epsilon_q)_{ex}$ , has been accomplished by conducting experiments on models subjected to uniaxial and biaxial states of stress, described in the following paragraphs.

Photoelastic behaviour under uniaxial state of stress has been studied using tension specimens. Fibre orientations with respect to a longitudinal edge of the specimen changed and kept at 0, 15, 30, 45, 60, 75 and 90 degree in order to obtain different states of strain for a fixed state of stress. In each case the isochromatic fringe order was measured with increasing load. A typical curve of fringe order as a function of applied stress has been shown in Figure 4.1 and was discussed earlier. The isoclinic angle was measured when the effect of initial birefringence could be neglected. The principal strains and their directions were determined by fixing strain gauges on the specimens. The strains can also be calculated from the known state of stress and the elastic constants of the material. Both the methods gave identical results. Measured values of fringe order, isoclinic angle, principal strain-difference and the direction of major principal strain have been given in Table 5.1 for a fixed state of stress (this state of stress was kept the same for all fibre orientations). Also given in Table 5.1 are the calculated values of  $(\epsilon_p - \epsilon_q)_{ap}$ ,  $(\epsilon_p - \epsilon_q)_{cr}$  and errors in the uncorrected and corrected values of principal strain-difference. It may be observed that the exact value of principal strain-difference is closer to the corrected principal strain-difference than the uncorrected one.

Table 5.1 Results of Photoelastic Analysis for a Uniaxial State of Stress

Fibre Orientation $\theta$ (degree)	*Fringe order N	*Isoclinic angle $\phi = \theta_{ap}$ (degree)	*Principal strain angle $\theta_{ex}$ (degree)	*Exact strain diff. $(\epsilon_p - \epsilon_q)_{ex}$ ( $\mu$ strain)	**Approx. strain diff. $(\epsilon_p - \epsilon_q)_{ap}$ ( $\mu$ strain)	**Corrected strain diff. $(\epsilon_p - \epsilon_q)_{cr}$ ( $\mu$ strain)	Error in uncorrected strains (percent)	Error in corrected strain (percent)
0	0.65	0	0	1747	1829	1774	-4.7	-1.5
15	1.24	30	32.8	3260	3230	3266	+0.9	-0.2
30	1.80	43	43.2	5144	4950	5150	+3.8	-0.1
45	1.90	53	50.40	6036	5320	6318	+11.9	-4.7
60	1.94	62	58.2	5720	5334	5534	+6.8	+3.3
75	1.77	72	70.3	4660	4844	4585	+4.0	+1.6
90	1.58	90	90	3980	4320	3946	+8.5	+0.9

\* Measured parameters

\*\* Calculated parameters

The last two columns show that the maximum error in uncorrected principal strain-difference (obtained from approximate strain-optic law, Eq. 5.10) is 12 percent whereas the error in corrected principal strain-difference is limited to less than 5 percent. The absolute magnitudes of error for the corrected and uncorrected strains have been presented in Figure 5.5. This clearly demonstrates that the correction indicated by Eq. (5.17) is in good agreement with experimental results.

Photoelastic behaviour under biaxial state of stress has been studied using a circular disc under diametral compression. The observations have been made for the cases when the load axis coincides with the fibre direction and when the two are at 30 degree to each other. In each case measurements concerning fringe order, isoclinic angle and state of strain have been made at three different points, whose locations are schematically shown in Figure 5.6. In both the cases the locations of the points with respect to the centre of the disc and fibre direction were the same. The directions of principal strains and principal birefringence (as indicated by isoclinics) have been shown in Figures 5.7 and 5.8. Photographs in Figure 5.9 show typical isochromatic and isoclinic fringe patterns. The actual state of strain was obtained by strain gauge measurements at the three points. The results of different



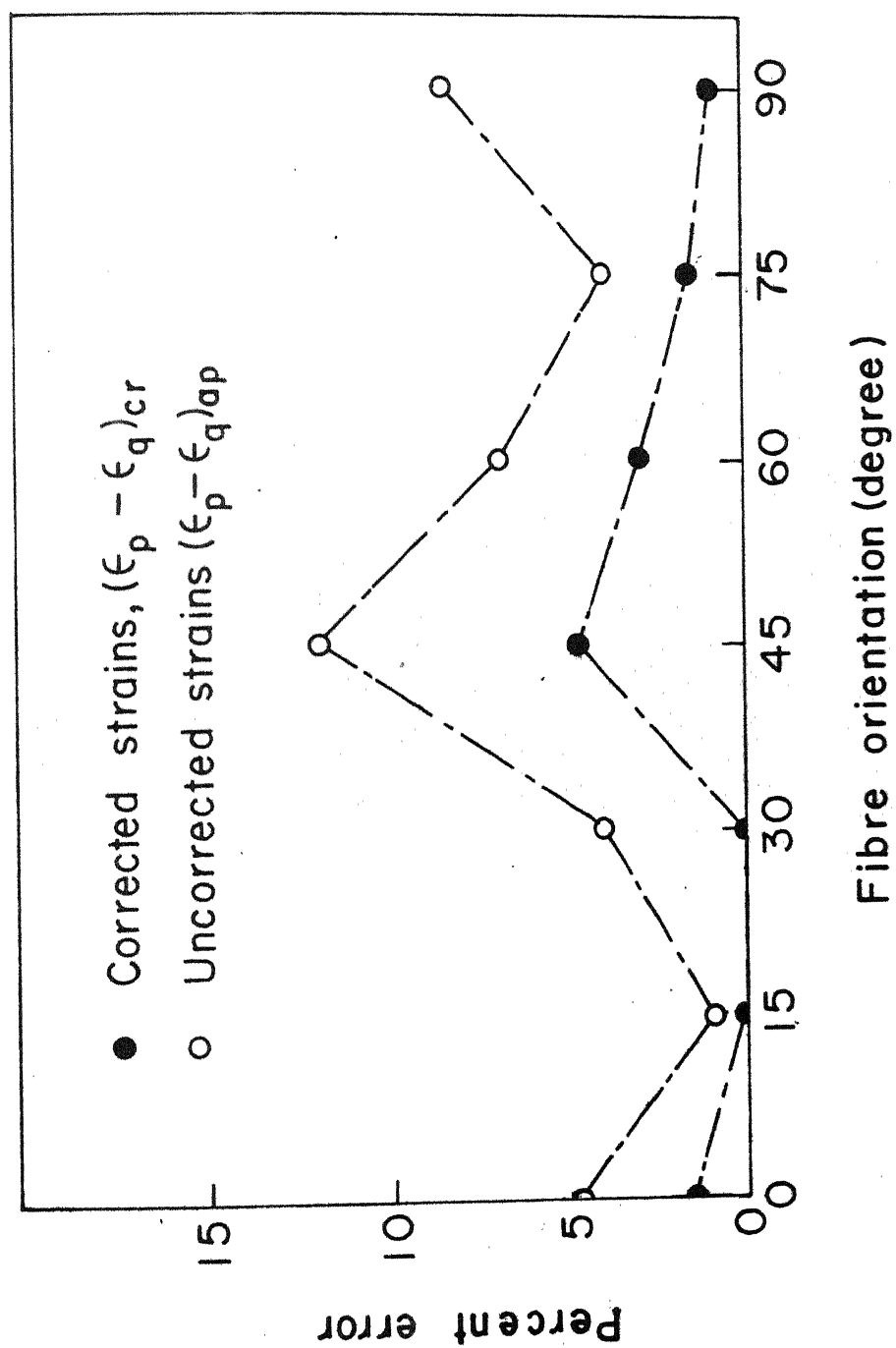


Figure 5.5 Errors in corrected and uncorrected principal strain-difference

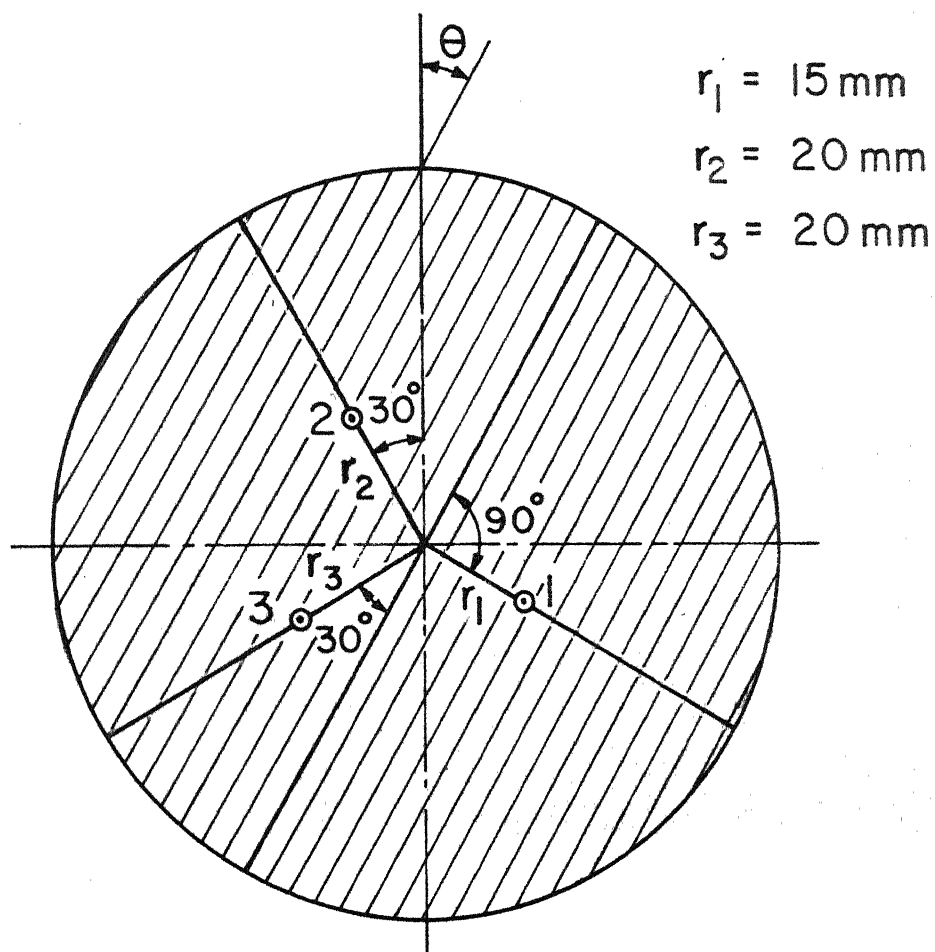


Figure 5.6 Schematic diagram showing the locations of the three points considered for analysis

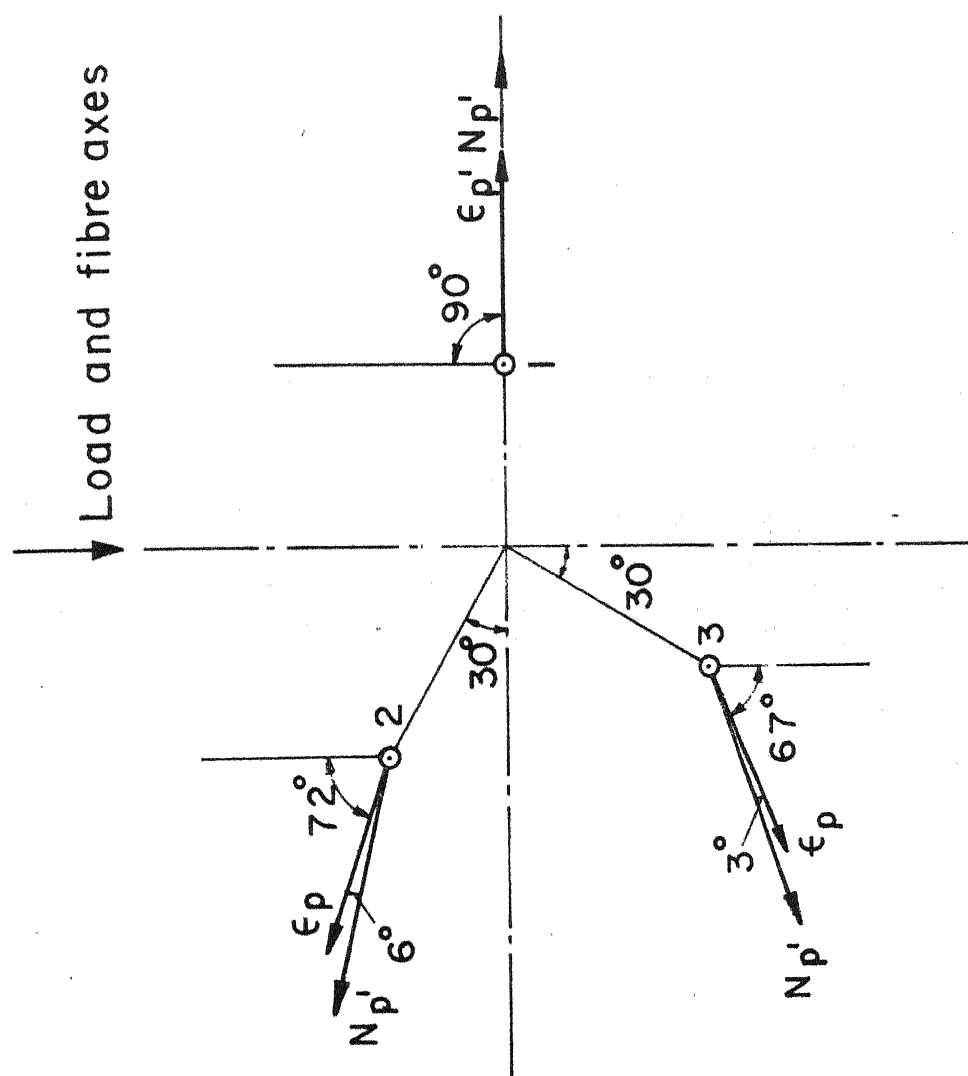


Figure 5.7 Directions of major principal strain and birefringence at the three points for disc orientation of 0-degree

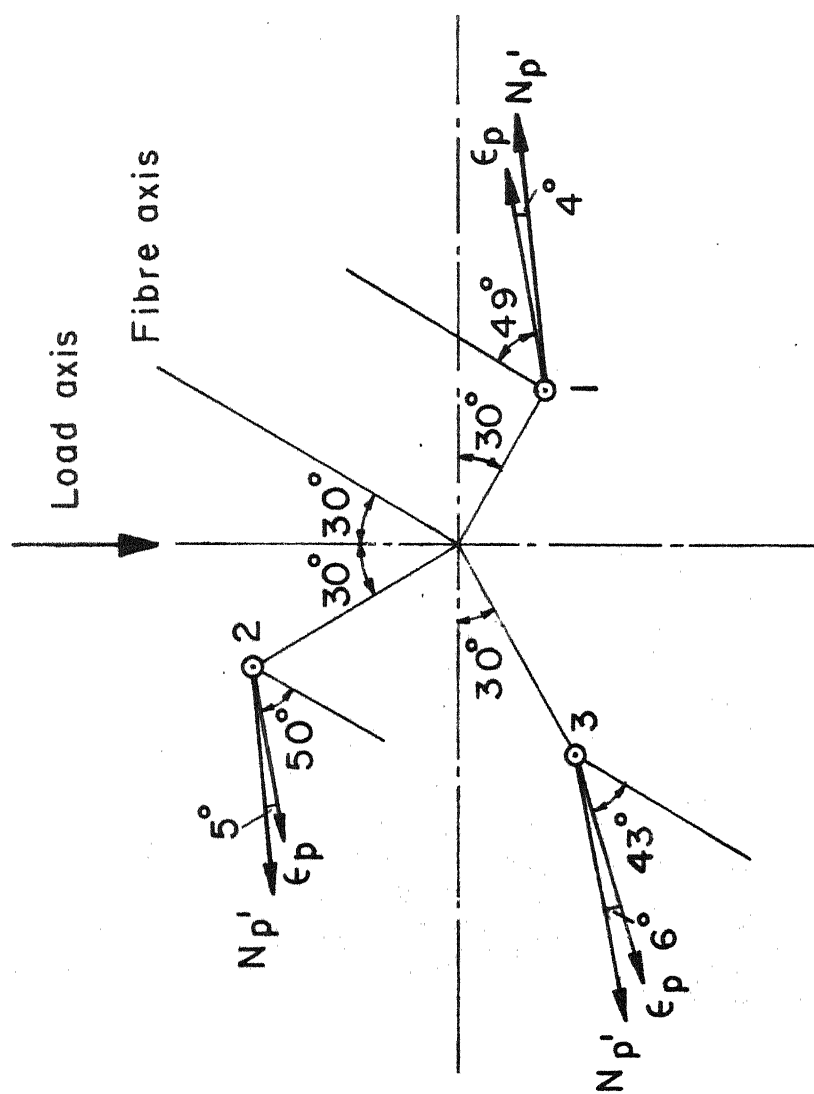


Figure 5.8 Directions of major principal strain and birefringence at the three points for disc orientation of 30-degree.

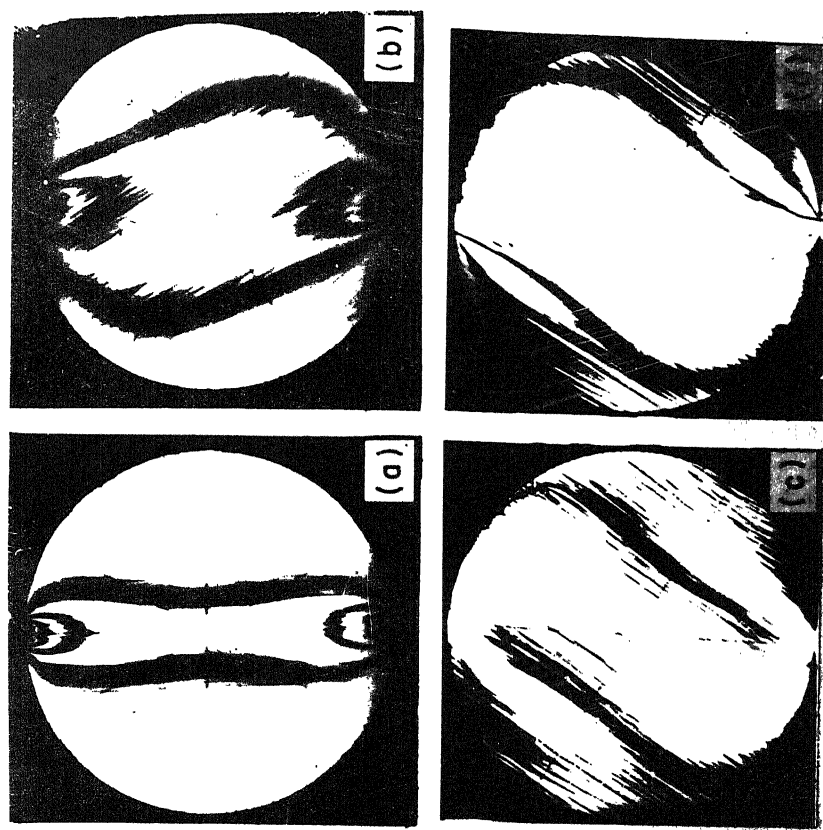


Figure 5.9 Isochromatics for disc orientation of (a)  $0^\circ$  and (b)  $30^\circ$  and isoclinics for disc orientation of  $30^\circ$  with isoclinic parameter (c)  $0^\circ$  and (d)  $15^\circ$ .

measurements and calculations have been given in Table 5.2. It is once again observed that in each case the exact principal strain-difference is closer to the correct values of principal strain-difference than the uncorrected one. It is observed that the percent error for corrected principal strain-difference is always less than that for uncorrected one. The maximum error in uncorrected principal strain difference is about  $\pm 6$  percent whereas for the corrected one it is limited to  $\pm 3$  percent only. This further demonstrates that the correction factor indicated by Eq. (5.17) is in good agreement with the experimental results for biaxial state of stress as well.

#### 5.5 CONCLUDING REMARKS

An approximate strain-optic law has been developed in this chapter which can be easily applied to obtain principal strain-difference and the directions of principal strains from the photoelastic observations. It has been experimentally established that the error in predicting the principal strain directions is limited to few degrees only whereas the error in the principal strain-difference is less than  $\pm 15$  percent. In view of the simplicity of the strain-optic law it is suggested that for preliminary stress analysis this error may be permitted. A correction factor has been developed which can be applied for a more accurate analysis. It has been experimentally established

that the correction factor indicated by Eq. (5.17) brings the corrected value of principal strain-difference within  $\pm 5$  percent of the exact principal strain-difference.

## CONCLUSIONS

Due to increasing importance of glass-fibre reinforced plastics in various industries, the present investigations were planned to obtain better understanding of the brittle coating method and the technique of transmission photoelasticity and to develop them to a state where they can be easily applied to the problems of stress analysis involving orthotropic materials. Based on the studies reported in this thesis the following conclusions can be drawn.

1. When a brittle coating analysis is carried out on the orthotropic materials, the coating cracks represent the directions of the principal strains in the specimen material underneath and not the directions of the principal stresses. This conclusion is valid for uniaxial as well as biaxial stress fields. Further, the threshold strain of the coating is not affected by the biaxiality of the stresses in the coating.
2. Optically superior photoelastic composite materials can be obtained by fulfilling the following two conditions:
  - (a) The refractive indices of the constituents of the composite should be matched as closely as possible.



- (b) The entrapped air in the composite should be minimised.
3. A poor matching of the refractive indices results into the following undesirable effects:
- (a) A parallel beam of light passing through the model appears smeared in the direction perpendicular to the fibres.
  - (b) Sharp boundaries of an object, when viewed through the model, appear smeared, again, in the direction perpendicular to the fibres. As a consequence very closely spaced straight parallel lines will not appear distinct.
  - (c) White light passing through the model will be split in its colours and exhibits a double spectrum symmetrical about the centre line.

The above effects are undesirable for photoelastic applications. The first two cause a reduction in the sharpness of isoclinic and isochromatic fringes. The third one will interfere in the analysis if white light is used.

It is suggested that the matching of the refractive indices be judged by the absence of above effects and not by visual inspection for transparency.

4. An experimental assessment of the exact theories of photo-orthotropic-elasticity (including a strain-optic law derived in the present work) shows that the photo-elastic response of orthotropic materials can be quite accurately predicted through these theories. However, no theory permits, evaluation of the individual strain or stress components or even the difference between their principal values from birefringence measured in a polariscope. The directions of principal stresses or strains also can not be established.
5. An approximate strain-optic law has been derived from an exact strain-optic law which in turn was derived from the well established theory of photo-elasticity of crystals. This law can be easily applied to obtain principal strains from the photoelastic observations. It has been experimentally established that the error in predicting the principal strain directions is limited to few degree only, and the error in principal strain-difference is less than  $\pm 15$  per cent.
6. A method has been developed by which a correction can be made in the approximate value of principal strain-difference. It has been experimentally established that the corrected value of the principal strain - difference is within  $\pm 5$  per cent of the exact principal strain-difference.

## REFERENCES

1. Lekhnitskii, S.G., Theory of Elasticity of an Anisotropic Elastic Body, translation, Holden-Day, Inc., San Francisco (1963).
2. Savin, G.N., Stress Concentrations around Holes, translation, Pergamon Press, New York (1961).
3. Konish, H.J. and Whitney, J.M., "Approximate Stresses in an Orthotropic Plate Containing a Circular Hole," J. of Comp. Mat., Vol. 9, p. 157 (1975).
4. Okubo, H., "The Stress Distribution in an Aelotropic Circular Disk Compressed Diametrically," J. of Mathematics and Physics, Vol. 31, p. 75 (1952).
5. Sarkar, K. and Sinha, P.K., "Stresses in Diametrically Compressed Composite Circular Discs," Trans. JSCM, Vol. 1, p. 17 (1975).
6. Al-Dabbagh, A., Finite Element Stress Analysis for Anisotropic Solids, Ph.D. Thesis, Dept. of Civil Engg., The University of Michigan, Ann Arbor (1970).
7. Sanford, R.J. and Beaubien, L.A., "Stress Analysis of a Complex Part: Photoelasticity vs. Finite Elements," Experimental Mechanics, Vol. 17, p. 441 (1977).
8. Daniel, I.M., Liber, T. and Chamis, C.C., "Measurement of Residual Strains in Boron-Epoxy and Glass-Epoxy Laminates," ASTM-STP 580, p. 340 (1975).
9. Rowlands, R.E. and Daniel, I.M., "Application of Holography to Anisotropic Composite Plates," Experimental Mechanics, Vol. 12, p. 75 (1972).
10. Pipes, R.B. and Daniel, I.M., "Moire Analysis of Interlaminar Shear Edge Effect in Laminated Composites," J. of Comp. Mat., Vol. 5, p. 225 (1971).
11. Daniel, I.M. and Rowlands, R.E., "Determination of Strain-Concentrations in Composites by Moire Technique," J. of Comp. Mat., Vol. 5, p. 250 (1971).
12. Daniel, I.M., Rowlands, R.E. and Post, D., "Strain-Analysis of Composites by Moire-Methods," Experimental Mechanics, Vol. 13, p. 246 (1973).

13. Cunningham, J.H. and Yavorsky, J.M., "The Brittle Lacquer Technique of Stress Analysis as Applied to Anisotropic Materials," Proc. SESA, Vol. XIV, p. 101 (1957).
14. Dally, J.W. and Alfirevich, I., "Application of Birefringent Coatings to Glass-Fibre-Reinforced Plastics," Experimental Mechanics, Vol. 9, p. 97 (1969).
15. Pipes, R.B. and Dalley, J.W., "On the Birefringent-Coating Method of Stress Analysis of Fibre-Reinforced Laminated Composites," Experimental Mechanics, Vol. 12, p. 272 (1972).
16. Horridge, G.A., "A Polarised Light Study of Glass Fibre Laminates," Brit. J. Appl. Phys., Vol. 6, p. 314 (1955).
17. Pih, H. and Knight, C.E., "Photoelastic Analysis of Anisotropic Fibre Reinforced Composites," J. of Comp. Mat., Vol. 3, p. 94 (1969).
18. Agarwal, B.D. and Chaturvedi, S.K., "Improved Birefringent Composites and Assessment of Photoelastic Theories," To appear in Fibre Science and Technology.
19. Sampson, R.C., "A Stress-Optic Law for Photoelastic Analysis of Orthotropic Composites," Experimental Mechanics, Vol. 10, p. 210 (1970).
20. Dally, J.W. and Prabhakaran, R., "Photo-Orthotropic-Elasticity," Experimental Mechanics, Vol. 11, p. 346 (1971).
21. Prabhakaran, R., "The Interpretation of Isoclinics in Photo-Orthotropic-Elasticity," Experimental Mechanics, Vol. 16, p. 6 (1976).
22. Bert, C.W., "Theory of Photoelasticity for Birefringent Filamentary Composites," Fibre Science and Technology, Vol. 5, p. 165 (1972).
23. Pockels, F., Lehrbuch der Kristalloptik, B.G. Teubner, Leipzig, Germany (1906).
24. Bhagavantam, S., Crystal Symmetry and Physical Properties of Crystals, Academic Press, London (1966).

25. Knight, C.E. and Pih, H., "Orthotropic Stress-Optic Law for Plane Stress Photoelasticity of Composite Materials," *Fibre Science and Technology*, Vol. 9, p. 297 (1976).
26. Pipes, R.B. and Rose, J.L., "Strain-Optic Law for a Certain Class of Birefringent Composites," *Experimental Mechanics*, Vol. 14, p. 355 (1974).
27. Prabhakaran, R., "Strain-Optic Law for Orthotropic Model Materials," *AIAA Journal*, Vol. 13, p. 723 (1975).
28. Pipes, R.B. and Dalley, J.W., "On Fibre-Reinforced Birefringent Composite Materials," *Experimental Mechanics*, Vol. 13, p. 348 (1973).
29. Mittal, R.K., "On the Effect of Residual Birefringence in Anisotropic Photoelastic Materials," *Strain*, Vol. 11, p. 55 (1975).
30. Cernosek, J., "On Photoelastic Response of Composites," *Experimental Mechanics*, Vol. 15, p. 354 (1975).
31. Dally, J.W., Link, J.A. and Prabhakaran, R., "A Photoelastic Study of Stress-Waves in Fibre-Reinforced Composites," *Proc. 12th Midwestern Mech. Conf., Developments in Mechanics*, Vol. 6, p. 937 (1971).
32. Rowlands, R.E., Daniel, I.M. and Prabhakaran, R., "Wave Motion in Anisotropic Media by Dynamic Photo-mechanics," *Experimental Mechanics*, Vol. 14, p. 433 (1974).
33. Ram Chand, "Development of Brittle Lacquer from Indigenous Materials for Experimental Stress Analysis," M.Tech. Thesis, Indian Institute of Technology, Kanpur (India) (1968).
34. Principles of Stress-Coat, A Manual for the Use with the Brittle Coating Stress Analysis Method, Magnaflux Corporation, Chicago, Ill., p. 55 (1955).
35. Jones, R.M., *Mechanics of Composite Materials*, Scripta Book Company, Washington, D.C. (1975).
36. Durelli, A.J., Phillips, E.A. and Tsao, C.H., *Introduction to Theoretical and Experimental Analysis of Stress and Strain*, McGraw-Hill Book Company, New York (1958).

37. Dally, J.W. and Riley, W.F., *Experimental Stress Analysis*, McGraw-Hill Book Company, New York (1965).
38. Fedorov, F.I., *Theory of Elastic Waves in Crystals*, translation, Plenum Press, New York (1968).
39. Richard, T.G. and Young, W.C., "Birefringent Response of a Potential Photoelastic Material with Variable Elastic Properties," *Experimental Mechanics*, Vol. 15, p. 226, (1975).
40. Richard, T.G., "The Mechanical Behaviour of a Solid Microsphere Filled Composites," *J. of Comp. Mat.* Vol. 9, p. 108 (1975).
41. Bhagvantam, S., "Photoelastic Properties of Crystals: Some New Results," *Acta Crystallographica*, Vol. 5, p. 591 (1952).
42. Hill, R., "Elastic Properties of Reinforced Solids; Some Theoretical Principles," *J. of Mech. and Phys. of Solids*, Vol. 11, p. 357 (1963).
43. Hill, R., "Self-Consistent Mechanics of Composite Materials," *J. of Mech. and Phys. of Solids*, Vol. 13, p. 213 (1965).

## APPENDIX A

### TRANSFORMATION RELATIONS FOR STRESSES, STRAINS AND MATERIAL PROPERTIES

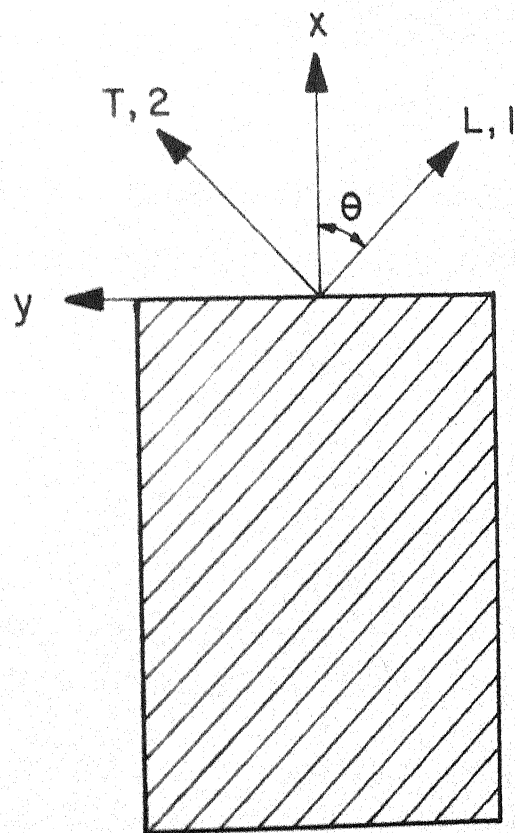
For an orthotropic lamina in the 1-2 plane (or L-T plane where L and T are the longitudinal and transverse symmetry axes of the material) as shown in Figure A.1, the strain-stress relation, in terms of engineering constants, for a plane stress state may be written as [35] :

$$\begin{bmatrix} \epsilon_1 \\ \epsilon_2 \\ \gamma_{12} \end{bmatrix} = \begin{bmatrix} \frac{1}{E_1} & -\frac{\nu_{21}}{E_2} & 0 \\ -\frac{\nu_{12}}{E_1} & \frac{1}{E_2} & 0 \\ 0 & 0 & \frac{1}{G_{12}} \end{bmatrix} \begin{bmatrix} \sigma_1 \\ \sigma_2 \\ \tau_{12} \end{bmatrix} \quad (\text{A.1})$$

If an axis normal to 1-2 plane is designated as 3, the Eq. (A.1) needs to be supplemented by the following equations:

$$\begin{aligned} \epsilon_3 &= -\frac{\nu_{31}}{E_3} \sigma_1 - \frac{\nu_{32}}{E_3} \sigma_2 \\ \gamma_{23} &= 0 \\ \gamma_{13} &= 0 \end{aligned} \quad (\text{A.2})$$

The strain-stress relation as given by Eq. (A.1) is referred to the principal material directions. However, the coordinate axes chosen for problems often do not coincide with the principal directions of orthotropy.



L-T Material symmetry axes

Figure A.1 An orthotropic plane lamina



It is, therefore, necessary to transform the strain-stress relations from one coordinate system to another.

Let there be another X - Y coordinate system making an angle  $\theta$  from the 1 or L - axis, the transformations for the stresses and strains can be written as:

$$\begin{bmatrix} \sigma_x \\ \sigma_y \\ \tau_{xy} \end{bmatrix} = [T] \begin{bmatrix} \sigma_1 \\ \sigma_2 \\ \tau_{12} \end{bmatrix} \quad (A.3)$$

$$\begin{bmatrix} \epsilon_x \\ \epsilon_y \\ \frac{\gamma_{xy}}{2} \end{bmatrix} = [T] \begin{bmatrix} \epsilon_1 \\ \epsilon_2 \\ \frac{\gamma_{12}}{2} \end{bmatrix} \quad (A.4)$$

where  $[T]$  is a transformation matrix given as:

$$[T] = \begin{bmatrix} \cos^2 \theta & \sin^2 \theta & 2 \sin \theta \cos \theta \\ \sin^2 \theta & \cos^2 \theta & -2 \sin \theta \cos \theta \\ -\sin \theta \cos \theta & \sin \theta \cos \theta & \cos^2 \theta - \sin^2 \theta \end{bmatrix} \quad (A.5)$$

The strain-stress relation, (A.1) in X - Y coordinate system is:

$$\begin{bmatrix} \epsilon_x \\ \epsilon_y \\ \gamma_{xy} \end{bmatrix} = \begin{bmatrix} \frac{1}{E_x} & -\frac{\nu_{yx}}{E_y} & -\frac{m_x}{E_L} \\ -\frac{\nu_{xy}}{E_x} & \frac{1}{E_y} & -\frac{m_y}{E_L} \\ -\frac{m_x}{E_L} & -\frac{m_y}{E_L} & \frac{1}{G_{xy}} \end{bmatrix} \begin{bmatrix} \sigma_x \\ \sigma_y \\ \tau_{xy} \end{bmatrix} \quad (A.6)$$

And the transformed engineering constants in terms of principal material-properties can be given as:

$$\begin{aligned} \frac{E_L}{E_x} &= \cos^4 \theta + \frac{E_L}{E_T} \sin^4 \theta + \frac{1}{4} \left( \frac{E_L}{G_{LT}} - 2 \nu_{LT} \right) \sin^2 2 \theta \\ \frac{E_L}{E_y} &= \sin^4 \theta + \frac{E_L}{E_T} \cos^4 \theta + \frac{1}{4} \left( \frac{E_L}{G_{LT}} - 2 \nu_{LT} \right) \sin^2 2 \theta \\ m_x &= \sin 2 \theta \left[ \nu_{LT} + \frac{E_L}{E_T} - \frac{E_L}{2 G_{LT}} - \cos^2 \theta \left( 1 + 2 \nu_{LT} + \frac{E_L}{E_T} - \frac{E_L}{G_{LT}} \right) \right] \\ m_y &= \sin 2 \theta \left[ \nu_{LT} + \frac{E_L}{E_T} - \frac{E_L}{2 G_{LT}} - \sin^2 \theta \left( 1 + 2 \nu_{LT} + \frac{E_L}{E_T} - \frac{E_L}{G_{LT}} \right) \right] \\ \nu_{xy} &= \frac{E_x}{E_L} \left[ \nu_{LT} - \frac{1}{4} \left( 1 + 2 \nu_{LT} + \frac{E_L}{E_T} - \frac{E_L}{G_{LT}} \right) \sin^2 2 \theta \right] \\ \frac{G_{LT}}{G_{xy}} &= \frac{G_{LT}}{E_L} \left[ 1 + 2 \nu_{LT} + \frac{E_L}{E_T} - \left( 1 + 2 \nu_{LT} + \frac{E_L}{E_T} - \frac{E_L}{G_{LT}} \right) \cos^2 2 \theta \right] \\ &\text{and} \\ \frac{\nu_{xy}}{E_x} &= \frac{\nu_{yx}}{E_y} \end{aligned} \quad (A.7)$$

## APPENDIX B

### FAILURE THEORY

In order to predict stresses in the specimen from observations of the crack patterns in the coating, some coating failure law must be utilised. Three laws of failure - maximum strain theory, maximum stress theory and the Mohr theory - have in the past been considered to represent the behaviour of coating. The maximum-strain and the maximum stress theories are not verified experimentally. The Mohr theory of failure is frequently employed to predict failure stresses in materials for which the ultimate compressive strength ( $\sigma_{uc}$ ) is much greater than the ultimate tensile strength ( $\sigma_{ut}$ ). Since it is well known that the compressive strength of a brittle coating greatly exceeds its tensile strength, the Mohr theory of failure would be appropriate for predicting its failure.

In this application of the Mohr theory of failure, three important cases arise:

- (i) For biaxial tension stress state ( $\sigma_p^c > \sigma_q^c > 0$ ), failure of the coating occurs when

$$\frac{\sigma_p^c}{\sigma_{ut}^c} \geq 1 \quad (B.1)$$

For this case the predictions of Mohr theory coincide with those of maximum stress theory of failure.

- (ii) For tension - compression state ( $\sigma_p^c > 0 > \sigma_q^c$ ) the failure relationship becomes:

$$\frac{\sigma_p^c}{\sigma_{ut}^c} - \frac{\sigma_q^c}{\sigma_{uc}^c} \geq 1 \quad (B.2)$$

- (iii) For biaxial compression state ( $0 > \sigma_p^c > \sigma_q^c$ ) the failure equation will be

$$-\frac{\sigma_q^c}{\sigma_{uc}^c} \geq 1 \quad (B.3)$$

In this formulation it is usual to assume that

$$\frac{\sigma_{uc}^c}{\sigma_{ut}^c} = K \quad (B.4)$$

In order to obtain the coating stresses from these failure equations, it will be necessary to evaluate the tensile and compressive strengths of the coating. Ultimate tensile strength of the coating is obtained by applying coating on a cantilever beam of the specimen material. The stresses in the beam under an end deflection are:

$$\begin{aligned} \sigma_L^S &= E_L^S \epsilon_L^S \\ \sigma_T^S &= 0 \end{aligned} \quad (B.5)$$

The minimum strain at which a crack appears at any point is given by  $\epsilon_L^S = \epsilon_t^*$ , where,  $\epsilon_t^*$ , is the threshold strain of the coating. Now introducing these

conditions in Eqs. (2.7) and solving for coating stresses, the ultimate tensile strength of coating is obtained as:

$$\sigma_{ut}^c = \sigma_p^c = \frac{E^c}{(1 - \nu^c)^2} (1 - \nu^c \nu_{LT}^s) \epsilon_t^* \quad (B.6)$$

The stress  $\sigma_q^c$  is given as:

$$\sigma_q^c = \frac{E^c}{(1 - \nu^c)^2} (\nu^c - \nu_{LT}^s) \epsilon_t^* \quad (B.7)$$

It may be noted that uniaxial stress in the specimen produces biaxial stresses in the coating due to mismatch between Poisson's ratios of the coating and the specimen. It is established practice to calculate  $\sigma_{ut}^c$  from Eq. (B.6) because the value of  $\sigma_q^c$  given by (B.7) is comparatively very small. Further, it has been established in Chapter - 2 that the threshold strain,  $\epsilon_t^*$ , is not affected by the biaxiality of stresses in the coating.

## APPENDIX C

### EVALUATION OF STRAIN - OPTIC PROPERTY ( $P_{22} - P_{23}$ )

As discussed in Chapter 5, the 2-3 plane of transversely isotropic composite behaves macroscopically as an isotropic plane to in-plane loads so that a theory applicable to microscopically heterogeneous but macroscopically isotropic material can be applied to obtain elastic and photoelastic properties of such a composite. Richard and Young [39] developed a composite which behaves in an isotropic, homogeneous manner on a macroscopic scale. The constituents of this composite are solid-glass microspheres embedded in a polyester matrix. The composites with variable mechanical and optical properties were obtained by changing the volume fractions of the constituents. For predicting the photoelastic properties of such composites, a theory has also been developed by them. According to this theory, the stress-fringe value  $f_{\sigma c}$  of the isotropic composite can be given as:

$$f_{\sigma c} = \frac{1}{X_g \frac{V_g}{f_{\sigma g}} + X_m \frac{1 - V_g}{f_{\sigma m}}} \quad (C.1)$$

where  $V_g$  is glass content;  $f_{\sigma g}$  and  $f_{\sigma m}$  are the stress-fringe values for the glass and matrix respectively, and

$X_g$  and  $X_m$  are respectively the ratios of principal stress difference in glass and matrix to that in the composite.

The values of  $X_g$  and  $X_m$  can be given as:

$$X_g = \frac{(\sigma_p - \sigma_q)_g}{(\sigma_p - \sigma_q)_c} = \frac{\sigma_{xg} - \sigma_{yg}}{\sigma_{xc}} \quad (C.2)$$

$$X_m = \frac{(\sigma_p - \sigma_q)_m}{(\sigma_p - \sigma_q)_c} = \frac{\sigma_{xm} - \sigma_{ym}}{\sigma_{xc}}$$

In these expressions the average coordinate stresses  $\sigma_{xg}$ ,  $\sigma_{yg}$ ,  $\sigma_{xm}$  and  $\sigma_{ym}$  can be evaluated by the following relations:

$$\sigma_{xg} = \frac{\sigma_{xc} E_g}{V_g (E_g + E_m R_3)}$$

$$\sigma_{yg} = \frac{\sigma_{xg} E_m}{E_c R_1} [v_g E_T - v_{23} E_g + (v_m E_T - v_{23} E_m) R_3]$$

$$\sigma_{xm} = - \frac{\sigma_{xc} E_m R_3}{(1 - V_g)(E_g + E_m R_3)} \quad (C.3)$$

$$\sigma_{ym} = \frac{\sigma_{xm} E_g}{E_c R_2} [v_g E_T - v_{23} E_g + (v_m E_T - v_{23} E_m) R_3]$$

where:

$$R_1 = E_m - E_g$$

$$R_2 = v_m E_g - v_g E_m \quad (C.4)$$

$$R_3 = \frac{(v_g E_T - v_{23} E_g) R_2 + (E_T - E_g) R_1}{(v_{23} E_m - v_m E_T) R_2 + (E_m - E_T) R_1}$$

Evaluation of average coordinate stresses given by Eq. (C.3) will require the values of elastic constants of the constituents together with the transverse modulus  $E_T$  and Poisson's ratio,  $\nu_{23}$ , of the composite. Due to practical difficulties associated with the direct determination of  $\nu_{23}$ , it was decided to calculate it theoretically following Richard [40]. Richard has shown that the mechanical properties of glass-microsphere-filled composite can be evaluated with a reasonable degree of accuracy using a self-consistent approach proposed by Hill [42, 43]. The properties of constituents for uni-directional model material developed in the present work are given in Table C.1. Knowing the constituents properties, volume fraction of glass fibres and the elastic properties  $E_T$  and  $\nu_{23}$ , the stress-fringe value,  $f_{\sigma c}$ , for a 2-3 plane-composite (light passes normal to 2-3 plane) can be evaluated from Eq. (C.1). The strain-optic property,  $(P_{22} - P_{23})$ , can be calculated from the following expression:

$$(P_{22} - P_{23}) = \frac{1}{f_{\epsilon c}} = \frac{E_T}{1 + \nu_{23}} \cdot \frac{1}{f_{\sigma c}} \quad (C.5)$$

Substitution of the Eq. (C.1) into (C.5) will yield:

$$(P_{22} - P_{23}) = \frac{E_T}{1 + \nu_{23}} \left[ X_g \frac{\nu_g}{f_{\sigma g}} + X_m \frac{1 - \nu_g}{f_{\sigma m}} \right] \quad (C.6)$$

The calculated properties,  $\nu_{23}$  and  $(P_{22} - P_{23})$  for uni-directional material ( $\nu_g = 0.165$ ) were found to be 0.34 and  $0.1016 \times 10^6$  fr/m respectively.



Table C.1 Properties of the Constituents of  
Unidirectional Model Material

Material	*Stress-fringe Value $10^3$ N/fr-m	Modulus of Elasticity $10^6$ N/m <sup>2</sup>	Poissons' Ratio
Fibres (E-glass)	238.2	72408.0	0.20
Matrix (Polyester +Dibutylphthalate)	32.5	4172.0	0.36

\*with  $\lambda = 5893 \text{ \AA}$

